

POLITECNICO DI TORINO

Master Degree Course
in Biomedical Engineering

Master Degree Thesis

CYBATHLON 2020 - Powered Exoskeleton Race



Supervisors
Prof. Marco Gazzoni
Prof. Dario Farina

Candidate
Andrea Pergolini

Academic Year 2018/2019

*To my Grandma Rita
and
my little nephew Giulio.*

Acknowledgements

I would like to take this chapter as a chance to express my immense gratitude to everyone who supported me during this internship of seven months. First of all, I want to express my immense gratitude to all my thesis supervisors, starting from Prof. Dario Farina, chairman of the Neurorehabilitation lab at Imperial College London (ICL), and Prof. Marco Gazzoni, LISiN director at the Politecnico di Torino, for the unbelievable opportunity they gave me and for the passion they transmitted to me.

Then, a huge thank you goes to Prof. Silvia Muceli and Dr. Deren Yusuf Barsakcioglu, at Imperial College London, for guiding me through the project and for supporting me during the whole internship period.

I would also like to thank all of the people of the Dario's fellas group at ICL, for having created the perfect work environment in which everyone can feel at home and welcome. In particular, a special thank goes to Irene, who I could always count on and that always supported me during these months; and Simone, who has helped me to overcome the difficulties of the project and for being a huge source of inspiration.

I can't forget to thank all the Coffe Break's people, of Dario's group and not, who I consider close friends and that helped make this experience perfect and unforgettable.

Thanks to all my Italian friends from the oldest ones to the Turin fellas. A special thank is necessary for Cekka and Chopper, great friends and flatmates who have borne me during these university's years; Giamma and Fice, that will always have a special place in my memories; and Simone, who I found again in London and that always encouraged me.

I would also like to thank Marianna, who shared with me this London experience and all the following thesis troubles.

Last but not least, I must thank my Mother and Father for making all this possible, for always being by my side and for making me become who I am; and my Sister for always being my first supporters and for believing in me, sometimes more than myself. Thank you for being such an amazing family.

Contents

1	Introduction	1
2	Powered lower limb exoskeleton	3
2.1	State-of-the-art Exoskeleton control	3
2.2	H2 exoskeleton	5
3	Experimental Protocol	8
3.1	CYBATHLON Powered Exoskeleton Race	8
3.2	Experimental procedure	11
4	Kinematics Recording and Processing	14
4.1	BTS Smart-DX Acquisition System	14
4.2	Markers Placement	15
4.3	Markers Position Pre-Processing	17
4.4	Evaluation of the Joints Kinematics	19
4.5	Inertial Measurement Unit Estimation	25
5	Back Muscle Exploration and Analysis	28
5.1	Back Muscles Study and Selection	28
5.2	High Density Electromyography Recording	29
5.3	Synchronization Framework	32
5.4	High Density EMG Processing	34
5.5	Estimation of Lower Limb Kinematics from the EMG features	37
5.6	Preliminary Study Results and Analysis	38
6	Bipolar EMG Recording and Processing	46
6.1	Feature and Advantage of the FreeEMG-1000 Acquisition System	46
6.2	Electrode Placement	48
6.3	EMG Processing	49
7	Estimation of Lower Limb Kinematics	52
7.1	Neural Networks	52
7.2	Regression with Feed Forward Neural Networks	54
7.3	Estimation of 6 DoF from EMG features	56
7.4	Estimation of 6 DoF from EMG and IMU features	58
8	Results and Discussion	60
8.1	Angles estimation from EMG features	60
8.2	Angles estimation from EMG and IMU	64

9 Conclusion and Future steps	67
Appendices	69
A Estimation of 6 DoF from EMG features: Results per Subject	70
B Estimation of 6 DoF from EMG and IMU features: Results per Subject	76

Chapter 1

Introduction

In this work, I present a novel intuitive and proportional myoelectric control algorithm to control a powered lower limb exoskeleton in order to compete in Cybathlon 2020 in Zurich. The main objective of the exoskeleton is to assist gait to those who have complete thoracic or lumbar spinal cord injuries (SCI). It aims to enable the user to perform tasks related to daily life activities, such as sitting down, standing up and walking. The thesis was carried out throughout an internship of seven months at the Neurorehabilitation Laboratory of the Imperial College London (ICL).

In the last decades, electromyogram has been the main information source to interpret and predict movement intention in prosthetics and orthotics field. This technique measures muscle activity and thus, it is affected by anatomical, physiological and acquisition factors. Despite these limitations, electromyogram has achieved proportional and simultaneous control of multiple degrees of freedom. Recently, some commercial Trunk-Hip-Knee powered exoskeletons have been developed to assist incomplete SCI during everyday life activities, or for rehabilitation purposes. The exoskeletons for complete SCI or paraplegic people developed by researchers are still mostly based on predefined gait and action enable from the user with a joystick. These assistive devices have already improved the lives of people with motor disabilities but they are neither intuitive for the user, nor practical to use. To overcome these difficulties for the user, I propose an intuitive and proportional myoelectric controller based on a Multi Layer Perceptron Neural Networks, which is able to regress the flexion/extension angles of the hip, knee and ankle joint from the upper body's muscles activity. We hypothesize that a relationship between the upper body muscles activities and the lower limb motion exists. The first step of my research project is to verify this assumption, thanks to the results of preliminary studies made during the internship. Then, once this assumption is verified, the final and principal goal of this research is to develop and verify the stability of a novel myoelectric exoskeleton controller. In order to validate the proposed method, I analyzed it in normally-limbed participants, which is a necessary basis for future testing in SCI patients. Ten able people participated in the experiment, after providing written informed consent and the procedure was approved by the local ethics committee of the ICL.

This dissertation presents in the second chapter the state of the art on the exoskeleton's control and the description of the exoskeleton on which is based this work. The third chapter shows the experimental protocol developed and followed during this research, starting from the required tasks of the Cybathlon race which are briefly

shown. Then, the use of the motion capture acquisition system and the consequent data processing are explained in the fourth chapter. Particular attention is given to the method for the hip knee and ankle joint angles calculation, which will be the targets for the Neural Network estimation, and the marker placement. These topics are described earlier than the other data type recording and elaboration because are valid for the entire dissertation. The fifth chapter presents a small stand-alone research project because it regards both the preliminary studies made in order to verify the aforementioned relationship between the upper body muscle and the lower limb kinematics. Therefore, it describes the high density surface electromyography setup used, the realized framework to concurrently record the motion and the muscles activities signals, and lastly, the neural network architecture used to verify the relation. The bipolar wireless surface electromyographic system is then shown in the sixth chapter, paying attention to the final realized electromyographic setup; which is used for the participants' study. A description of the Neural Network architecture is then made in the seventh chapter, and how these networks are used for the estimation of the angle, focusing on the different input features and network layers utilized. In the last two chapters, I present the results of the entire work and the conclusions with some suggestions for future steps to improve the research done.

Chapter 2

Powered lower limb exoskeleton

The first chapter initially gives a panorama of the state of the art in exoskeleton control's strategies besides a brief description of different assistive device classifications. Then, a description of the exoskeleton on which this thesis work is based is given to the reader in order to better understand some control choice made, e.g. number of degrees of freedom available.

2.1 State-of-the-art Exoskeleton control

As technology is becoming smarter and safer, the development of exoskeletons for physical aid represents one of the most addressed mobility assistance options. Exoskeletons can be used for substituting the therapists in repetitive rehabilitation exercises or assisting healthy people with heavy loads carrying or physically demanding jobs. Moreover, they are useful for assisting people suffering from muscular weakness or regaining locomotion ability for paraplegic or quadriplegic people. In this thesis, I will focus only on the medical exoskeleton devices, thus, only those devices which have medical purposes.

Exoskeletons are thought in different architectures to assist their users' movements. The research has been mainly focused on lower-limb devices, because they address basic and fundamental motion tasks of daily life, like walking or standing. Moreover, leg exoskeletons have particular cognitive and physical requirements from the emerging human-robot interaction systems. Many categories can be found to classify exoskeletons. For example, they can be passive or powered. Yet they can be rigid or made entirely out of soft materials. There is really no established correct way to categorize exoskeleton. However, some nomenclature conventions are adopted from a literature review in this dissertation.

Exoskeletons are firstly classified accordingly with the covered joints. Thus, they are distinguished among:

- trunk–hip–knee–ankle–foot (THKAF);
- hip–knee–ankle–foot (HKAF);
- trunk–hip–knee (THK);
- hip–knee (HK);
- knee–ankle–foot (KAF).

This first classification allows dividing multi-joint exoskeleton from orthotics and single joint devices. Then, two major categories are easily recognizable and separable between all the medical exoskeletons, which are rehabilitative and mobility aids. Rehabilitation exoskeletons can perfectly recreate the same motion repeatedly thousands of times. Patients are thus able to perform more exercise repetitions in the same amount of time and with higher consistency. Rehabilitation medical exoskeletons assume that the user will improve his physical condition until he will no longer need to use the assistive device. An exoskeleton used as mobility aids instead, assumes that users will not get better and they will rely on the wearable device for the rest of their lives. Both categories may rely on different control strategies of the exoskeleton. In recent years, the research mainly focused on the robotic development rather than control strategy. For this reason investigating an innovative and subject intuitive control strategy, like the one in this thesis work, it is a challenging and open research objective.

Even though different control approaches can be easily found in a literature review, it is still a challenge to develop natural and efficient assistive strategies. The major complexity in realizing those controllers is due to the existence of bidirectional interaction between the exoskeleton and the wearers. The device provides power and concurrently gives sensory feedback information to the wearers, whereas, the user sends the movement intention to the exoskeleton and undergoes the action of it. While the research direction is more involved in the hardware level, the greatest lack is in a high-level controller which interprets the feedback and the user intention information. Actually, there are different, purpose dependent, control strategies. The main utilized controller strategies found in the literature [25] for rehabilitation and mobility aids exoskeleton are sensitivity amplification, predefined gait, model-based, predefined action based and biomedical signals based.

- **Predefined gait trajectory control.** This is the easiest and most basic control strategy for a medical exoskeleton. The exoskeleton is basically a pre-programmed wearable robot that executes predetermined motions. The desired joint trajectories are recorded from an able person or extrapolated from gait analysis data, and then replayed on an exoskeleton. To improve the flexibility and usability of the controller, different trajectories are sometimes postures dependent. The user control is made through a joystick usually placed in the crutches. This control strategy has the lowest level of interaction between the human and the device. This kind of assistance mainly targets people partly/completely losing normal voluntary movements like quadriplegic, gait disorders patients and SCI patients. The reason is essentially a lack of detectable information useful for understanding the wearer intention.
- **Model-based control.** This control structure relies on a human–exoskeleton model. The desired robotic actions are mainly computed considering gravity compensation or the detection of the shift of the center of mass. An example of these is the zero moment point (ZMP) balance criterion. This control strategy requires a numerous sensors to recognize kinematics and dynamics variables of the human-exoskeleton system. Moreover, the control strategy completely depends on the accuracy of the model. Thus, a less accurate model means not accurate control. Model-based control target at assisting paraplegic people with daily-life movements, it can augment the wearer’s staff-holding capability

and it is suitable for muscular weakness people.

- **Sensitivity amplification control.** This controller is based on an inverse dynamic model of the human-exoskeleton system. Thus, it is a model-based controller but it is distinguished from it because the exoskeleton power is wearer dependent. The force exerted by the user is detected from the exoskeleton and used in a feedback loop of the controller. Unfortunately, external disturbance force can also be amplified by the controller, which makes it unstable. It is mostly used to handle exoskeletons which increase the load-carrying capability of a user or for rehabilitation exercise purposes.
- **Predefined action based on gait pattern.** Some exoskeletons provide assistance using passive springs or pneumatic cylinders. This means systems controlled only by activation of these elements. Predefined action based control strategies distinguishes from the predefined trajectory because they act concurrently with expected gait events. Therefore, the system does not continuously follow recorded joint trajectories, but it waits for specific events. Similar to the predefined gait trajectory, this control strategy is suitable for people partly/completely losing normal voluntary movements like quadriplegic, gait disorders patients and SCI patients.
- **Biomedical signals control.** This control strategy relies on electrical signals detectable from the wearer. These medical exoskeletons record bio-electrical information from the user body and produce a proportional motor activation. This control strategy can be suitable for rehabilitation purposes as well as increasing the load-carrying capability of a user.
- **Hybrid assistive strategy.** The exoskeleton control is executed by applying different assistive strategies. For a specific gait state, the efficacy of assistance could be improved. However, the transition between each strategy should be taken into account to avoid discontinuity or uneven outputs.

These briefly described control strategies are mainly used in the manufacturing and research field. This thesis is an initial study made to realize a novel and intuitive biomedical signal based controller. More specifically a myoelectric intuitive and proportional control, thus based on the wearers muscle activity detection. Obviously, this view is given to the reader to know that also other control strategy exist.

2.2 H2 exoskeleton

The robotic exoskeleton available in the laboratory is the H2 [16]. It presents the hip, knee and ankle joints actuated on both legs. H2 is an HKAF exoskeleton designed for adult stroke patients with a maximum height of 1.95 m and a maximum body weight of 100 kg. It can be also adopted with spinal cord injuries (SCI) patients who suffer hemiplegia or paraplegia. The mechanical design of the exoskeleton has been made taking into account that it should be ergonomic, lightweight and robust. The H2's mechanical structure is primarily made of aluminum 7075 considering its resistance and lightweight. Because of that, the final exoskeleton weights, including its battery pack, is around 12 kilograms. In order to be adaptable to different users the length



Figure 2.1: The H2 exoskeleton[16], a bilateral hip, knee and ankle active joint rehabilitation device.

of the thigh and shank segments' aluminium structure can be modified via two telescopic mechanisms. The same telescopic bar system is used in the exoskeleton's ankle joint. The device is designed to permit active and passive movements only in the sagittal plane and limited passive movements, only in the hip joint, of about 20 degrees in the transverse plane to let the user be able to turns while walking. The range of motion of the hinged hip, knee and ankle actuated joint is limited for safety reasons. Moreover, the H2's mechanical structure is designed to unload its own weight through the aluminium frame to the ground, otherwise, the user would have felt an extra weight during the utilization.

In exoskeletons, not every type of actuator can be used, because it requires high torques concurrently with lower speeds. The H2 actuators in the hip, knee and ankle joints are a 100 W (Maxon EC60) brushless DC motors with a nominal torque of 220 mNm. Moreover, in order to reduce speed and increase torque, the motors shaft are coupled to a Harmonic Drive gearbox (CSD-20-160- 2AGR). The exoskeleton is designed as an autonomous device, so, its power supply, made of a high capacity battery, can provide enough power for an independent use of the device. In addition, the battery pack has been specifically developed for the H2.

In wearable robotic devices, to guarantee the wearers safety and control the user-exoskeleton interactions are fundamental. H2, in order to determine the angular positions and velocities of the active joints and the interaction torque, presents the following sensors placed in the structure:

- 6 potentiometers, which detect the angular position in the hinged hip, knee and ankle joint.
- 18 Hall Effect sensors, which detect the angular velocity in the hinged hip, knee and ankle joint.
- 24 strain gauges, placed at each link, which measure the interaction torque be-

tween the exoskeleton and the wearers. A full Wheatstone bridge connection is used to amplifying the output of the strain gauges 500 times and in order to have the torque measurements in a range from -50 to $+50$ Nm.

- 4 foot switches, two in each plantar surface of the foot, which binary detect the heel and toe ground contact. They are based on resistive sensor and are useful to detect the different gait phases.

H2 is developed as a wearable device for gait rehabilitation in a clinical environment, but it also allows users to perform sit-to-stand and stand-to-sit movements. In the H2 an impedance controller is available, in order to assist the user in completing the gait movements. Despite the partially different rehabilitation aim, this exoskeleton has been choose because it presents an open architecture with wired and wireless communication's interfaces. These features allow the H2 to be easily integrated with other systems and to be used for combined studies, such as human-machine interfaces.

Chapter 3

Experimental Protocol

In this second chapter, a general view of the Cybathlon competition is given to the reader; paying attention to what the exoskeleton race requires. Then, a description of the experimental procedure specifically created is made. The realized protocol is thus based and oriented on the tasks required from the Cybathlon. This is the first study in the laboratory that aims to take part in the race, thus only the fundamental Cybathlon task will be explored.

3.1 CYBATHLON Powered Exoskeleton Race

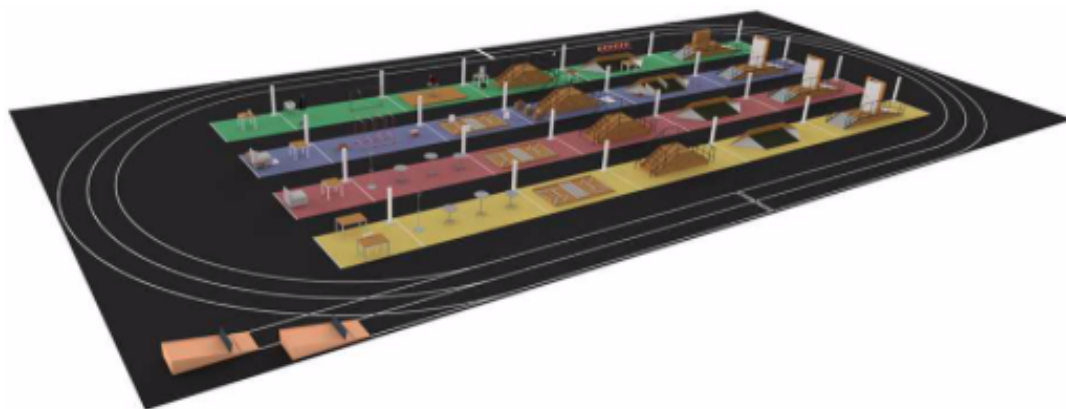


Figure 3.1: Example of the competition field and tracks [20]. Clearly recognisable the two tracks for the FES Bike Race. In the middle the four parallel tracks for the Arm Prosthesis, Leg Prosthesis, Exoskeleton and Wheelchair Race.

This thesis work aims to realize a high-level controller for Spinal Cord Injury (SCI) people in order to compete in the non-profit CYBATHLON 2020 exoskeleton race. The main goal of the competition is to promoting research, development, and implementation of advanced assistive technology for everyday use by disabling people. Moreover, the competition invites to create a common platform where engineers, people with disabilities and general public meet and dialogues each other. Technical assistance systems are used by millions of people with disabilities in their everyday lives. These devices often lack practical usability, which disappoints users, with the

results that new technologies are either not being used and not even accepted. Besides, the public environment often makes the use of assistive technologies close to impossible, due to architectural barriers. The wish of the CYBATHLON is to break down barriers between the public, people with disabilities and engineers through organizing a unique competition. Each team is tested on courses designed to show how well suited a given technology is with everyday tasks, like climbing stairs or opening doors. The CYBATHLON has six different races and disciplines:

- Brain-Computer Interface (BCI) Race, where pilots with quadriplegia use BCI to control avatars in a computer game. The aim of this race is to improve the BCI technology in order to create an interface able to control devices like wheelchairs.
- Functional Electrical Stimulation (FES) Bike Race, where pilots with paraplegia are enabling to perform a pedalling movement on a recumbent bicycle thanks to the FES.
- Powered Arm Prosthesis Race, where pilots with unilateral or bilateral amputation can compete. The prosthesis has to include the wrist and can utilize any kind of control.
- Powered Leg Prosthesis Race, where pilots with unilateral or bilateral transfemoral amputation have to perform various movements using any kind of active or passive prosthetic device.
- Powered Wheelchair Race, where pilots with severe walking disabilities using a powered advance wheelchair can compete. The aim is to create assistive devices able to overcome obstacles such as stairs or doors.
- Powered Exoskeleton Race, where pilots with complete thoracic or lumbar spinal cord injury can compete using an exoskeleton. The aim is to create a device able to walk and master other everyday tasks.

Each of the six disciplines has specific tasks to achieve and rules to follow. However, the common and most important rules are about the safety of the pilots.

Pilots with complete thoracic or lumbar SCI equipped with an exoskeleton are challenged by tasks related to daily life activities. During the race, the pilots are asked to solve as many tasks as possible in a given time. In order to compete in the race, the exoskeleton and the pilot need to satisfy certain minimum requirements.

- the SCI pilots need to be at least classifiable as AIS A or B [5], with a complete loss of motor function and with leg paraplegia.
- SCI Pilots with higher lesions level, affecting the control of the trunk and/or neck, must be evaluated individually; because they must have enough voluntary control and strength to hold crutches and stabilize the trunk for safety reasons.
- For control purposes, any kind of input device or automated gait intention detection strategy is allowed.
- To mobilize the exoskeleton any type of actuation (other than combustion) is allowed.

- The maximum weight of the exoskeleton (excluding the pilot) is limited to 75 kg.
- The exoskeleton control can be hybridized with the use of FES. Moreover, surface and/or implanted technologies are allowed.
- The Pilot must wear a helmet during the race and the use of handrails or crutches is allowed.

The exoskeleton hardware criteria are all satisfied from the H2 exoskeleton on which the controller is based. In addition, also the controller object of the thesis is clearly allowed.

The specific exoskeleton race tests the exoskeleton-pilot in condition related to activity often required during the day of an able person. The required tasks for the exoskeleton race are:

1. SIT AND STAND. In the first part of the task, the pilots are asked to sit down and stand up from a sofa. Then, in the second part, pilots are asked to manipulate objects while standing.
2. SLALOM. In this task, pilots have to negotiate a slalom track composed of single pieces of furniture.
3. RAMP AND DOOR. In this task, the pilots are asked to climb and descend ramps, ring a doorbell and pass through a doorway. Thus, the ability to negotiate steep inclines and to navigate in confined space is tested.
4. ROUGH TERRAIN. It requires to step over obstacles on the ground and to accurately control the positioning of the feet.
5. TILTED PATH. Negotiating a tilted path in an exoskeleton is challenging as it requires abduction/adduction in the hip and pronation/supination in the ankle. A tilted path with different surfaces is used to create the challenge of such a situation.
6. STAIRS. This task tests how well the exoskeleton supports the action of ascending and descending stairs.

For the realization of some of these tasks, an advanced control system is required. As already said, this is the first study made in the lab aiming at the exoskeleton race. Thus, I focus on the fundamental activity without which the attendance is not possible. The essential task I recognize in all the required activity is walking, which is also a frequent activity during daily life. Moreover, I considered in the study the sitting-standing task, which does not require a specific environment in the race and is fundamental to rest for the pilot. Thus, during the entire study, the walking and sitting tasks will be the target of my controller, because selected as fundamental tasks for the race.

3.2 Experimental procedure

The definition of a precise experimental protocol to follow during each study made in the internship is essential for more reason. Firstly and most practical reason, because during the execution of an experiment every step of it need to be previously deeply defined in order to focus only on the study goal. Thus, the definition of a protocol allows to specifically define which are the objectives of the study and how the researcher wants to reach and test it. In this case, as already explained, the aim is to realize a myoelectric exoskeleton control to perform walking and sitting/standing tasks. Moreover, this aim implies the presence of a volunteer on which the myoelectric activity is detected, which leads to a second important reason for defining a protocol. When a person is involved in an experiment, they must provide written informed consent and moreover, the experimental process needs to be previously approved by the local ethics committee of the ICL. Therefore, the first step of the internship was to create a detailed protocol, where every activity require and every recording made from a volunteer are precisely described.

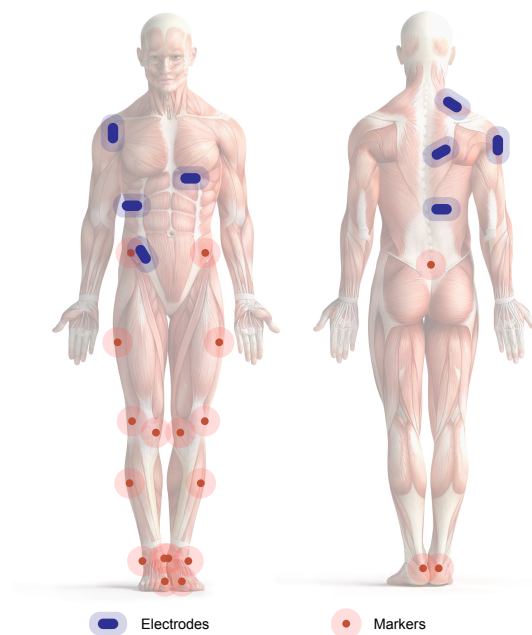


Figure 3.2: The scheme of the experimental setups made for the final study. As it is described in the picture, the reds dots represent the passive ball-shaped markers and the blue rectangle, instead, are the bipolar EMG probe. An idea of the position of each marker and sensor on the subject's body is thus visible.

The experimental procedure defined is slightly different between the preliminary study and the final one. These differences regarding the different acquisition systems used and everything that follows it. Therefore, in this paragraph, I will describe only the activity required to participants and I will leave the setup description to other chapters. Nevertheless, figure 6.2 shows the scheme of the final study setup. In every case, as it is visible, the setup involves the placement of grids or electrodes on the subject upper body right side and of reflective ball-shaped markers on specific

lower limb anatomical landmarks.

In every experiment realized during the internship, the activities required to participants are three: standing, walking and sitting, which are shown later in the chapter following the procedure order. At the beginning of each experiment, it is explained to the participant that each task has to begin and end with him in the rest position, i.e. standing position. Moreover, the rest position needs to be maintained for at least 5 seconds at the beginning of each task. During the whole experiment, the start and the end of the acquisition are communicated verbally to the participants. Lastly is required to the subject to maintain the resting position at the end of each task until verbal confirmation of the end of the acquisition. Before the beginning of the true experiment, the researcher have to takes some anatomical measures from the subject body. He is measured taking into account the motion capture marker placement, thus after the realization of the setup. These measures are essential for the calculation of the joints centers of rotation because obtained from anthropometric measurement based equations. The essential measures are reported in table 3.1.

Measure Label	Anatomical Measure
La	Asis distance [cm]
Lc	Thigh length [cm]
Cc	MidThigh Circumference [cm]
Lg	Calf lenght [cm]
Cg	Calf circumference [cm]
Wm	Malleolus width [cm]
Hm	Malleolus height [cm]
Lp	Foot length [cm]
Bp	Foot breadth [cm]
Dk	Knee circumference [cm]

Table 3.1: participants anatomical measures necessary to estimate the joints centers of rotation.

When this preliminary information is explained to the subject, the real experiment can begin. Therefore, the researcher will perform a practical demonstration of each task before the actual recording.

The first task required is standing. The subject has to maintain the standing position for 20 seconds in the middle of the motion capture zone. This task is needed to normalize the kinematics joint angles and to obtain the natural pose of each subject body segment. This task is done just once in the beginning of the experiment.

Secondly, the walking task is required. The subject has to walk at a self-paced walking for the whole length of the motion capture zone, trying to follow the rhythm of the metronome. He has to start walking inside the motion capture zone from a standing position and end, inside the motion capture volume, maintaining a standing position at the end. Prior to the task recording, the subject is required to perform some demo walking trials to get used to the walking rhythm. The metronome is always set between 70-75 bpm, to normalize the walking rhythm between participants. The task is repeated 10 times, 5 times starting with the right leg and 5 with the left one. Between each repetition, the subject will have 30 seconds to rest and to return to the starting point.

The third and last required task is sitting. The subject has to frontally flex the

upper body in order to sit in a stool using the upper limb to support the movement and then extend the upper body while is sitting. Then, frontally flex the upper body in order to stand up from the chair using the upper limb to support the movement and extend the upper body in the end of the standing movement. This specific movement will be repeated twice inside a recording. As well as for the walking task, the subject has to follow the rhythm of the metronome and in the begging, some sitting trial will be done to let the subject be used to the rhythm. The metronome is set to 30 bpm for each subject and it beat the beginning of each partial movement. This task will be repeated 4 times. Between each repetition, the subject will have 30 seconds to rest. After each acquisition, the integrity of the EMG and motion capture data are checked. Moreover, the motion capture data can often present some missing information due to covered markers. In case of problems is thus asked to the subject to repeat the problematic task.

The defined experimental process allows having all the information needed for the joint angles' estimation during the realized tasks. Indeed, I have the target signals for the Neural Network estimation, the motion capture data, and the input feature from the EMG recording. I used the experimental protocol in normally-limbed participants, which is a necessary basis for future testing in spinal cord injured. Ten able body people participated in the final experiment, after providing a written informed consent of it. This experimental process defines the base for the entire study.

Chapter 4

Kinematics Recording and Processing

This chapter covers everything that concerns the motion capture data recording and processing. Firstly, I describe the acquisition system and markers placement. Secondly, the applied pre-processing to markers' coordinates is explained, with particular attention on the tracks gap-filling procedure. Thirdly, I focus on the joint angles, with an explanation of the method used to calculate the six lower limb flexion/extension degree of freedom. Finally, I explain how the equivalent information of an Inertial Measurement Unit (IMU) is estimated from the pelvis markers.

4.1 BTS Smart-DX Acquisition System

The motion capture acquisition system available in the lab is the Smart-DX 700 from *BTS Bioengineering* [21]. It has eight infrared digital cameras with a resolution of 1.5 Mpixel. During the study, the maximum resolution of the cameras is always set, which implies a sampling frequency of 250 Hz. Otherwise, the system is able to record at 1000 fps with a minor resolution. The accuracy of the system is 0.1 mm on a motion capture volume of 36 m³ (4 x 3 x 3 m). The Smart-Dx is a passive marker-based system, where markers are illuminated from infrared lights mounted on each camera. Thus, the markers are retroreflective balls with 1 cm diameter or smaller. The Smart-DX integrates and synchronizes all the information from the cameras, the bipolar electromyographic devices, the sensorized platform and from other general purpose input.

The acquisition system needs to be calibrated before each experiment, which consists of two different kinds of acquisition. Firstly, a static acquisition of a tripod with three different marker's number on the axes, to determine the global reference frame of the motion capture volume. Secondly, the recording of a moving marker's wand, to estimate the calibration matrix. This matrix is essential to maps the 3D real coordinates of the markers into the 2D image domain. The calibration matrix is usually recovered linearly via a Direct Linear Transform method, which will not be explained because not central for the thesis purpose. Thanks to the calibration procedure, the average and standard deviation error between the real and the recorded marker position is guaranteed to be under 0.5 mm for each camera. Otherwise, a new calibration of the system is required. The system is ready to record when the calibration process is ended. The output signals are the three spatial coordinates of

each reflective marker. Therefore, the global 3D position of each marker, referred to the global reference frame of the motion capture volume, is obtained from each recording. The Smart DX also provides an analysis software, which allows to create customized experimental protocols and visualize the marker position, velocity and acceleration. It can identify and associate each recorded marker to one of the realized model, which will be explained in the following chapter. It is also useful to eliminate the presence of unreal marker, due to reflecting materials present in the volume, or correct other noise sources.

4.2 Markers Placement

The first step of using a motion capture system is the realization of the marker placement model. The model's definition set where markers need to be placed on the subject. Some prior knowledge about the utilization of a motion capture system is needed for the definition of the model and the use of the system. Firstly, the minimum number of markers for each body segment is three. This number allows defining a plane between the markers, which permits to calculate a reference frame for the segment and thus the 3D position and orientation of it. This process will be explained in the chapter 4.4 when the calculation of a local reference frame is described. Secondly, the maximum visibility of each marker needs to be guaranteed from each camera inside the motion capture volume. Therefore, the camera and marker perfect placement need to be checked before realizing a recording. Thirdly, placing additional markers near and around the body joint allows us to better define the joint centers and motion, e.g. twist of the proximal segment on the distal one. Lastly, it is necessary to define a lower limb mechanical model as a serial kinematic chain, taking into account the desired number of rigid body segments and the desired degree of freedom (DoF) of each joint. Therefore, it is suggested to place markers at bony anatomical landmarks, because it minimizes sliding and allows regression for the localization of the joint centers. Considering all the aforementioned guidelines, besides of a literature review of pre-realised marker placement model, I use a slightly modified Davis-Helen Hayes lower limb protocol [24]. The difference between the reported protocol and the one used reside in the presence of four additional markers in the medial position of the knee and ankle joints [3], as is shown in figure 4.2a. The selected marker placement is thus composed of a set of 19 passive ball shaped markers, subdivided along the lower limb as is described in table 4.1. Each anatomical landmark is found feeling the subject's skin and paying attention on the symmetry of the placement between the two sides. Despite of this, the markers placed in the segment's mid point, e.g. RTHI or RTIB, are placed not symmetrically between the two sides to easily recognize them on the recording. Figure 4.1 shows an example of the complete marker placement. The marker placement is based on a subdivision of the lower limb in seven rigid body segments; which are pelvis, right/left thigh, shank, and foot. Each body segment is considered connected to the other with a single DoF rotary joint. The lower limbs are so defined as the serial kinematic chain reported in figure 4.2b. The presence of two markers on opposite sides of the knee and ankle joints allows us to easily define the position of the joints center of rotation as the average position of them. Regarding the hip joints center instead, it will be calculated thanks to an anthropometrics-based conditioning [1], based on the anatomical measure explained in paragraph 3.2. The first acquisition with the

Anatomical landmark	Marker label
Left Anterior Superior Iliac	LASI
Right Anterior Superior Iliac	RASI
Sacrum	SACR
Right/Left Thigh mid point	RTHI/LTHI
Right/Left Knee Lateral epicondyle	RKNE/LKNE
Right/Left Knee Medial epicondyle	RKNM/LKNM
Right/Left Tibia mid point	RTIB/LTIB
Right/Left Toe	RTOE/LTOE
Right/Left Heel	RHEE/LHEE
Right/Left Ankle Medial malleolus	RANM/LANM
Right/Left Ankle Lateral malleolus	RANK/LANK

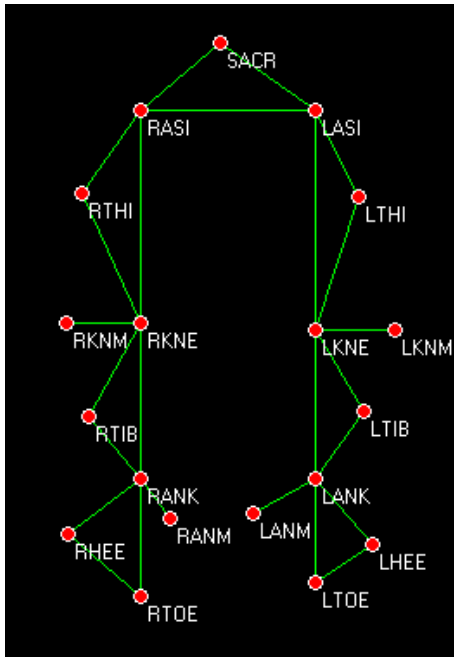
Table 4.1: The description of the markers placement models. A label is associated to each marker positioned above each anatomical landmark.



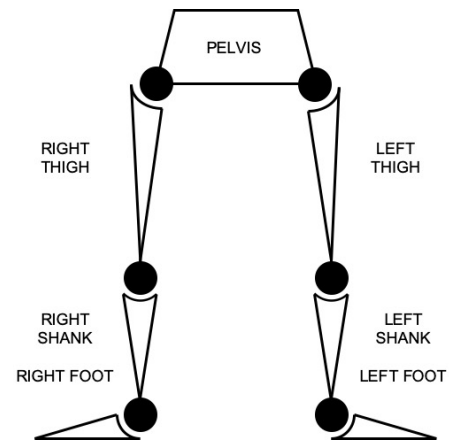
Figure 4.1: The complete markers' placement realized during an experiment. It is visible the symmetry between the markers on the two sides of the body placed above specific bony anatomical landmarks and the not symmetry of the others. Each marker is placed feeling his anatomical landmark that minimize sliding and maximize its visibility.

system is always a static standing recording, in order to calibrate the joints' neutral angular displacement and the relative position between each body segment. An association of each recorded reflective object with a marker of the model is needed after each acquisition. The motion capture system only records the spatial position of each reflective material that at least two cameras can see. It is not able to real-time associate and labels a recorded object with a marker of the model. This procedure needs to be done from the user at the end of the recording. Therefore, thanks to the aforementioned tracking software provided by *BTS Bioengineering*, I recognize and associate each recorded object with a model's marker from the 3D

visualization. This process allows to label each reflective object with the name of the model and it is simplified from the software marker's auto detection. This means that the user needs to select a marker only in one frame, then the software recognizes and associates the label, to the selected marker, for the whole duration of the signal. Therefore, the software is not able to autonomously label the marker but it is able to recognize each different reflective object of the recording. In the end of the labeling procedure, the kinematics information of each marker is ready to be exported in Matlab for the pre-processing and the angle joint estimation. Thus, the output of the motion capture system is a 3 spatial coordinate signal for each labeled marker.



(a) The motion capture marker placement model used during the whole study. It is a modified version of the Davis-Helen Hayes lower limb protocol



(b) The considered model of the lower limb as a serial kinematics chain. the Hip - Knee - Ankle joint are thought to be as single DoF rotary joint in the sagittal plane, because of the H2 exoskeleton active joint

Figure 4.2: The motion capture marker placement model and the lower limb mechanical model as a serial chain

4.3 Markers Position Pre-Processing

The output of the motion capture system, after the previously explained association, is the 3D coordinates of each marker during the recording time. Each output file is exported as a *.tdf* and open with a given function in Matlab. This function is provided by the *BTS bioengineering* with the system. The pre-processing comprises three different signal's elaboration. Firstly, a filling gap procedure of the motion missing information. Secondly, a resampling procedure of the marker track, to obtain the same number of samples of the concurrently recorded electromyographic information. Lastly, a filtering of the marker position.

Unfortunately, during the recording, a marker can be occluded from the camera and disappear from the recorded signal. When this happens, the motion capture approaches fail, and in the correspondent samples a *Not a Number* (NaN) is inserted. Where a NaN is present, the marker signals position shows missed information that needs to be filled. The missing position of the marker can be reconstructed from the previous and following samples of the same signals with an interpolation technique. Moreover, the worst problem happens when the missing information is in the beginning or end of the marker position when no prior or posterior knowledge is available. In this scenario, interpolation methods fail and different completion algorithms are used. Obviously, the first approach to avoid this missing information problem is understanding which is the cause of the missing data during the recording. However, a signal gap can always be present in the marker position. The first step of the kinematics pre-processing is thus to find and fill the gap in the marker tracks. When a NaN is found, I use three different reconstruction techniques. Two different signals interpolation methods and a Kalman filter based completion algorithm [17]. In the realized code, a linear and a spline interpolations of the marker positions are compared with the signals extrapolated from the third method and with the original and gaped signal. The results are shown to the user which can decide between the three different techniques. An example of it is shown in figure 4.3. The choice is

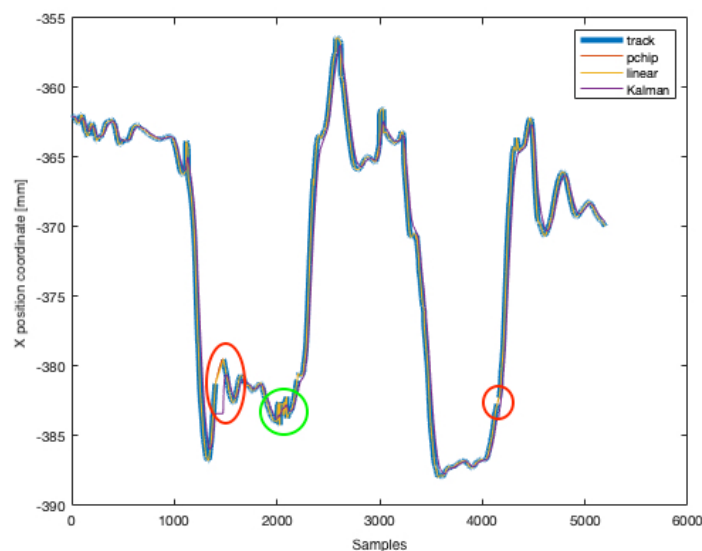


Figure 4.3: In the figure can be seen an example of the Matlab figure from where I decided which interpolation method to use. Moreover, highlighted in red, an example of the missing information gap and of the three different estimations. Besides, highlighted in green, an example of strong high frequency noise due to jitter.

left to the user because, as previously explained, each method can be optimum in different missing data conditions. For example, the linear interpolation is optimum when the gap is present during a slowly or constant variation of the marker position. On the contrary, spline interpolation is better when the signals vary rapidly and non linearly. Lastly, the Kalman filter based is the best choice when an extrapolation of the information is required. Once every marker's track has been checked and there are no NaN in the signals, the marker positions need to be up-sampled. This step is due to the different sampling frequency between the motion capture systems (250

Hz) and the electromyography acquisition systems (1000 Hz or 2048 Hz). The two different signals need to have the same length in terms of samples for the last step of the study, the exoskeleton kinematics estimation. The up-sample of the marker position is basically an ulterior interpolation of the signals. In other words, to increase the number of samples a replica of the aforementioned spline interpolation process is done; as if a gap is present between each sample. This is done, in the realized Matlab code, thanks to an already developed function and present in the software. Lastly then, all the marker coordinates are low pass filtered with a 6th order Butterworth at a cut off frequency of 5 Hz. The filter is applied to limit the bandwidth of the kinematics information and to eliminate high frequency noise. The filter is usually able to eliminate most of the rapid and unreal change in the reported position of a stationary or quasi-stationary marker calls jitter. An example of this noise source is shown in Fig. 4.3. After this last step, each marker position signal is smooth and clean from noise sources, with the correct number of samples for the final estimation and without missing information. Thus, the marker coordinates are ready to be used for the joint kinematics estimation.

4.4 Evaluation of the Joints Kinematics

In the end of the previously explained pre-processing three X-Y-Z spatial coordinates, of each labeled marker, is available. These signals represent the global position in the motion capture volume of each model's marker. In order to better explain the following joint angles estimation, a definition of global reference frame and local reference frame need to be given to the reader. A global reference frame is a fixed reference frame in the environment, the motion capture volume in this case, and not to the moving subject. It is commonly used to describe the motions of different body parts present inside the environment. A local frame, instead, is a moving reference frame that moves with the moving body. This frame can translate and rotate accordingly with the refereed body part. It is easy to confuse, after these two definitions, a reference frame with a coordinate system. Thus, a prior definition of coordinate systems needs to be made, to explain the difference between it and a reference frame. The coordinate system determines the way one describes/observes the motion in each reference frame, e.g the Cartesian or Polar are coordinate system. As explained in the chapter 4.2 the lower limbs of the subject are considered as a serial mechanical chain constitute of 7 rigid body segment. A local reference frame can be associated with each body segment, to describe its position and orientation, and to do that the marker's coordinates can be used. Whereas, a global reference frame is set and associate with the motion capture volume, thanks to the calibration procedure. The aim of using the motion capture in this study is obtaining the flexion/extension angle for each hip - knee - ankle joint of the lower limbs. This objective is due to the degree of freedom that the exoskeleton hardware allows. The realized code for the estimation of the joints angles can calculate, from the given motion capture data, the whole position and orientation of each rigid body of the chain. Thus, instead of using an easier method, I realized a general lower limb kinematics estimation, to have a better estimation of the desired degree of freedom. Moreover, in this way, I have a ready platform to calculate more degrees of freedom in the prevision of an exoskeleton's hardware improvement. The joint kinematics estimation is subdivided into four steps. First of all, a local marker-based reference

frame calculation. Followed by the joint center's identification, through the calculated local reference frame. In order to clarify for the reader, the local frame calculated in the first step are only useful for the joint center's estimation. These frames are not able to describe the orientation of each rigid body of the defined lower limb chain. Thirdly, a second local reference frame definition is done, this time each frame is embedded in each segment of the chain. These embedded frames are based on the anatomical notable points estimated and calculated in the second step. Finally, the real angles joint estimation is done, considering the relative motion between two adjacent body segments and following the recommendation of the International Society of Biomechanics [3] [19]. These resumed angles estimation steps follow the procedure made in [1] and they are now deeply explained.

As already said, the first step calculates an orthogonal uvw reference frame based on three selected markers. The selected markers around the right foot, for example, are the RTOE, RHEE and RANK as shown in figure 4.4a. Indicating with the marker's label the instantaneous spatial position of the selected marker and with $\hat{i}\hat{j}\hat{k}$ the unit vectors of the global reference frame, the following operations are done to calculate the uvw reference frame for the right ankle.

- u axis is defined parallel to the line that connects RTOE and RHEE

$$\begin{aligned} RTOE - RHEE = (RTOEx - RHEEx)\hat{i} + (RTOEy - RHEEy)\hat{j} \\ + (RTOEz - RHEEz)\hat{k} \end{aligned} \quad (4.1)$$

$$RTOE - RHEE = \|RTOE - RHEE\|\lambda \quad (4.2)$$

$$\lambda = \frac{RTOE - RHEE}{\|RTOE - RHEE\|} = Cux\hat{i} + Cuy\hat{j} + Cuz\hat{k} \quad (4.3)$$

- w axis is defined perpendicular to the three marker's plane

$$\begin{cases} RTOE - RANK = (RTOEx - RANKx)\hat{i} + \\ (RTOEy - RANKy)\hat{j} + (RTOEz - RANKz)\hat{k} \\ RHEE - RANK = (RHEEx - RANKx)\hat{i} + \\ (RHEEy - RANKy)\hat{j} + (RHEEz - RANKz)\hat{k} \end{cases} \quad (4.4)$$

$$(RTOE - RANK) \wedge (RHEE - RANK) = w_{foot} = \|w_{foot}\|\nu \quad (4.5)$$

$$\nu = \frac{w_{foot}}{\|w_{foot}\|} = Cwx\hat{i} + Cwy\hat{j} + Cwz\hat{k} \quad (4.6)$$

- v axis is defined to make a right-handed triad with u and w

$$\mu = \nu \wedge \lambda = Cvx\hat{i} + Cvy\hat{j} + Cvx\hat{k} \quad (4.7)$$

The $\lambda\mu\nu$ unit vector triad of the right ankle is so defined, where they respectively indicate the uvw axes' direction of the reference frame. The $\lambda\mu\nu$ triad allow me to have a coordinate system to describe the position of the different point in the local frame relative to the global reference frame, defining the following rotation matrix:

$$\begin{bmatrix} Cux & Cvx & Cwx \\ Cuy & Cvy & Cwy \\ Cuz & Cvz & Cwz \end{bmatrix} \quad (4.8)$$

The columns of the matrix 4.8 are the direction cosines and they define the orientation of each local frame axis relative to the global frame. It is important to emphasize that the nine matrix elements are not independent. In fact, six scalar equations may be written, that reduce the number of independent elements to three. In summary, the independent elements are three scalar independent quantities, that define the relative orientation of the frame. This explained method to calculate the ankle reference frame has been realized by me in a Matlab function. A similar process is done for each joint that connects two rigid body segments of the considered lower limb's serial chain. The marker's selection and the selected axes direction for each segment are reported in the following. Thus, Considering the right calf in figure 4.4b:

- I place the origin of the reference frame in the RKNE.
- The RKNE, RTIB and RANK marker form a plane and u axis is defined perpendicular to it.
- The v axes is defined parallel to the line between RKNE and RANK
- the w axis is defined to form with v and u a right-handed system.

The same considerations are done to realize the left calf rigid body reference frame; substituting the three markers with the respectively left side LKNE, LTIB and LANK. Considering then, the pelvis joints in figure 4.4c:

- I place the origin of the reference frame in the SACR.
- The SACR, RASI and LASI marker form a plane and the w axis is defined perpendicular to it.
- The v axes is defined parallel to the line between RASI and LASI
- The u axis is defined in order to form with v and w a right-handed system.

In the end of the first step, I have five orientation matrix that allows me to describe the marker's position in each different local frame calculated. This step is essential for the following process, where anthropometric measurement based equations are applied in order to estimate the joint centers and the segment centers of gravity. I will now show how the joint centers are estimated from the markers' positions described in the calculated local frame, using the anatomical measure taken and explained in 3.2. Considering the local reference frame uvw of the pelvis, the position of the marker in the sacrum and the ASIS breadth; the following prediction equation are used to estimate the position of the right and left hip joint centers of rotation.

$$\begin{aligned}
 Hip_r = SACR + (0.598)(ASISbreadth)\hat{u} - (0.344)(ASISbreadth)\hat{v} \\
 - (0.290)(ASISbreadth)\hat{w} \quad (4.9)
 \end{aligned}$$

$$\begin{aligned}
 Hip_l = SACR + (0.598)(ASISbreadth)\hat{u} + (0.344)(ASISbreadth)\hat{v} \\
 - (0.290)(ASISbreadth)\hat{w} \quad (4.10)
 \end{aligned}$$

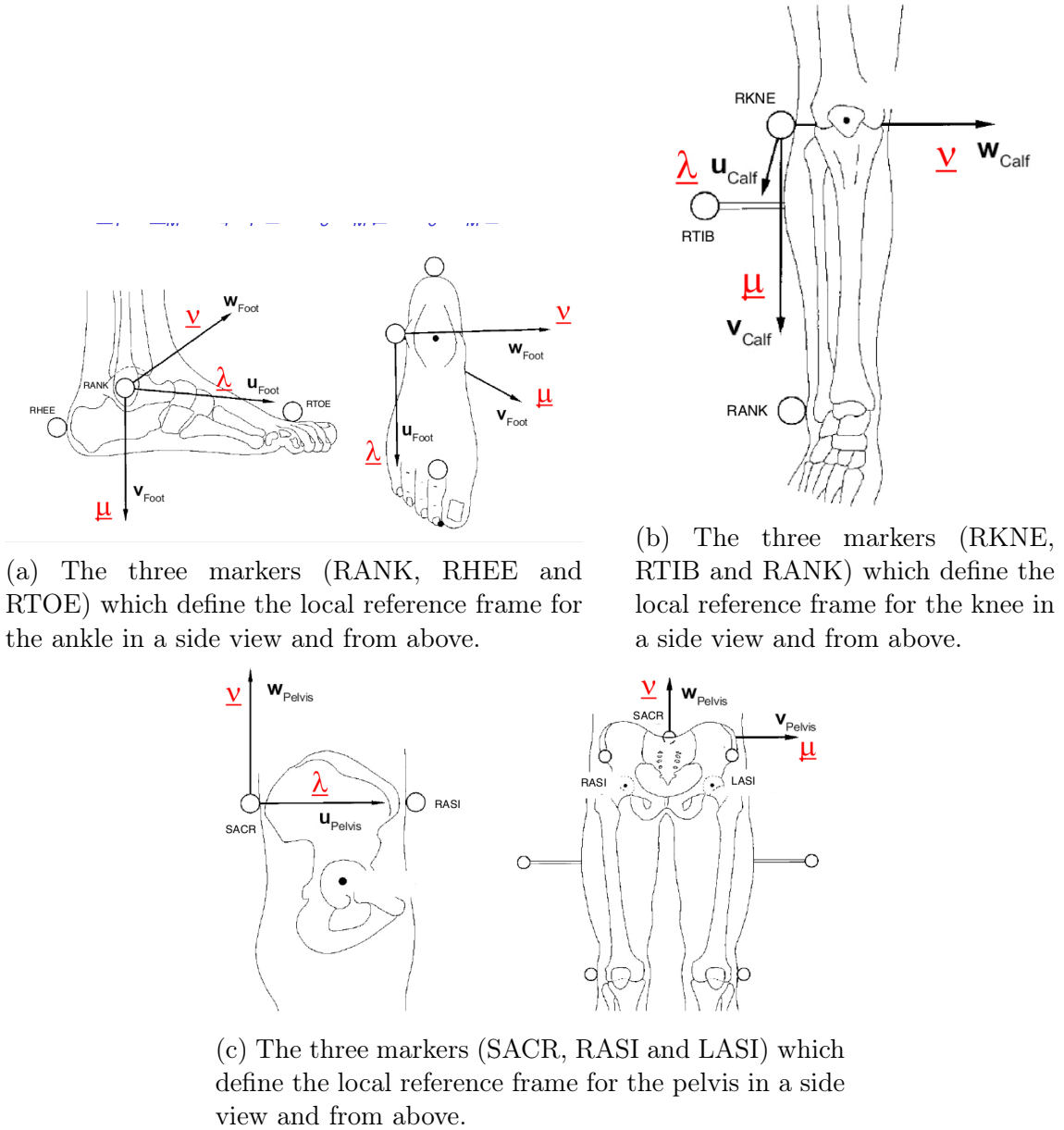


Figure 4.4: The three different markers selection for the local reference frame definition

Where the coefficients have been taken from [1] and are based on direct 3D measurements of 12 normal participants, and on stereo X rays of a normal subject. It is necessary to pay attention to the reference frame used in the equation. Each marker position or equation member needs to be described in the same reference frame to correctly estimate the anatomical notable points. Therefore, the SACR position in the equation 4.9 is previously pre-multiplied with the transposed of the matrix 4.8 in order to describe its position in the local pelvis frame. Moreover, I also estimate the knee and ankle joint center using the prediction equation.

$$Knee_r = RKNE + (0.500)(Kneediameter)\hat{w}$$

$$Knee_l = LKNE + (0.500)(Kneediameter)\hat{w}$$

$$\begin{aligned}
 Ankle_r = RANK + (0.016)(Foot_{length})\hat{u} + (0.392)(Malleolus_{height})\hat{v} \\
 + (0.478)(Malleolus_{width})\hat{w}
 \end{aligned}$$

$$\begin{aligned}
 Ankle_l = LANK + (0.016)(Foot_{length})\hat{u} + (0.392)(Malleolus_{height})\hat{v} \\
 - (0.478)(Malleolus_{width})\hat{w}
 \end{aligned}$$

Then, as a validation of the explained calculi, I compare it with the knee and ankle joints center of rotation position calculated as the average point between the medial and lateral marker. Now that the joint centers are calculated, the center of gravity of each segment and other notable points are obtained from anatomical-based calculi. The prediction equation used for that will not be shown because the obtained notable points are not used in the continuing of the angles' estimation, in fact, they are useful to describe the translation of the segment on the space. The second step of the realized procedure is thus finished and thanks to it I have the relative position of the joints center in each local frame.

The third task in these angles joint estimation regards becoming able to determine the orientation of each segment in 3-D space. This is done by calculating an embedded reference frame (xyz) in each body segment, that will define how each rigid body is oriented and positioned relative to the global reference frame. The origin of each xyz reference frame is located in the segment centers of gravity and it allows to know the position of each segment. As already said this information is obtained but not used in the following of the study. The rigid body's orientation description, instead, is obtained from the relative orientation of each embedded segment's frame compared to the global one. The segments frame are calculated following the same principle of the first step, but this time using the estimated joints center. The difference between the first local frame and these resides in the direction of the axes, which now is an anatomical segment direction. Besides the fact that these are embedded in each body. Thus, for the thighs segments, the x axis lays from distal to proximal on the line between the knee and hip joints center. The xz plane is formed by the hip joint center, the position of the thigh marker, and the knee joint center. The y axis is perpendicular to the xz plane, points in an anterior direction and so complete a right-handed triad. In the case of the calves, the x runs from distal to proximal direction on the line between the ankle and knee joints center. The xz plane is formed by the knee joint center, the position of the marker in the calf and the ankle joint center. The y axis is perpendicular to the xz plane, points in an anterior direction and in this way it completes a right-handed triad. Lastly for the feet, the x axis lays between the toe and the heel marker's position. The xy plane is formed by the ankle joint center and on the heel toe marker's position. The z axis is at right angles to the xy plane. Figure 4.5 illustrates how the frames are at the end of the procedure. I am now able to describe the orientation of each body segment compared to the global fixed reference. This means that I already know the desired angles joints information, I just need to correctly extrapolate them from the relative orientation of each reference frame.

This is done in the final step, which is the estimation of the rotation angles. This final step relies on the relative motion between two adjacent bodies' segments and extrapolates the anatomical angles from it. Firstly, since the orientation is specified by three independent angles, as described in 4.8, we need to specify the three axes

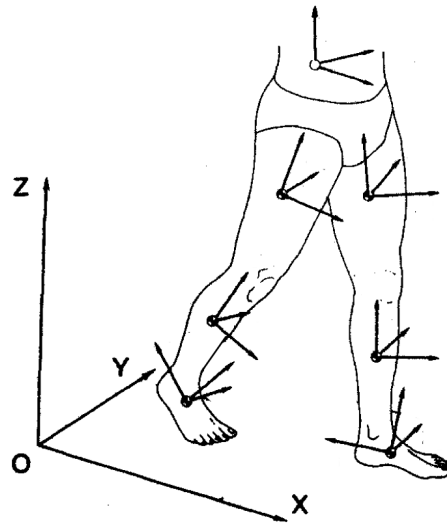


Figure 4.5: The segment's local reference embedded in the center of gravity of each segment. Note the axes direction and the relative orientation of each reference frame compare to the global.

about which the corresponding rotational motions occur. If these axes are not correctly selected from the embedded reference frames for each segment, the obtained angles will not be coincident with the anatomical ones. Following [19], the first two axes, called body fixed, are two of the embedded reference frame axes from the two adjacent body segments in relative motion. Thus, their direction is already specified by the unit vectors calculated in the previous step. The third axes, called floating, is the unique common perpendicular axes of the first two bodies fixed. Therefore, the orientation and the unit vector of the floating axes is given by the cross product of the body fixed's unit vectors. This axis is called floating because is not fixed and its direction depends on the movements of the two considered body segments. The first two relative rotations between the body segments may be thought as a spin of each body about its own fixed axis while the other body remains stationary. The magnitude of these spin rotations is measured by the angles formed between the floating axis and the embedded axes of the stationary body. The third relative rotation occurs about the floating axis and is measured by the angle between the two body-fixed axes. A graphic example of this process is shown in figure 4.4. These three angular coordinates are the independent information that provides the relative orientation of the two adjacent bodies and a general geometric description of Euler angles. The concept of Euler angles is thought to be known to the reader. Due to the embedded reference frames previously defined, these three angles exactly describe the three degrees of freedom of each anatomical joint. Mathematically speaking, in order to clarify the concept, an example of the estimation of the angle between the thigh and the calf is shown. In the following, I will indicate with I, J, K the unit vector triad of the thigh reference frame and i, j, k the unit vector triad of the calf reference frame. Moreover, I will use e_1, e_2 and e_3 for the joint rotation axis. Where, e_1 is the axes about the flexion/extension rotation and it has the same direction of I ; e_2 is the floating axes and e_3 is the same of k , meaning the tibial internal/external rotation axes. Keeping in mind these variable names, the joint angles α (flexion/extension)

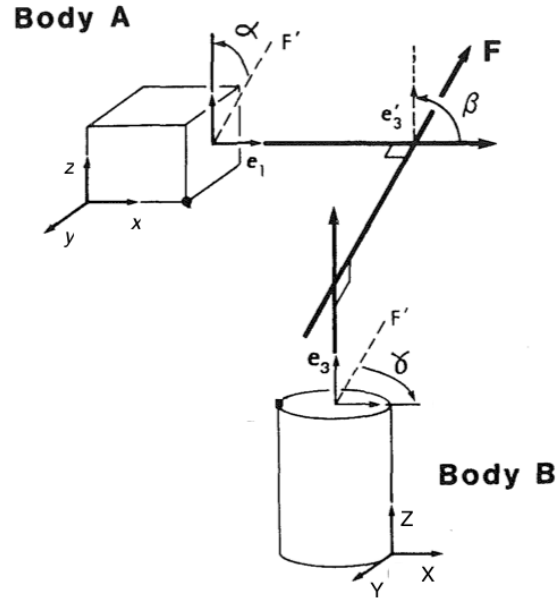


Figure 4.6: A description of a general joint frame (e_1, e_2, e_3) definition for the angles estimation between two adjacent segments. e_1 is coincident with x of the body A, e_1 with Z of the body B and the calculated floating axis is shown. The $\alpha\beta\gamma$ are thus the estimable angles.

β (abduction/adduction) γ (internal/external rotation) are estimated.

$$e_2 * K = \cos\left(\frac{\pi}{2} + \alpha\right) = -\sin(\alpha) \quad (4.11)$$

$$\begin{cases} e_2 * i = \cos\left(\frac{\pi}{2} + \gamma\right) = -\sin(\gamma) \text{ left knee} \\ e_2 * i = \cos\left(\frac{\pi}{2} - \gamma\right) = \sin(\gamma) \text{ right knee} \end{cases} \quad (4.12)$$

$$I * K = \cos(\beta) \begin{cases} \text{R knee adduction} = \beta - \frac{\pi}{2} \\ \text{L knee adduction} = \frac{\pi}{2} - \beta \end{cases} \quad (4.13)$$

Making the same evaluation for the other body segment is possible to calculate each considered joint angle. As explained in the beginning of the chapter, the realized procedure allows obtaining more joints angles than needed. Therefore, in the following of the dissertation, only the α angle for each joint will be considered. Hereafter, I will refer to angles joint to indicate only every flexion/extension angles estimated. Once all these steps are realized the angles joint estimation is ended and the desired information is ready for the Neural Network use.

4.5 Inertial Measurement Unit Estimation

The Inertial Measurement Unit (IMU) is a not optical motion capture sensor, which is able to give to the user from three to six degrees of freedom. These sensors are widely used, in the literature, for a lower accurate gait analysis and/or for robotic and prosthetic control [10] [15]. From this knowledge comes up the idea of integrates an IMU as an input feature in the Neural Network control. In order to

not insert another sensor in the already highly complex and elaborate experimental protocol and not to add an ulterior sensor on the subject, I decided to estimate the information received from an IMU directly from the motion capture information, since optical motion capture systems are used to validate and evaluate the IMU system features. Thus, the information that I can extrapolate from the sensor is basically the same, only a bit less accurate. Obviously, in the follow-up case of a real-time application with an exoskeleton, a real IMU will be applied to the subject body due to the lack of presence of an optical motion capture system. The IMU estimated information is the tilt, obliquity and rotation of the subject's pelvis. This placement decision is due to gait's consequent pelvis movement. The application of this IMU is thought as a way to close the loop between the EMG input and the estimated output kinematics of the Neural Network. As shown in the final results, the application of this IMU as input feature increases the quality of the estimation of the angle.

The aforementioned pelvis tilt, obliquity and rotation DoFs are obtained thanks to the already calculated pelvis embedded reference frame, explained in the chapter 4.4. The three degrees of freedom are thus calculated from the relative orientation of the pelvis frame to the global motion capture reference. The realized function that calculates the segment reference frame, in order to give to the user the three independent orientation information, returns the rotation matrix between the global and the embedded frame. Thus, to estimate the IMU information, I only need to consider the rotation matrix achieved from three simple rotation about each axis and the extrapolate the angles from this matrix. The three consecutive rotations that occur are:

- γ around the vertical axes for the internal/external rotation;
- α around the anterior/posterior axes for the tilt information;
- β around the medial/lateral axes for the obliquity.

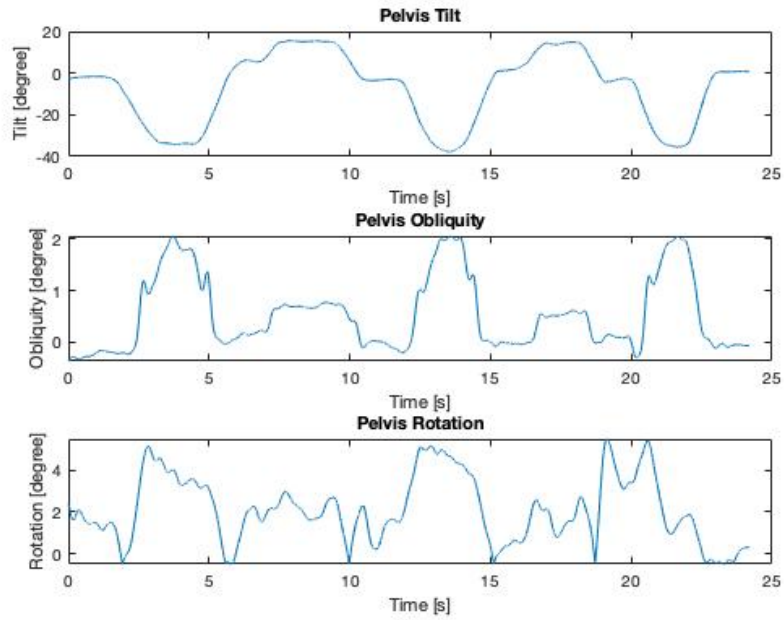
From the so composed rotation matrix the desired angles are calculated from the following equation:

$$\alpha = \arcsin(r_{(32)}) \quad (4.14)$$

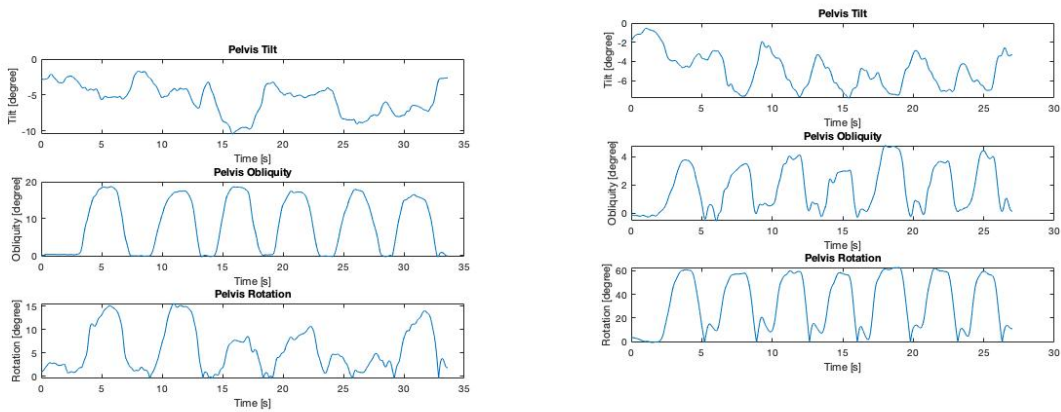
$$\beta = \arccos\left(\frac{r_{(33)}}{\cos(\alpha)} + k * \frac{\pi}{2}\right) \quad (4.15)$$

$$\gamma = \arccos\left(\frac{r_{(22)}}{\cos(\alpha)}\right) \quad (4.16)$$

To validate and verify the functionality of the estimation, three basic tasks have been recorded. Each of the three tasks consists in the movement of the pelvis for every single degree of freedom. Thus, the first is a simple internal-external rotation of the pelvis, the second a tilting of it and the final an oblique movement of the pelvis. The results of this validation are reported in figure 4.7.



(a) The IMU tilt, obliquity and rotation DoFs measured from the subject pelvis during a simple frontal flexion.



(b) The IMU tilt, obliquity and rotation DoFs measured from the subject pelvis during a simple lateral flexion.

(c) The IMU tilt, obliquity and rotation DoFs measured from the subject pelvis during a simple rotation about the longitudinal axes.

Figure 4.7: The validation of the tilt, obliquity and rotation IMU measure estimation.

Chapter 5

Back Muscle Exploration and Analysis

In this chapter, I describe both preliminary studies made at the beginning of the internship. The first challenge of my work is to understand if a physiological relation exists between the trunk muscles activity and the lower body movements. The exploration and analysis of the back muscles activity is realized in two pilot studies following the experimental procedure explained in chapter 3.2. In the beginning of the chapter, the literature studies, which create the base for the existence of the relationship and thus for these pilots, are shown and explained to the reader. Subsequently, I describe the high density surface electromyogram used during these preliminary studies, and why it is helpful to realize the back muscle exploration. Thirdly, a fundamental synchronization framework is briefly shown. This framework is essential for the execution of the experimental procedure. Then, a description of the high density electromyography features selection and extraction is given to the reader, followed by a short explanation of the neural network architectures used for the angles' estimation. Lastly, the results thus obtained are deeply analyzed where the goodness of the estimation is used as a quantification of the relation existing between the selected muscles' activity and the lower limbs motion.

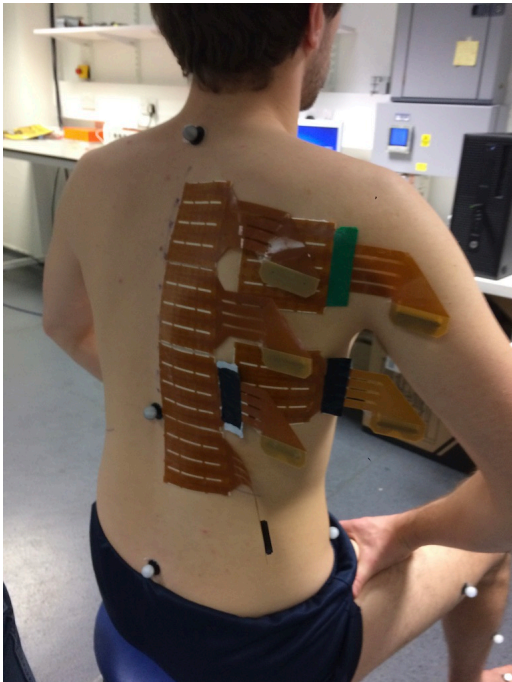
5.1 Back Muscles Study and Selection

The back's muscles are classified as stabilizers and mobilizers of the spine [2]. They allow linking the thorax and the spine to the pelvis. The deepest of these back's muscles produce high and constant magnitude of torque/force with the main purpose of maintaining the stability of the spine and of the whole upper body. This is defined as the global stabilizer function of these muscles and it is mainly realized from the deep muscles of the Erector Spinae group and the Abdominals. Back's muscles also work on maintaining the stability of the upper body segments and of the spine curvature, which action is classified as local stabilizer function and it is mainly due to the Abdominal and Trapezius. The most superficial back's muscles, moreover, have a mobilizer function of the spine and of the upper body. In addition, they show a non-continuous and direction dependent muscle's activity, producing large range of movements of the body's segments. Thus, the first theoretical relation of the back's muscles with the lower body activity is due to the necessity of maintaining the stability of the upper body during the motion. These attended muscles activities

are confirmed in other literature studies during daily life activity, such as walking [11] or sitting and standing [4]. The first pilot study is made in order to verify the existence of this relation, and it is realized trying to cover with the high density EMG as more surface as possible on the right side of the back. This is done because, in this way, we expect to detect the activity from the maximum number of muscles possible, both superficial and deep. The choice of cover only the right side, instead, is due to the number of channels available. Moreover, if a relationship exists, the activation of the right and left muscles would mostly be inverted to each other. Lately, taking into account the muscle synergy theory [7] [8] during gait, the group of muscles studied in the second pilot is changed. The synergy theory supposes the existence of a modular organization in motor control. This means that the control problem is reduced to modulating an appropriate selection of an adequate number of motor modules, also called muscle synergies. It results in a simplified control strategy of movements. The theory is that the central nervous system controls muscles' activation using a set of basic control elements and each synergy defines a group of muscles that are coactivated, thus working as a single functional unit. Therefore, the selected muscles for the second study are supposed to be related to each other and with the lower limb motion through the synergy theory. From the aforementioned synergy's articles during daily life activities, I add to the selected muscles the descending Trapezius, the anterior Deltoid and the posterior Deltoid. Summarizing, for the first study we want to analyze as max right side back's muscles as possible covering the whole right back's side of the subject. For the second pilot, instead we target 5 specific muscles; the anterior and posterior Deltoid, the ascending and descending Trapezius, and the Erector Spinae group.

5.2 High Density Electromyography Recording

In both preliminary studies made, the high density surface electromyography (HD-sEMG) is used to study the muscles' activation during the experimental procedure's required tasks. The advantages of using HD-sEMG are many, from the chance to extract physiological information, such as muscle fatigue or conduction velocity [9] to the possibility of estimating motor unit discharge patterns [12] [13]. Basically HD-sEMG makes available a higher quantity and variability of EMG data. The acquisition system used in these preliminary studies is a "LISiN-OTBioelettronica, QUATTROCENTO" configured to a sampling rate of 2048 Hz. The EMG signals are recorded in a monopolar mode acquisition from each electrode and they are amplified with a gain of 10000, band-pass filtered at a selected bandwidth of 10–500 Hz (eighth-order Bessel filter) and converted with a 16 bit analog digital converter. In both preliminary studies, the reference electrode for the measurement is placed at the right clavicle. As anticipated, the first pilot provides an HD-sEMG recording from 384 channels, the maximum amount of the system, using six semi-disposable adhesive grids of 64 electrodes, each arranged in 8 rows and 8 columns with 8 mm of inter-electrode distance. The grids are placed above the right back side of the trunk between the 7th cervical vertebra and the 12th thoracic vertebra. They are thus placed in the subject's back right side trying to cover as max surface as possible of it. The grids placement is shown in figure 5.1. In order to have a lower electrode-skin impedance, prior to grids' placement, the subject's skin is shaved, if necessary, lightly abraded and cleaned with alcohol. This procedure must be always



(a) A clear view of the grids' placement. In order to make the placement repeatable and precise the spinous process of the vertebrae are counted and marked.

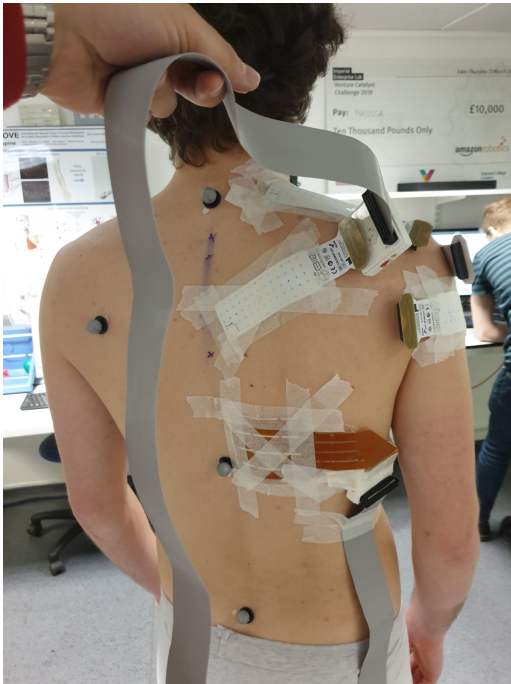


(b) The entire setup connected setup. It is clearly visible from this picture the complexity of the setup. The acquisition system is also visible and it is above a wheeled chair to allow the researcher to follow the subject during the execution of the tasks.

Figure 5.1: The placement of the six grids above the right back side of the subject for the first pilot study.

done before the grids' placement in an HD-sEMG recording. Moreover, the grids and the last part of the connecting pending cable are tightened to the subject body; with the aim of reducing the movement of them, having the matrix' best adhesion possible and decreasing the presence of motion artifact in the recording. Figure 5.1b shows, in addition of the grids' placement, the complexity of the setup. During the experiment, it is asked to the subject to walk around the lab' space and to sit and stand. In the meantime, the researcher must follow the subject, due to the length of the cables that connect the grids and the system, and in order to do that the acquisition system is placed on a moving chair. This operative choice carries on a lot of noise sources, from the chair's vibration interference, to the high probability of motion artifacts.

The second pilot study, differently from the first, provide the recording of 320 EMG channels from five semi-disposable adhesive grids of 64 electrodes and 8 mm of inter-electrode distance but, one arranged in 8 rows and 8 columns whereas, the other, arranged in 5 rows and 13 columns. In the second pilot, the placement is more muscles specific, due to the results of the first study, and to the precise muscle activity researched. The targeted muscles selected, as already mentioned, are the descending Trapezius, with the grid placed on the line between the 7th cervical vertebra and the acromium, the anterior Deltoid, which has the muscle's fiber following the line



(a) A clear view of the back's grids placement. In order to make the placement repeatable and precise the spinous process of the vertebrae are counted and marked.



(b) A clear view of the Deltoids and descending Trapezius grids' placement. To notice the different kind of matrices used and the specific muscles targeting.

Figure 5.2: The placement of the five grids of the targeted muscles of the subject for the second pilot study.

between the acromium and the thumb, and posterior Deltoid, with the grids placed to cover the whole muscle belly that lays in the line between the acromium and the little [8]. The remaining grids are placed between the 9th and the 6th thoracic vertebra, in order to cover the erector spinae group muscles, and between the 5th and the 1th thoracic vertebra along the line that connects 8th thoracic vertebra and the acromium, to cover the ascending Trapezius. The described grids' placement is shown in figure 5.2. The reader also notices that, even in this second pilot study, the same cables connection and the same use of the chair is done for the execution of the experiment. During the grids' placement is asked to the subject to realize isometric contraction of the targeted muscle, in order to better visualize and feel the muscle belly and border under the skin.

When the desired grids placement is done it is possible to start with the EMG recording. Firstly, the correct placement above the muscle and the goodness of the signals needs to be verified. Therefore, isometric contractions of each selected muscles are required to the subject, this request allows checking the whole amount of available channels. Once the setup is ready and checked, it is possible to proceed with the real experimental procedure. Unfortunately, the HD-sEMG from *OT-Bioelettronica* is not directly compatible with the motion capture system previously described in chapter 4. The aim of the studies require to have both information perfectly synchronized to each other, otherwise, it is impossible to verify if a relation exists. Moreover, for the final angles' estimation with the Neural Networks, the Input and Target signals must have the same amount of sample. The essential

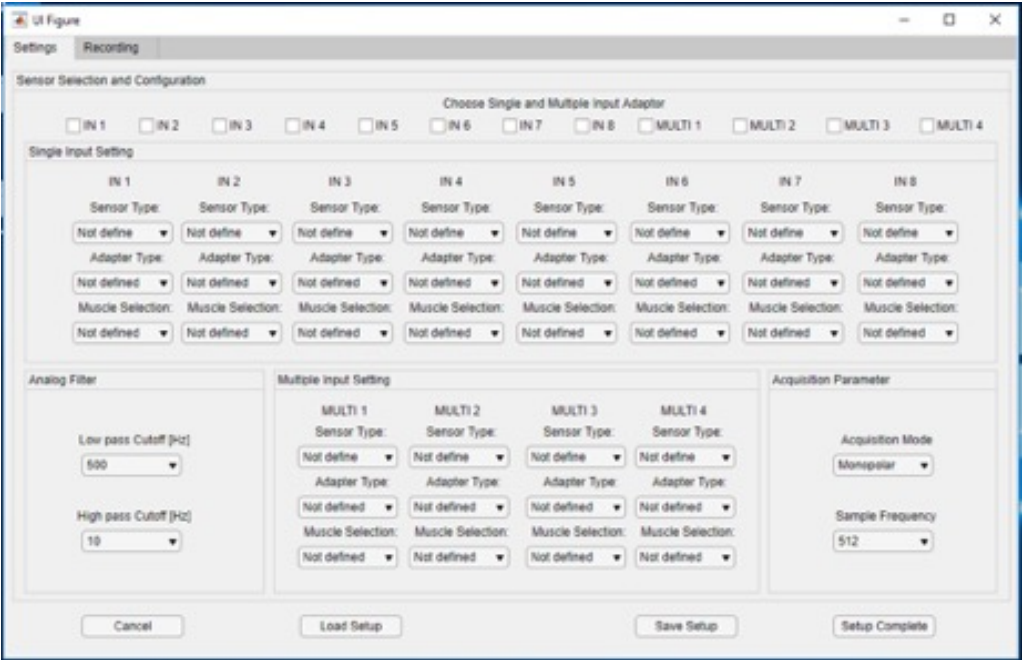
synchronization of the data from the two systems is made thanks to an acquisition and synchronization framework realized on Matlab and explained in the following paragraph.

5.3 Synchronization Framework

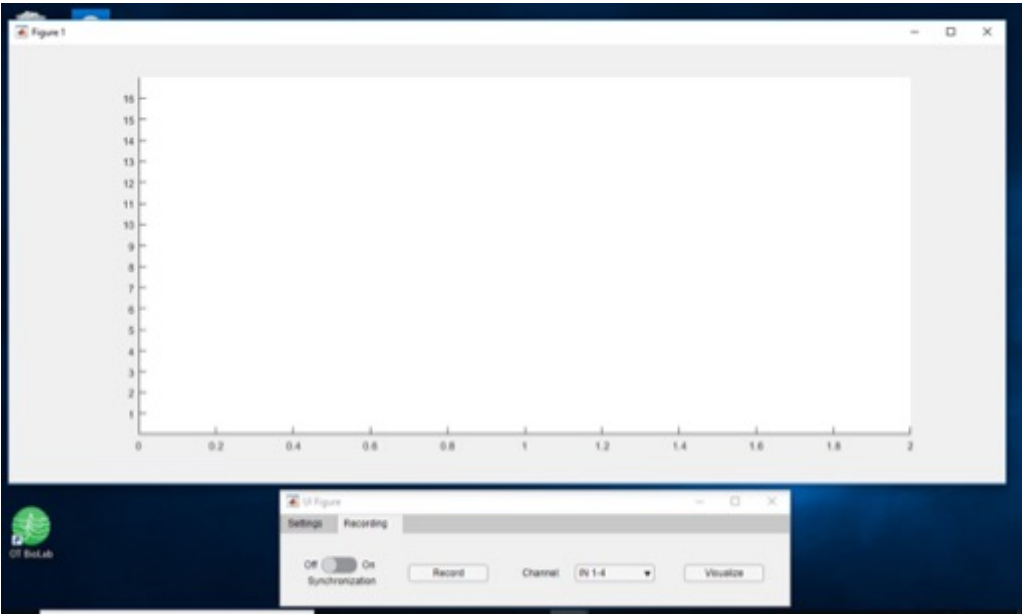
The framework mainly aims to allow the user to synchronize the recording of the HD-sEMG data with the motion capture signals and moreover, trying to do that in the easiest way possible. Firstly, in order to be able to synchronize the signals, an Arduino board is used as a Trigger signal generator. I choose an Arduino microcontroller, because it is easily programmable on Matlab to generate a square wave and because it is trouble-free to connect to other devices. A trigger signal is the most used way to synchronize two acquisition devices because it can be used to start the acquisition on the rising edge and stop it on the downing edge. Unfortunately, neither the Quattrocento neither the Smart-Dx have a programmable trigger input, but only accessible analog input. Moreover, it is necessary to take into account the different sampling frequency between the two devices. The Smart-dx has a frame rate of 250 fps whereas, the Quattrocento of 2048 Hz. Therefore, the trigger can only be used in an offline synchronization, through identifying and cutting both the recorded signals on the trigger's rising and downing edge. This means that, after this choice, the Arduino's trigger is what determines the start and stop of the recording. The user will thus consider the recording started only on the trigger activation.

This is already enough to have synchronized data, but, in this way, it is necessary to start three different acquisition, one for each device, in order to do the recording. Taking into account the already complex experimental process, where the tester has to carry the system behind the subject during the execution of the tasks, this solution is not practical. In order to simplify the acquisition, a stand-alone Matlab object able to merge the Arduino and the HD-sEMG recording has been created. This specific Matlab framework is not only able to start the recording from the Quattrocento and turn the Arduino trigger on, but it completely substitutes the OTBioelettronica software for the EMG acquisition. It allows real-time visualizing and operating, directly from Matlab, on everything that concerns the EMG acquisition and the Arduino. Moreover, with the framework the possibility to start the trigger and the EMG acquisition concurrently is integrated into the developed user interface. Summarizing, this object eliminates the needing to start and manage two different devices separately. I cannot show and deeply explain the realized code in this dissertation because it contains private information from the OTBioelettronica company. This private part takes care of setting all the acquisition system's registers, through sending essential binary string to them. These strings set the channel's gain, the cutoff frequency of the filter inside the system, the available channels, the grids' type connected to the system and all the other system's settings. Moreover, the application is not specific for the experimental setup used in these studies, but it is able to set and create every available setup of the device. Figure 5.3 shows an example of the framework's user interface during the acquisition and the settings' definition.

The communication between the PCs and the Quattrocento, for the real-time acquisition and visualization, is based on a TCP/IP communication. A listener in the open TCP/IP channel continuously refreshes and acquires specific buffer size of data



(a) The Settings user interface. The user can define the acquisition settings from this window panel, before switching to the recording.



(b) The Recording user interface. From this panel, the user can visualize one Quattrocento channel at time and switch between them.

Figure 5.3: The Quattrocento Matlab object realized for the synchronization framework.

from the system, until the acquisition is stopped. Unfortunately, the object is not able to integrate the Smart-dx. This means that the motion capture files are copied in the PCs and elaborated from the object after the recording. As explained, the signals are cut on the rising and downing edge of the Arduino trigger and the motion data are then up-sampled in order to match the EMG signals samples number. Thank to the framework is thus possible to have the data synchronized. Moreover, It is possible to have an easier execution of the experimental procedure. In the end, the framework gives in outputs the two different information ready for the following processing.

5.4 High Density EMG Processing

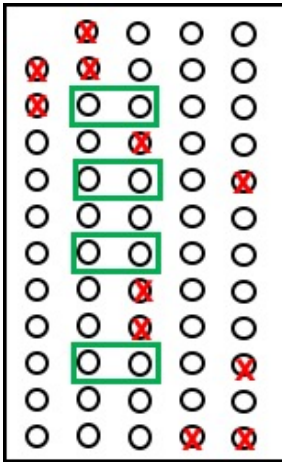
The recording framework allows me to have the motion capture and EMG signals synchronized and ready to use in Matlab. The EMG processing is the same for both preliminary studies, and it consists of a pre-processing followed by a features selection and extraction of the EMG data. During the realization of the recording, some electrodes can slightly disconnect from the skin, causing an infinite electrode-skin impedance, or, the connection between the electrodes and the acquisition system cannot work, due to broken channels. In both scenarios, the unavailability of these signals is caused and these data are eliminated. Moreover, due to the proximity to the heart, the monopolar signals acquired are strongly affected by the EKG artifact. In order to eliminate this cross-talk source a single differential spatial filter between each adjacent electrodes is applied.

Spatial filter evaluates the linear combination of the muscle activity electrical potential withdrawn from two or more different skin points. Thus, a differential amplifier is the easiest spatial filter possible. They are useful to emphasize some signals source and attenuate others. Compared to the monopolar mode, the single differential is the linear combination of two adjacent electrodes of the grids and it allows to emphasize the sources that are closer to the skin. Moreover, due to its impulse response, it allows removing non-traveling components, such as DC component and common mode interference. Therefore, in this study, the EKG noise is almost eliminated with the application of the spatial filter, due to its higher spatial selection and the fact that the EKG source is almost common in each electrode. Using HD-sEMG with electrode grids, it is essential to verify the direction on which the single differential filter is calculated because it needs to be applied following the direction of the muscles' fiber. Hereafter, I refer to all the recorded channels to indicate the full number of available signals, after discarding the bad contacts and the single differential application.

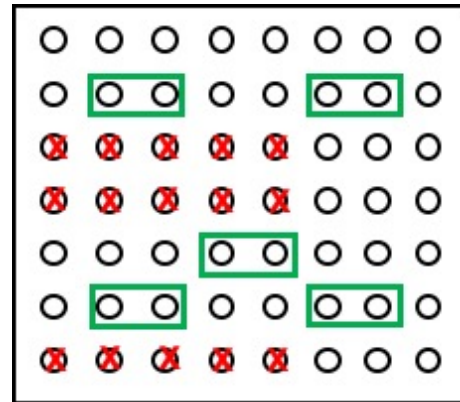
The channels are then band-pass filtered with a fourth-order Butterworth digital anti-causal filter, with a pass-band between 10–500 Hz to limit the bandwidth. The aim of the pre-processing is attenuating dc offset, motion artifacts, and high-frequency noise in order to have the highest signal noise ratio possible. A common noise source in the high density EMG recordings is due to the relative motion between the electrodes and the skin. If an electrode is moved or the skin is stretched, the distribution of charge at the electrode-skin interface is disturbed. This causes a large differential signal detected by an electrodes pair, which is indicated as motion artifact. Unfortunately, due to the high dynamicity of the required protocol tasks, some of the channels show strong motion artifact, which sometimes completely cover

the muscle activation. The cause and the consequence of this problem will be better analyzed and explained in paragraph 5.6 when the results of the preliminary studies are analyzed.

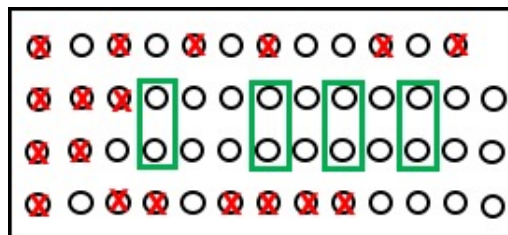
On one hand, the large number of channels available with the HD-sEMG is obviously useful, because it allows seeing more information than a bipolar acquisition. On the other hand, for a Neural Network application, the amount of channels present will require an enormous computational cost. Therefore, since the grid's inter-electrode distance is 8 mm, signals from adjacent channels are highly correlated. For this reason, I execute a dimensionality reduction process of the available data via features selection. Firstly, a channel selection of the available EMG channels is made and showed in figure 5.4. The choice of the selected electrode is based on the spatial distributions of the grid's electrodes, taking into account the presence of the unavailable or noisy channels. The signals from the selected channels are then full-wave rectified and low-pass filtered with a second-order zero-lag Butterworth digital filter, the cutoff frequency at 5 Hz, to obtain the muscle activity envelopes. The so extracted envelopes is the first selected feature for the Neural Network input. In addition to channels selection, the representations of the EMG in the principal component space, extrapolated with Principal Component Analysis (PCA), is selected as the second EMG feature. The PCA is a blind source separation technique that uses an orthogonal transformation to convert a set of possibly correlated variables into a set of uncorrelated linear variables. Thus, it allows estimating the signals' source that contains the maximum energy in the original data. The PCA is applied to the muscle activity envelope in two different ways. Firstly, I extrapolate the principal component from the envelope of the whole amount of selected channels together. Fifteen principal components are sufficient to describe the 95% of the total variance in both studies. Secondly, I calculate the principal components from the selected channels of every single matrix, taking the first three principal components because sufficient to describe the 95% of the total variance. This second principal component analysis is done to study the correlation between every single muscle and the kinematics and it is done only in the first pilot.



(a) The grids placed above the ascending and descending Trapezius. The noisy and deleted channels together with the selected are indicated.



(b) The grids placed above the Erector Spinae. The noisy and deleted channels together with the selected are indicated.



(c) The grids placed above the anterior and posterior Deltoid. The noisy and deleted channels together with the selected are indicated.

Figure 5.4: The channels selection made in all the placed grids. The red crosses indicate noisy and eliminated channels. The green rectangles indicate the selected channel for the features extraction.

The described feature selections are chosen from a literature review of myoelectric prosthetic control [6] [14]. The aim of both preliminary studies is to understand the best muscles' selection for the control purpose, that is why I chose two features based on the amplitude or energy of the signals and not others. In the end of the explained processing, the selected features are ready for the Neural Network inputs and estimation. The selected feature allows me to reduce the number of channels from 382 and 320, respectively first and second pilot, to 60 and 42 muscles activity envelopes channels or 15 principal components, without losing information from the recorded EMG data. Moreover, thanks to it, the neural network training will have a largely reduced computational cost.

5.5 Estimation of Lower Limb Kinematics from the EMG features

The estimation of the measured angles joint from the EMG features selected is done with a Neural Network architecture, thus use to regress the joint kinematics from the muscles' activity information. The EMG signal is known, in the literature, to be associated to the force produced by the muscle. The forces produced by the muscles acting on the body segment joint determining the motion of them. Therefore, a well-defined relationship between the position of a body segment and the force that moves it is present. We thus assume that the Neural Network can learn the relations between the EMG and the force and the successive force-position. Moreover, differently from the precedent cited study, I assume that the Neural Network can learn the associations between muscle activity and the kinematics of body segments not directly connected to the detected muscles, but associated with it for the consequence of the considered motion. I use for the regression a static Multi Layer Perceptron artificial NN, due to its simple architecture and to the fact that I was not certain to succeed in finding the aforementioned association in the begging of the thesis. A description of the Neural Network is shown in chapter 7, where the same architectures are used for the main study of the dissertation.

Three different MLP architectures are tested for each different input group, which are four due to the features selection made. This is done to find the best MLPs architecture, if exist, and because sometimes different architectures can produce completely different results. All the MLPs have one hidden layer with a number of hidden neurons varying between 5 and 15, for a PCA input, and between 10 and 20 for the channel selection input. The neurons in the hidden and output layers had a sigmoid and a linear activation function, respectively. During the training, the estimation error is monitored to evaluate the presence of overfitting. It is required for each MLP architecture to learn the association between the EMG features and only one angle joint at a time. This means that six different Neural Network, with the same architecture, are trained to estimate the six different lower limb degrees of freedom. The MLPs are trained using the Levenberg–Marquardt back-propagation algorithm. The realization of the architectures, the NN training, and the NN test are done in Matlab. A four-fold cross-validation procedure is used to evaluate the MLP performance. Three out of the four repetitions of the sitting task and eight out of ten repetitions of the walking task are used for training/validation data set, whereas the others are used for the test set and thus to evaluate the behavior of the MLP in presence of novel inputs. The detail of the Neural Network architecture used and of the data set realization will be described in chapter 7 when the main study is explained.

I am interested in assessing if a regression is possible and, in the positive case, how accurately each single DoF is estimated from the different input. Therefore, the performance of the MLPs in the estimation of each angle is evaluated through the coefficient of determination (R^2) and the mean relative error (rE). The network output is low-pass filtered at 2 Hz to match the frequency content of the network target, figure 5.5. Such a cutoff frequency may appear low, compare to the kinematics one. Preliminary tests were done limiting the kinematics bandwidth differently at 5 Hz, but with it, I obtained the best matching of the target power spectral density.

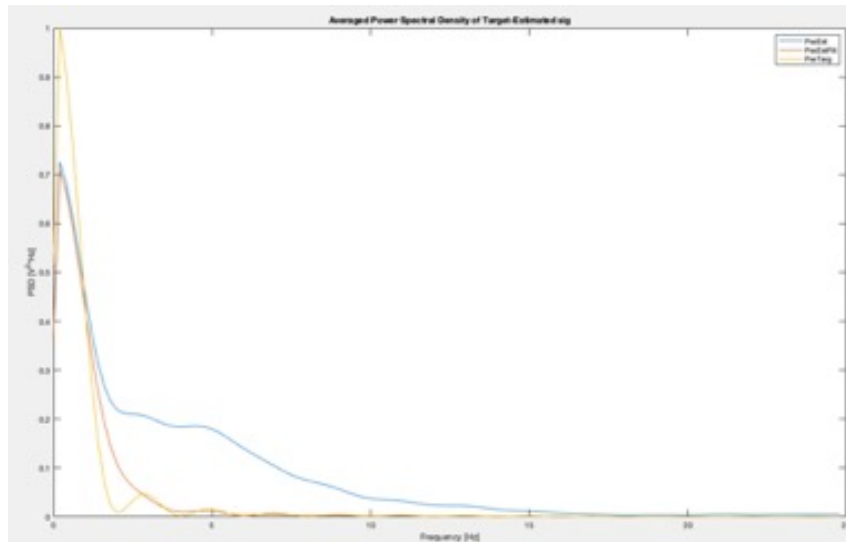


Figure 5.5: Power Spectral Density (PSD) of one of the calculated angles' joint, superimposed to the PSD of the MLPs output and the PSD of the filtered NN output. It is evident how the filtered output better matches the frequency content of the target.

The outcome results allow me to understand the strength of the relation between the selected muscle and the monitored motion or to evaluate new EMG grid placement and configuration in case of bad results. To sum up, the NNs are trained firstly with the channels selected and the principal components from each matrix and tested. Then, the training is done with all the channels selected and the principal component extracted from all the channels.

5.6 Preliminary Study Results and Analysis

In this paragraph, the results of both the preliminary studies are shown and explained. Firstly, I will analyze the results of the first pilot. Starting with the results obtained from the single matrix features as input and followed from the overall channels used together. Then, the decision made on these results are explained and the follow up for the second preliminary study are shown. Thirdly, the results of the second pilot and the choice made on it are described and lastly, an analysis of the whole results is made in order to explain the decision of moving to another acquisition system for the primary study.

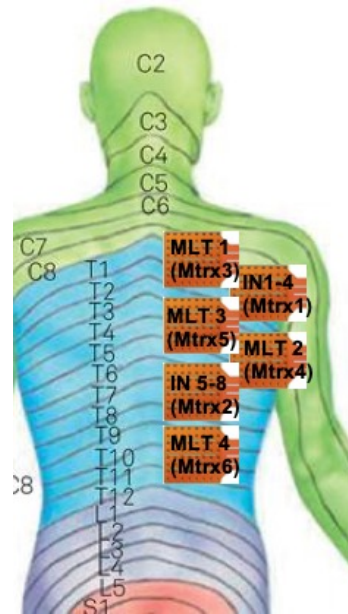


Figure 5.6: A representation of the grids placement for the first preliminary study. It also show the position of each matrix related to the innervation level. The will of detecting signals above the T12 is shown.

The grids' placement of the first pilot, shown in 5.1, is summarized in figure 5.6. In the beginning of the study, the kinematics and the extracted envelope are visual analyzed, in order to recognize if a precise muscles' activation pattern occurs during the requested movements, as shown in figure 5.7. Due to the high number of EMG channels available, an average envelope from all channels of each matrix is used to have an overall activation map and it is superimposed to a calculated anatomical' angle. From this initial analysis is already possible to get some useful information about the realized grid's placement and setup. It is clear from figure 5.7, that with this grid placement the activation pattern is positively concurrent on the kinematics change but negatively almost the same for each matrix. Moreover, for the matrix placed laterally, the signals are highly attenuated compare to the other and sometimes the activation is not present. These problems are probably due to the presence of the scapula immediately under the upper lateral grid and to the high fat layer on the lower later grid. This visual analysis already shows that a change in the grid placement may be necessary, because of the data redundancy and of the lack of information. Due to the averaged technique used, that highlights the common part in the signals, the heart-beat peaks are clearly present and recognizable in the measure. Besides, as shown in figure 5.8, a clear problem of motion artifact in some electrode recording is often present, due to the pending cables oscillation. This noise is occasionally present in this kind of acquisition but not that often as in this study. This noise causes the elimination of a huge number of channels from the grids, especially for the electrodes in the corner of them. In the first place, a better bandage and fixation of the grids is usually sufficient to solve the problem. Unfortunately, I will show that this is not the case.

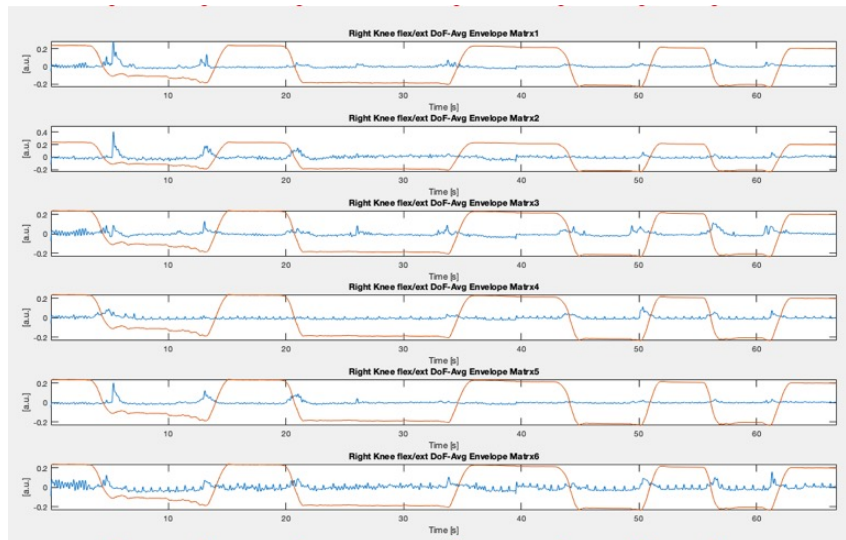


Figure 5.7: In blue the averaged muscle activation envelope and in orange the right knee flexion/extension angle calculated. Both signals are normalized in amplitude to allow a common scale. The reader notices the concurrence between the muscles' activation and the change in the angles. Moreover in the 4th and 5th row is evident the presence of EKG artifact in the envelopes.

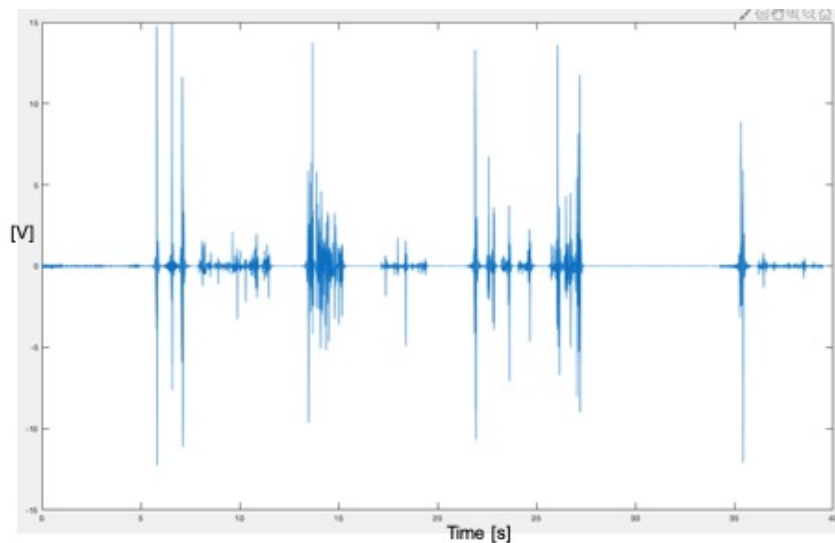


Figure 5.8: An example of heavy motion artifact present in the EMG recorded. The visible peaks are three order greater than the muscle activation and thus completely cover it. This reported signal is unusable and deleted.

The overall results of the MLP tests with the channels selection from each grid as input are now analyzed. Group data are represented in figure 5.9, which shows the average coefficient of determination (R^2) and the mean relative error (rE) between the measured and the estimated joint angles for the six DoF and for the six different matrices used as input. It is clear from the obtained R^2 and rE value, that a good association with the lower limb movement is possible only with matrix 2, placed between T7-T9, and Matrix 3, placed between C7-T3, which are mostly above the erector spinae group the Trapezius muscles respectively. The best R^2 , obtain for the

average Hip left angles estimation, is anyway not good enough to declare that an estimation is possible only with this input. Moreover, the average 4-fold rE obtained from all the matrix is always around 10% of the range of motion, with peaks of 25% as is visible from the standard deviation. These results are confirmed from the group data rrepresented in figure 5.10, which shows the average R^2 and rE for the six DoF with principal component extracted from each matrix as input. The overall results are slightly better than the previous and they confirm matrix 2-3 as the two with the best performance. Unfortunately, they also confirm that a good estimation of the joint angles from a single matrix is not possible but that a relationship could exist between some of the muscles covered and the lower limb motion.

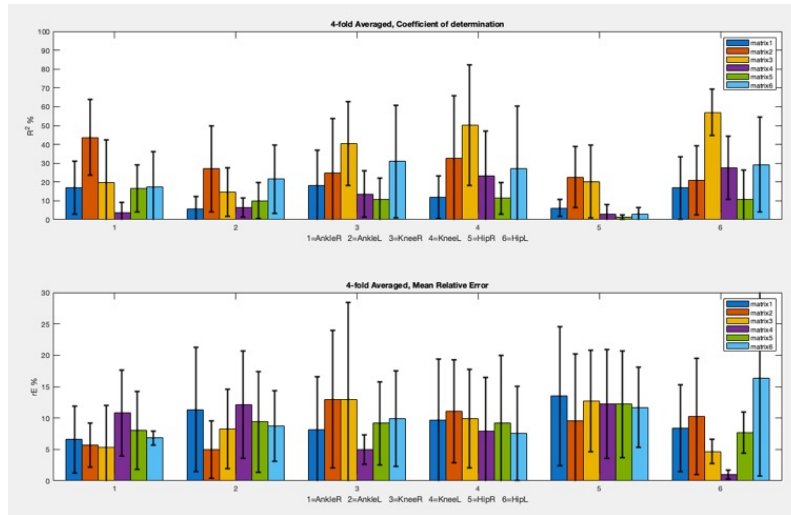


Figure 5.9: The average 4-fold R^2 coefficient, on top, and the average 4-fold rE, on the bottom, for the six angles joint estimation and for the six different channels selection envelopes from each matrix used as input. Matrix 2-3 shows the best results of this group data.

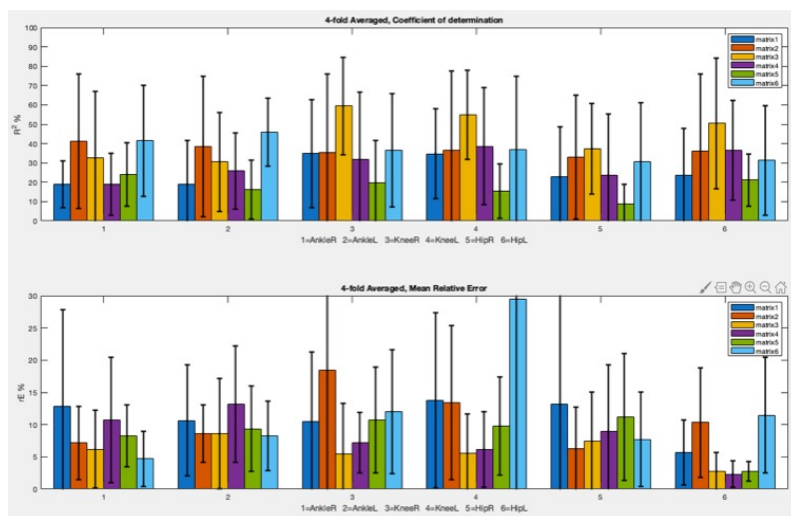


Figure 5.10: The average 4-fold R^2 coefficient, on top, and the average 4-fold rE, on the bottom, for the six angles joint estimation and for the six different principal components from each matrix used as input. Matrix 2-3 shows the best results of this group data.

The certainty of the need to drastically change the grids' placement is given from the group data of the six DoF estimation, obtained from the overall channel selection and principal components as input to the NN. These results are respectively shown in figure 5.11 and 5.12. Despite the already bad results obtained from every single matrix, adding all the recorded information for the estimation causes even worst results. The average R^2 for all the DoF estimated is the 20% of correlation and the average rE is the 15% of the range of motion for either inputs. These results do not allow to define that a relationship between the muscles activation and the analyzed motions exists.

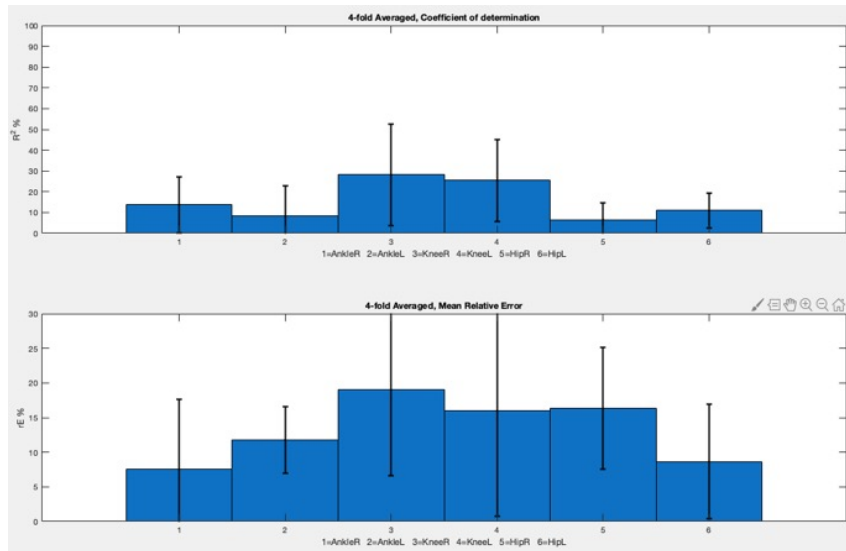


Figure 5.11: The average 4-fold R^2 coefficient, on top, and the average 4-fold rE, on the bottom, for the six angles joint estimation obtained with the channels selection envelopes as input.

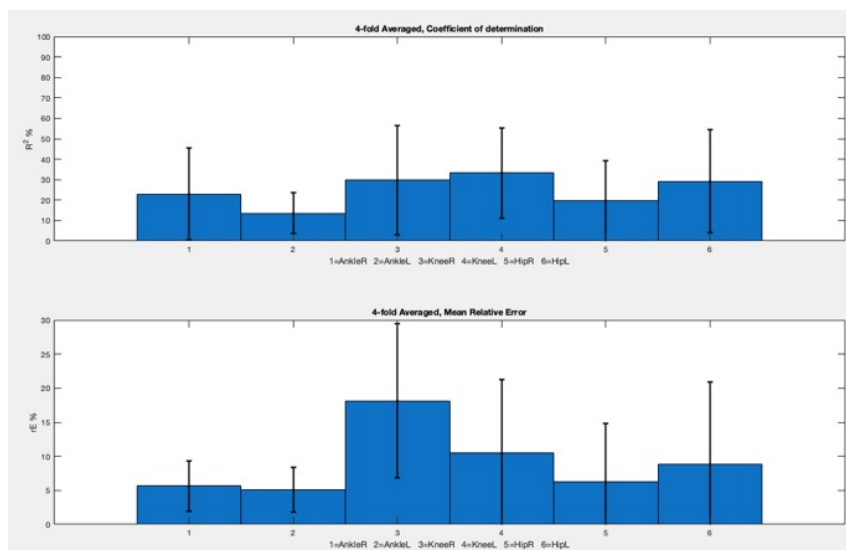


Figure 5.12: The average 4-fold R^2 coefficient, on top, and the average 4-fold rE, on the bottom, for the six angles joint estimation obtained with the principal components as input.

In the end, resuming the information obtained from the first pilot, the matrix 2 and 3 placed between T7-T9 and C7-T3, respectively, have shown a possible strong association with the lower limb kinematics. This pilot has also shown the necessity of taking major care in the grids fixing and placement. Moreover, the idea of covering as more surface as possible of the back to obtain the maximum information has proven to be wrong.

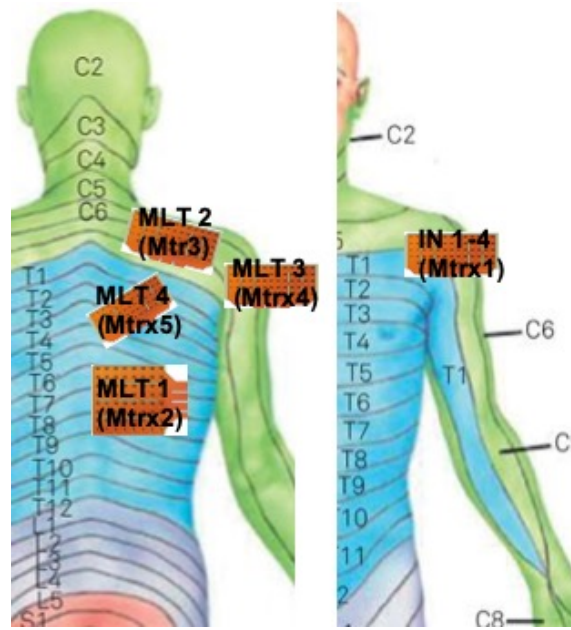


Figure 5.13: A representation of the grids placement for the second preliminary study. It also show the position of each matrix related to the innervation level.

The second pilot grids' placement is summarized in figure 5.13, which shows the choice of maintaining the two best grids of the first pilot. Both are only lightly shifted from before, in order to have a more specific muscle targeting. Group data of the six DoFs estimation for the principal components input from all the matrix together are represented in figure 5.14. The average coefficient of determination and the mean relative error between the measured and the estimated joint angles obtain from the 4-fold cross-validation of the best architecture tested is shown. The obtained results are basically the same of the first pilot in terms of R^2 and rE. The reason for these bad estimations can be due to the redundancy of information between each principal component extracted. Despite the showed results, the reason of pursuing this setup in the final study is given from the results obtained with the channels selection input. The group data of the best architecture tested with the channel selection input are shown in figure 5.15. It is clear and evident a big improvement in terms of average 4-fold R^2 and rE compare to every other aforementioned result. They show an average R^2 of 50% between all the joint, with peaks of 80% of correlation for the left hip and knee angles estimation. Moreover, the average rE is largely decreased, passing from an average of 15% of the previous test to an average between all the joint of 5% of the range of motion. An example of the best angles' estimation obtained is shown in figure 5.16, within the bottom of the figure the average signals from each different matrix. From these results is clear that an association between the activity pattern of the selected muscle and the lower limb motion is possible.

In addition, it is necessary to take into account that the motion artifact problem is still present in some of the EMG signals used for the estimation. Therefore, even better results are possible from these muscle selection, because the average 4-fold R^2 and rE values reported consider also some bad estimation caused by the noise presence. This can also be the reason for the worst estimation made by the PCA, in which the sources with higher energy are highlighted. The thus obtained results from the channel selection input open the chance for a stronger intuitive myoelectric controller if the motion artifact problem can be overcome.

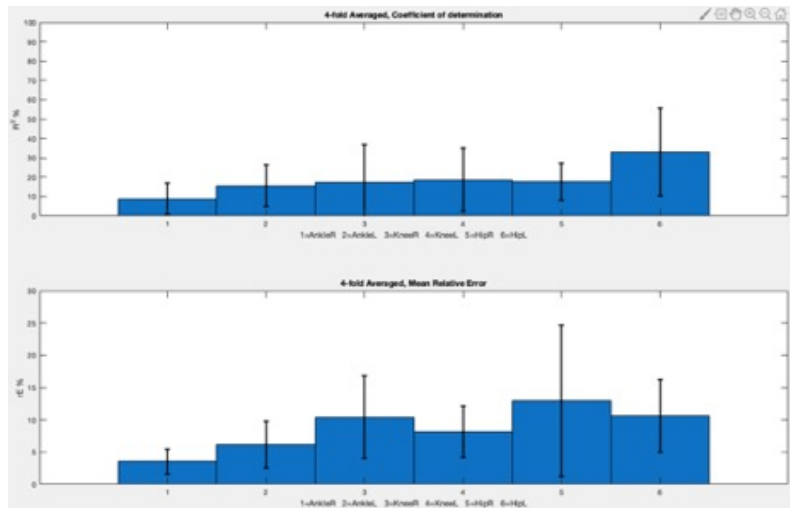


Figure 5.14: The average 4-fold R^2 coefficient, on top, and the average 4-fold rE, on the bottom, for the six angles joint estimation obtained with the principal components as input.

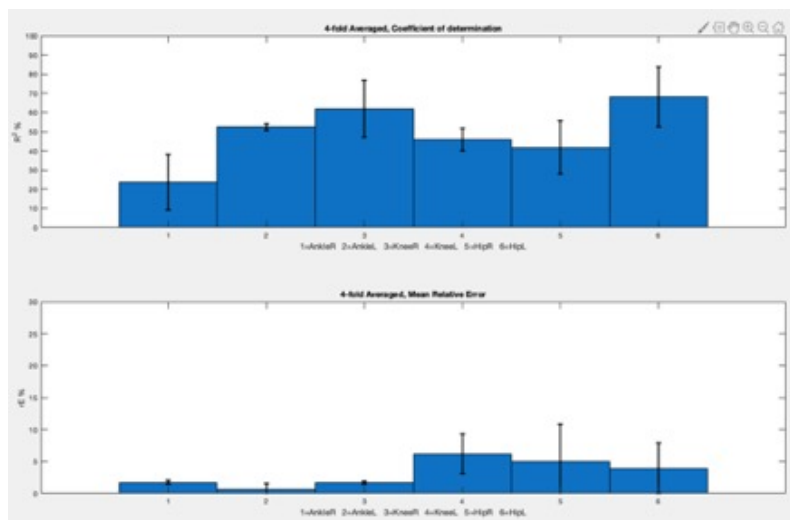


Figure 5.15: The average 4-fold R^2 coefficient, on top, and the average 4-fold rE, on the bottom, for the six angles joint estimation obtained with the channels selection envelopes as input. The average R^2 between all the joint is 50%, with peaks of 80% of correlation for the left hip and knee angles estimation. the average rE is of the 5% of the range of motion between all the joint.

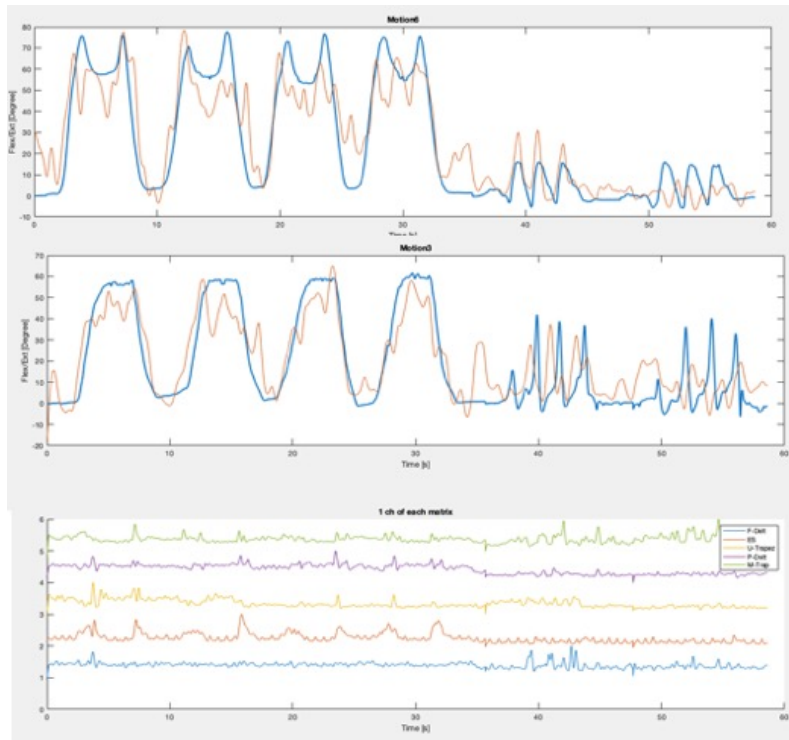


Figure 5.16: In the two top rows, the blue signals are the target angles and the orange the obtained estimation from the MLPs with the envelopes features. In the bottom rows, the concurrently average envelopes from each matrices. Notice the activation pattern present between the envelopes and the angles change above it.

Chapter 6

Bipolar EMG Recording and Processing

This chapter covers the description and the utilization of the wireless bipolar acquisition system used in ten able participants' study. Firstly, I introduce the main features of the system and the reasons for switching from the HD-sEMG. Then, I focus on the utilization of it in the experimental protocol, making a description of the bipolar electrode placement. Finally, I describe the EMG signals processing and feature selection made for the subsequently angles estimation.

6.1 Feature and Advantage of the FreeEMG-1000 Acquisition System

The FreeEMG-1000 is a surface electromyography device with eight wireless probes. This acquisition system is thought to realize dynamic analysis of muscles' activity. It is a 4G technology device and this is its major advantage for the study objective. Indeed, signal accuracy in absence of wires, together with lightness and reduced size of the probes are features that enable users to perform analyses of any type of movement. The system communicates with a PC through the supplied USB receivers and can manage up to 20 probes simultaneously. Moreover, the system is developed and integrate with the Smart-Dx motion capture system used in the study for the kinematics recording. The receiver's connection to the motion capture station allows to concurrently record both information from the same PC. Thus, the system is perfectly suited for the experimental protocol objective, without other integration needed. Each probe is equipped with internal memory to ensure uninterrupted recording in case of temporary connection loss and to allow for acquisitions in wide spaces and open fields. The probes are directly attached to snap connected pre-gelled electrodes, with no need for additional fastening; which means, no skin preparation is necessary. The probe has a 16 bit resolution with a sampling frequency of 1 KHz. A gain of 1000 and a high pass filter at 10 Hz are applied to each recorded signal from the probe's hardware. LiPo battery, rechargeable with proprietary charger are mounted in each probe, allowing over 6 hours of continuous acquisition. A weight of about 13 grams, battery included, and extremely reduced dimension, allows the subject to easily forget the presence of the devices on the skin. The system and the probes are shown in figure 6.1.



Figure 6.1: The FreeEMG-1000 a wireless surface bipolar EMG Acquisition System by BTS-Bioengineering.

The advantages and disadvantages of this system are evaluated, comparing the aforementioned system's features with the HD-sEMG used during the preliminary studies. Firstly, the huge disadvantage is the enormous loss of information, due to the not high density EMG recording. Indeed, HD-sEMG is mostly used, in the research field, for proportional control. On one hand, the variability and quantity of information available from HD-sEMG are thus not even comparable with the described wireless system. On the other hand, in order to make the most of the HD-sEMG, different and more complicated feature selection for the control purpose needs to be studied. This study aims to find a relation between the back muscle and the lower limb kinematics. Moreover, the goal is to understand if the possibility of proportional control exists. Therefore, a comparison of different feature selection is not even thinkable yet. During chapter 5, the huge amount of channels eliminated, due to motion artifact, have been shown and analyzed. This noise source is due to the flat cable connection between the acquisition system and the placed grids and to the oscillation of those cables caused by the high dynamicity of the required tasks. Analyzing these problems and concurrently keeping in mind the aforementioned features of the Free-Emg system, the possible advantages of switching to the wireless device are clear. Moreover, if the researched relation exists between the selected muscles and the lower limb motion, it will be possible to obtain a controller also from a minor number of data. Thus, the lack of information on the Free-emg system should not be the cause of missing the relationship or find a control strategy. Comparing the advantages and the disadvantages, keeping in mind the aim and the stage of this study, the Free-Emg seems the correct choice for the continuation.

6.2 Electrode Placement

The bipolar electrodes placement for the study on ten able participants is based on the good results obtained in the last pilot. The Free-Emg has eight bipolar probes available. Therefore, the first five probes are placed in order to target the same muscle of the last preliminary study, which are ascending and descending Trapezius, anterior and posterior Deltoid and Erector Spinae. From the pilot, it is clear the necessity of realizing an adaptive filter for the EKG interference in the electromyographic signals. Thus, the sixth is placed above the heart, in order to record a derivation of the electrocardiograph. Precisely, placed in the left side fifth intercostal space, correspondent to the fifth precordial leads derivation. In addition, to use the entire number of available probes, I place the 7-8th probes targeting the internal and external Obliques Abdominal.



Figure 6.2: The bipolar EMG setup for the final study. Notices the less complexity than the HD-sEMG and the lack of connective cables. The probes are placed targeting ascending and descending Trapezius, anterior and posterior Deltoid, internal and external Obliques Abdominal and Erector Spinae

The choice of these two additional muscles targeted comes from the literature review made in the preliminary study, chapter 5. Moreover, the innervation zone of these muscles is above the required minimal lesion height for an SCI person to, unfortunately, become paraplegic. Differently from the HD-sEMG where the grid's placement objective is to cover as max as possible the muscle's belly, bipolar electrodes need to be placed in a more precise position avoiding the muscle's innervation zone and placing the probes between it and the ligament. The correct electrodes positioning is done in this study following the SENIAM location directive [23]. The

precise description of each sensor is explained and described in Table 6.1 and an example of it is shown in figure 6.2.

Targeted Muscle	Sensor location and Placement
Erector Spinae	At 2 finger width lateral from the proc. spin. of L1-T6
ascending Trapezius	At 2/3 on the line from the trigonum spinea to the T8.
descending Trapezius	At 50% on the line from the acromion to the spine on vertebra C7.
anterior Deltoideus	At one finger width distal and anterior to the acromion.
posterior Deltoideus	In the area about two finger breaths behind the angle of the acromion.
internal Obliques Abdominal	In the area about two finger breaths medial to the anterior superior iliac spine
external Obliques Abdominal	At 50% on the line from the lower edge of the eighth rib to the anterior superior iliac spine

Table 6.1: The bipolar electrodes placement used in the experimental protocol. It follows the location recommendation from the SENIAM.

When the correct location is found the two electrodes are placed on the skin with an approximate distance of 20 mm. The inter-electrode distance is guaranteed from the fixed diameter length of the pre-gelled electrodes. Lastly, when all the probes are correctly placed and connected, is required to the subject to perform an isometric contraction of each targeted muscle. This operation is done to check the correct placement and the detected signals of each probe.

6.3 EMG Processing

The electromyographic signals acquired with the bipolar device are pre-processed in the same way as the HD-sEMG. The eight bipolar signals thus are bandpass filtered with a 6th order Butterworth between 10-500 Hz. Differently from the previous pre-processing where the same filter was already applied from the acquisition system, with this device this filtering action is essential to limit the signal in the EMG bandwidth. Moreover, differently from the preliminary study, the digital filters are always causal, in anticipation of a real time application of the setup where anti-causal filters are not applicable. This creates a possible phase displacement problem due to the filters' application. For this reason, the filter applied to the motion capture signals and to the EMG has the same order and type. A previous filtering action was tried with a finite impulse response (FIR) filter, because of its linear relation between the phase displacement and the order of it. Fortunately, the Butterworth filtering phase displacement doesn't cause a miss synchronization of the two signals, moreover, the FIR filter tested has a minor attenuation in the

stop-band, which causes a not perfect limitation of the bandwidth of the signals. Then, a Notch filter at 50 Hz is applied to be sure to reject the network interference.

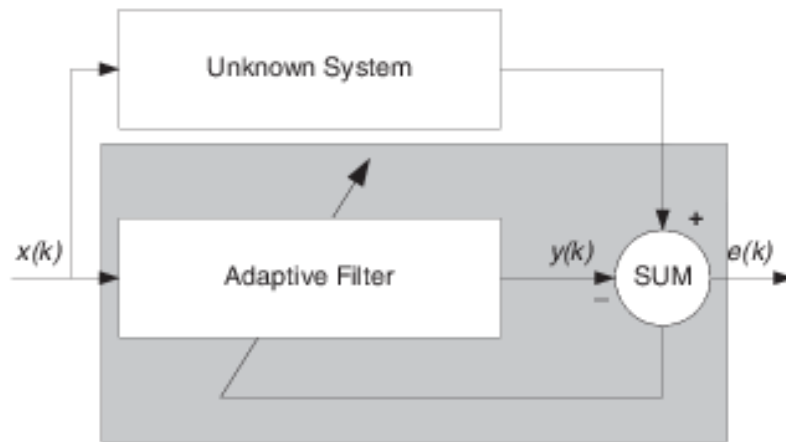


Figure 6.3: The Recursive Least Square (RLS) Adaptive filter algorithm. Where the Adaptive filter box calculate and update the filter's coefficient. x is the electrocardiographic signal, y the signals estimate from the minimization algorithm and e is the filtered signals.

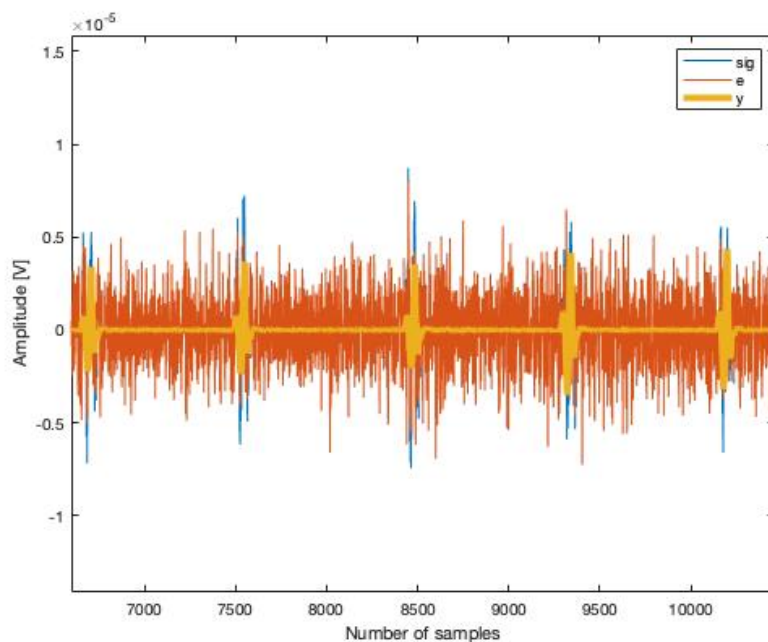


Figure 6.4: Example of the original EMG signal superimposed to the signal to eliminate, y , estimated from the adaptive filter and the filtered signal, e .

Lastly, a Recursive Least Square (RLS) Adaptive filter is applied to attenuate as much as possible the electrocardiography artifacts present in some channels. The RLS algorithm, on which this filter is based, has an increased complexity and higher computational costs compare to other adaptive filters but, at the same time, it is

more reliable. This filter is based on a minimization problem of a weighted linear least square cost function. The coefficients of the filter are thus found from the minimization of the cost function relating to the input signals, which is the EKG. Figure 6.3 shows the explained process. For this reason, an acquisition of the EKG signals is necessary to adapt the coefficients of the filter. Before giving the EKG measure in input to the RLS algorithm, the signal is filtered between 0.005-100 Hz in order to limit the signal bandwidth to the one of the electrocardiography. The adaptive filter always attenuates the EKG interference present in the bipolar recorded signals but is not always able to completely reject it. Figure 6.4 shows an example of the application of the adaptive filter where the noise is not completely removed.

The filtered seven bipolar channels are then processed to realize a feature extraction. The feature selection of the EMG is based on the preliminary study. The redact number of channels does not need a dimensionality reduction operation, a PCA application will then be useless. Besides, the best results in the preliminary pilots studies are obtained from the envelope of the channels' selection. Lastly, as already discussed, the thesis aims to find a relation that allows the lower limb estimation from the selected muscles' activity. Therefore, an evaluation of the different performance obtained from different EMG features is left for future studies. The only EMG features selected and used are thus the muscle activity envelopes of each bipolar sensor. In order to calculate it, the signals are full-wave rectified and low-pass filtered with a second-order zero-lag Butterworth digital filter with a cutoff frequency at 5 Hz. The seven input features for the Neural Network estimation are thus extracted.

Chapter 7

Estimation of Lower Limb Kinematics

This chapter covers both different regressions of the joint angles tested. Firstly, a brief introduction about some basic Neural Networks knowledge is given to the reader. Then, the feed forward neural network used for the regression purpose in this thesis is shown and the realized data set for the training of it is described. Lastly, the different architectures tested for each different input features are explained, together with the parameters used to evaluate the estimation results.

7.1 Neural Networks

This paragraph only aims to introduce to the reader, simplistically, some basic concepts regarding Neural Networks. It must not be taken as a specific and in-depth explanation of the Neural Networks theory, for which the reader has to refer to other apposite texts. The only objective of this paragraph is to briefly describe the useful and essential topics needed to understand the neural network architecture used in the following of the chapter.

In this study, the Neural Networks are used to estimate the hip, knee, and ankle flexion/extension angles joint from the electromyographic features. An artificial neural network is a massively parallel distributed processor that has a natural propensity for storing experimental knowledge and making it available for use. It resembles the brain in respects of knowledge, which is acquired through a learning process, and of inter-neuron connection strengths, known as synaptic weights, which are used to store the knowledge. When we talk about a Neural Network we actually have three basic elements the Neurons, the Architecture, and the Learning algorithm.

Firstly, the Neurons are the processing elements and they are characterized by an activation function. Neurons can use any differentiable transfer function to generate their output and the type of them change according to the network's implementation. The simplest network is the Perceptron [22]. It is formed by a single neuron with various inputs connected and it allows to classify only in two classes. Figure 7.1. The Neuron takes the value of the variables in inputs from the environment by means of weighted connections. The weighted sum is transformed by the activation function and the output is returned as network output. Another kind of neuron, used in this dissertation, is the one based on the sigmoid activation function. Differently, from before, the sigmoid function can have any value in the range between 0

and 1 as input, and a small change in the weight causes a small change in the output.

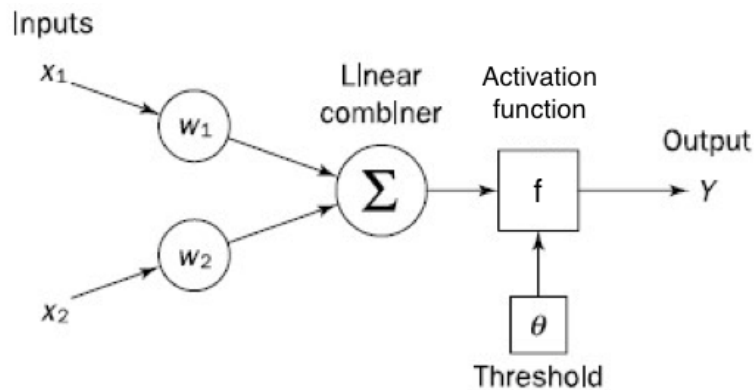


Figure 7.1: An elementary Perceptron with 2 inputs. Each input is weighted with an appropriate weight w . The sum of the weighted inputs and the bias forms the input to the transfer function f . The threshold is present to classify the output as integer, e.g. if greater than the threshold means class one.

Secondly, the architecture defines the network structure, which is the number of artificial neurons in the network and their inter-connectivity. The architecture of the aforementioned Perceptron is the simplest possible because formed of one only neuron. To overcome non linear problems, such as the one in this work, we need multi layer neural networks. These networks are composed of several neurons connected among them and organized in layers. This NNs thus have a certain number of neurons organized in input, hidden and output layers. The input layer is composed of neurons that receive input directly from the environment. The neurons in the output layer, instead, produce and return the final outputs to the environment. Lastly, the neurons in the hidden layer cope with the elaboration of the data. Moreover, depending on the different interconnections' ways between neurons, a Neural Network can be differently classified. Therefore, multi layer NN are defined feed forward when the connections between neurons are only made forward and do not form a cycle.

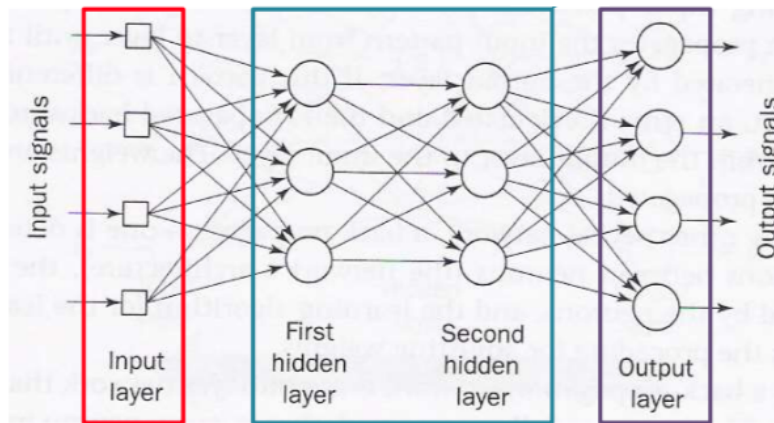


Figure 7.2: A Feed Forward Multi Layer Neural Network. Highlighted in red the neurons of the input layer. In purple the neurons which form the output layer. The two hidden layer present are, instead, highlighted in blue, both composed by three neurons.

Last but not least, the learning algorithm is the procedure used to perform the learning process which works by modifying the synaptic weights of the network. The learning process can be carried out in a Supervised and Unsupervised way. The aims of the study require a Supervised learning process which means that a training set consisting of input vectors and the corresponding desired outputs are provided to the NN. Supervised learning thus adjusts the synaptic weights accordingly to the error between the network outputs and the targets of the NN. The developed learning algorithms are mostly based on the backpropagation theory. Initially, in the backpropagation algorithm, a training input is presented to the network input layer. The network, then, propagates it from layer to layer until the output is generated by the output layer. If the estimated output is different from the target, an error between them is calculated. Then, this error is propagated backward from the output layer to the input ones. During the error back propagation, the weights of each interconnection are modified.

7.2 Regression with Feed Forward Neural Networks

The estimation of the measured joint angles is done with a Neural Network (NN) from the EMG features selected. The NN is thus able to regress the joint kinematics from the muscles activity information. The EMG signal is known, in the literature, to be related to the force produced by the muscle. The forces produced by the muscles acting on the body segment joint determining the position of it and the motion of the segments. Therefore, a well-defined relationship between the position of a body segment and the force that moves it is ensured. In this thesis, I assume that the Neural Network can learn the associations between the EMG features and the force and the successive force-position relation. Moreover, I assume that the Neural Network can learn the relationship between muscle activity and the kinematics of body segments not directly connected to the measured muscles, but associated with it for the consequence of the considered motion. Feed forward multi layer perceptron (MLP) neural networks are used for the angles joint regression's purpose.

This kind of network often has one or more hidden layers of sigmoid neurons followed by an output layer of linear ones. Multiple layers of neurons with nonlinear transfer functions allow the network to learn nonlinear relationships between input and output vectors, whereas the linear output layer is most often used for nonlinear regression problems. The used NNs are thus made of an input layer receiving information from outside, one or more sigmoid hidden layers elaborating the information, and a linear output layer that returns the result of the learning process to the user. Figure 7.3 shows an example of the architecture used.

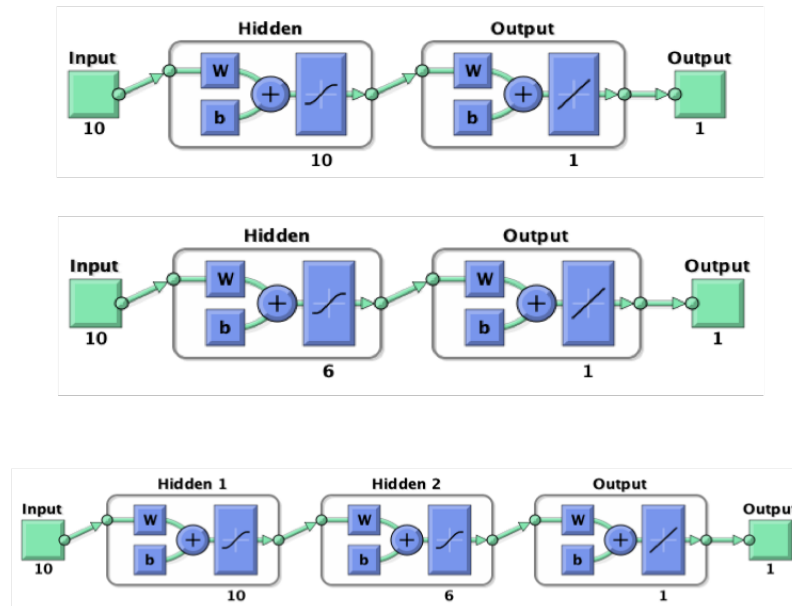


Figure 7.3: Three of the MLPs architectures tested. All of them show 10 neurons in the input layer, due to the seven EMG and three IMU inputs, and one linear neuron in the output layer. The hidden layer are respectively composed by 10 or 6 sigmoid neurons forming one hidden layer or in 10 and 6 sigmoid neurons forming two hidden layers.

The described networks are trained using the Levenberg–Marquardt back-propagation algorithm. This algorithm employs the average squared error between the network outputs and the target outputs (mse) for measuring the learning performance of the network. This means that the error between the current network output and the desired output is calculated during the learning phase and propagated backward to adjust the weights connecting the NN layers. Before the realization of the training, the weights and the biases of the network must be initialized. The MLPs are supervised networks. Therefore, for the learning process, a collection of input features and output targets is necessary, usually indicated as data set. It is generally difficult to incorporate prior knowledge into a neural network, therefore the network can only be as accurate as the data that are used to train it. It is important that the data set covers the range of inputs for which the network will be used. After the data have been collected, they need to be pre-processed, and they must be divided into subsets. The pre-process is different for each data type and consists of each already explained signal elaboration plus a normalization in terms of the mean and standard deviation of them. The normalization is done in order to improve the computational cost and the results of the training algorithm. Moreover, it is necessary

for the sigmoid neurons domain. The division of the data set, instead, consists of the subdivision of it in the training, validation and test set. which are respectively the data collection used for train, validate and test the Neural Network during and after the training procedure. The data set, in this study, is formed from the EMG, IMU and kinematics signals concurrently recorded during the progress of the experimental procedure. Then, every separated recording of the whole experimental protocol is concatenated and divided into training/validation set and test set. Three out of the four repetitions of the sitting task and eight out of ten repetitions of the walking task are used for training/validation set, whereas the others are used for the test set and thus to evaluate the behavior of the MLP in presence of novel inputs.

7.3 Estimation of 6 DoF from EMG features

Eighteen multilayer perceptrons (MLPs) are used to estimate the flexion/extension angles of the six hip, knee, ankle joints of the lower limbs. I thus use three different architectures for each different angle, intending to obtain an accurate estimation for each DoF. In this first estimation, the bipolar EMG channel envelopes are used as input features to the MLPs to estimate one of the angles as target. Even if the EMG signals are recorded only from the right side of the body, also the left lower limb angles are estimated from them. The three MLPs architectures tested for each angle have one hidden layer with a number of neurons varying between 6 and 7 or two hidden layers with a number of neurons of 7 and 6, respectively. The number of neurons in the hidden layer is selected from preliminary tests executed. The three different architectures are tested for each angle in order to evaluate how much the NN structure influences the results. During training, the estimation error is monitored, checking that is not indicating any major problems. The validation and test curves have to be similar. If the test error curve has a significant increment before the validation ones, then it is possible that some overfitting might occur. As already mentioned, the neurons in the hidden and output layers have a sigmoid and a linear activation function and the MLPs are trained using the Levenberg–Marquardt back-propagation algorithm.

A four-fold cross-validation procedure is used to evaluate the different MLP architecture performance. Cross-validation is a statistical method used to estimate the skill of machine learning models. It is commonly used in applied machine learning to compare and select models for a given predictive problem. The procedure differently divides the data set into training/validation and test set. The number of folds is chosen such that each train/test group of data samples is large enough to be statistically representative of the broader data set. When each training is done, a novel input from the test set is given to the NN in order to evaluate the performance of the architecture.

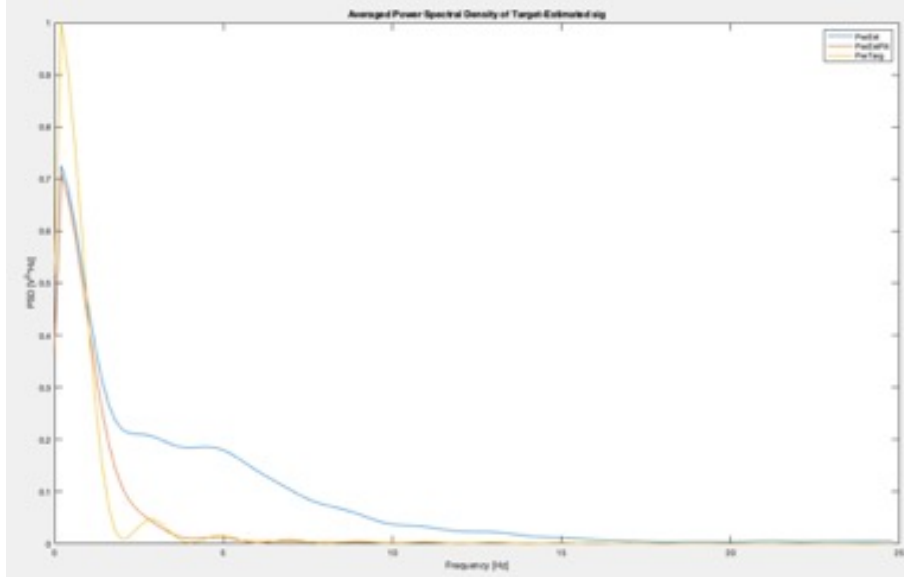


Figure 7.4: In yellow the Power Spectral Density (PSD) of one of the calculated angles' joint, superimposed to the PSD of the MLPs output, in blue, and the PSD of the filtered NN output at 2 Hz, in orange. It is evident how the filtered output better matches the frequency content of the target.

The network output is low-pass filtered at 2 Hz to match the frequency content of the flexion/extension angles joint. Such a cutoff frequency may appear really low, but for the signals collected in this study, the network target had the majority of the power in the frequency band below 2 Hz. Preliminary tests were done limiting the kinematics bandwidth to 5 Hz as is done in the pre-processing. Therefore, I further low-pass filtered data at 2 Hz. Figure 7.4 shows the power content of the kinematics and of the network output filtered and not.

Lastly, the performances of the MLP in the estimation of each angle are evaluated through the coefficient of determination R^2 and the mean relative error (rE). Which respectively are:

- R^2 , the percent variability in the actual angular values explained by the estimated values.

$$R^2 = 1 - \frac{SS_{res}}{SS_{tot}} \quad (7.1)$$

Where SS_{tot} is the total sum of squares

$$SS_{tot} = \sum_i (y_i - \bar{y})^2$$

SS_{res} is the sum of squares of residuals and f_i is the estimated vector.

$$SS_{res} = \sum_i (y_i - f_i)^2$$

\bar{y} is the mean of the observed data y

$$\bar{y} = \frac{1}{n} \sum_{i=1}^n y_i$$

- rE , the magnitude of the difference between the measured and the estimated value divided by the range of motion.

$$rE = \frac{|y_i - f_i|}{\max y - \min y} \quad (7.2)$$

These parameters evaluate the results in terms of error between the signals' amplitude, rE , and in terms of relation between the signals progress and shape, R^2 . In figure 7.5 an example of the estimation evaluation for one subject is shown. The reported R^2 and rE , used for the results evaluation, are always mean and standard deviation value from the 4-fold cross validation procedure.

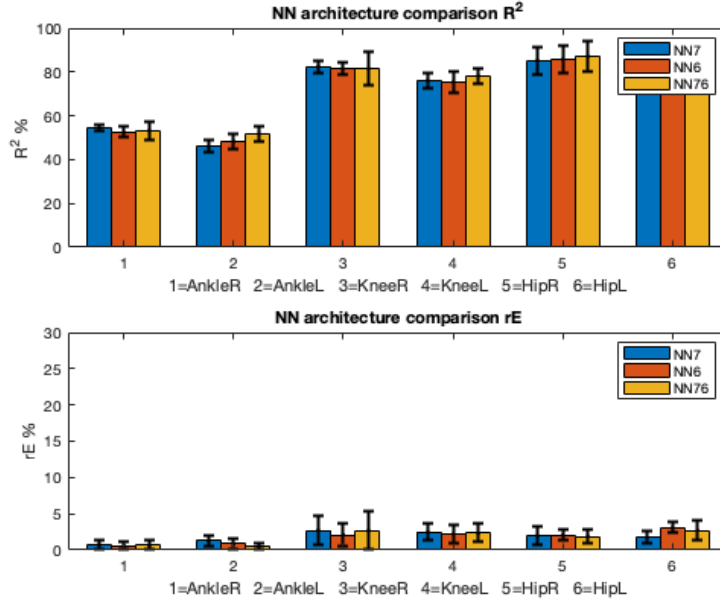


Figure 7.5: The coefficient of determination (R^2) and the the mean relative error (rE) obtained from one subject. Each group represent one estimated angle. Each bar in each group of three represent one architecture tested.

7.4 Estimation of 6 DoF from EMG and IMU features

Eighteen multilayer perceptrons (MLPs) are used to estimate the flexion/extension angles of the six hip, knee, ankle joints of the lower limbs. I thus use three different MLPs for each different angle, intending to obtain an accurate estimation for each DoF. In this second estimation, the bipolar EMG channel envelopes are used together with the tilt, obliquity, and rotation IMU information as input to the MLPs to estimate one of the angles. As before, also the left lower limb angles are estimated from the IMU data and the EMG features from the right side of the body. Three MLPs architectures are tested for each target angle; where two of these have one hidden layer with a number of neurons varying between 6 and 10 and the other one has two hidden layers with number of neurons of 10 and 6 respectively. The three different architectures are tested for each angle in order to evaluate if the architecture largely influences the estimation results. During training, the estimation

error is monitored, checking that is not indicating any overfitting problems. Therefore, the validation and test curves are continuously observed, looking that they have similar errors. The neurons in the hidden and output layers have a sigmoid and a linear activation function, respectively, and the training algorithm is always the Levenberg–Marquardt back-propagation algorithm. A four-fold cross-validation procedure is, as well as the first test, used to evaluate the three different architectures. Following the training, the test set is applied to the NN in order to evaluate the performance with novel input. The network output is low-pass filtered at 2 Hz to match the frequency content of the flexion/extension angles joint because, as in the first evaluation, the network targets have the majority of the power in the frequency band below 2 Hz.

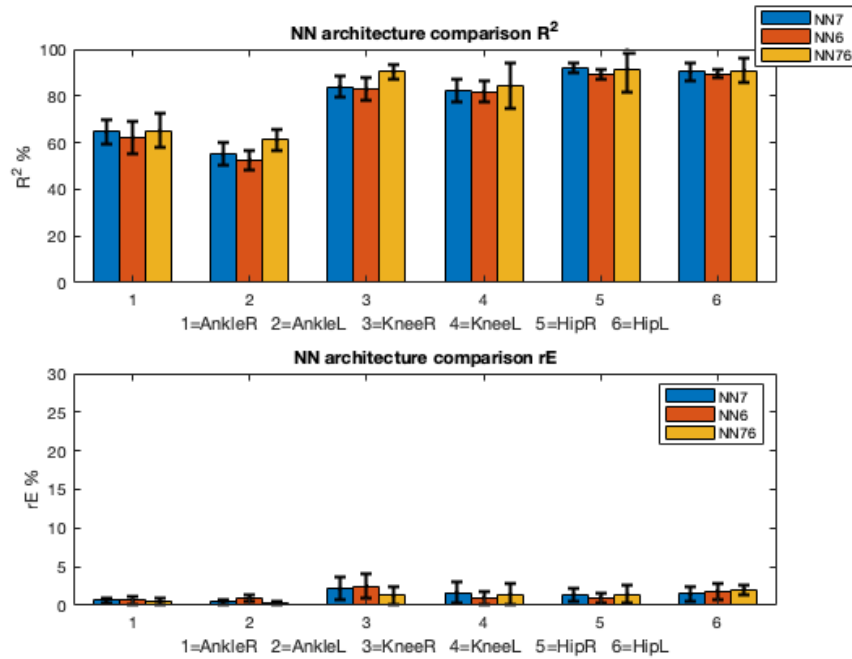


Figure 7.6: The coefficient of determination (R^2) and the the mean relative error (rE) obtained from one subject. Each group represent one estimated angle. Each bar in each group of three represent one architecture tested.

Lastly, the estimation's performances of each angle are evaluated through the coefficient of determination (R^2) and the mean relative error (rE). Described in equation 7.1 and 7.2. In figure 7.6 an example of the estimation evaluation for one subject is shown. The reported R^2 and rE are always mean and standard deviation values from the 4-fold cross-validation procedure.

Chapter 8

Results and Discussion

In this chapter, I will describe the results obtained from the execution of the experimental protocol on 10 able people. I will show the qualitative results of the regression, focusing on the difference between the estimation and the angles joint target, and the quantitative results, in terms of the subject's average R^2 and rE .

8.1 Angles estimation from EMG features

Initially, I proceed by analyzing the results qualitatively, comparing some of the target angles joint, with the predicted signals from our MLPs. Figure 8.1 shows an example of the left hip kinematics prediction which depends only on the EMG features. The reported example presents respectively two sitting/standing action followed by two walking tasks. The good performances of the networks are easily appreciable. On one hand, it is visible that the goal to find a relation between the selected muscles and the lower limb flexion/extension angles has been reached. Demonstration of that, it is the good estimation obtained and moreover the concurrency between the change in the kinematics and in the muscle activation envelopes. On the other hand, it is also clear that the estimation made with only the EMG as input is not always enough robust for stable control. Moreover, small rapid variations in the predicted signal, despite the low pass filter applied, are always present. These variations represent the larger source of error between the target and the output in every estimation. In figure 8.2 is shown an example of right hip angle joint estimation where the first two tasks in the signals are due to a sitting/standing action and the following two are due to the walking task. The sitting/standing predictions are accurate and stable as well as the gait ones even if slightly worst due to the more rapid variation of the motion.

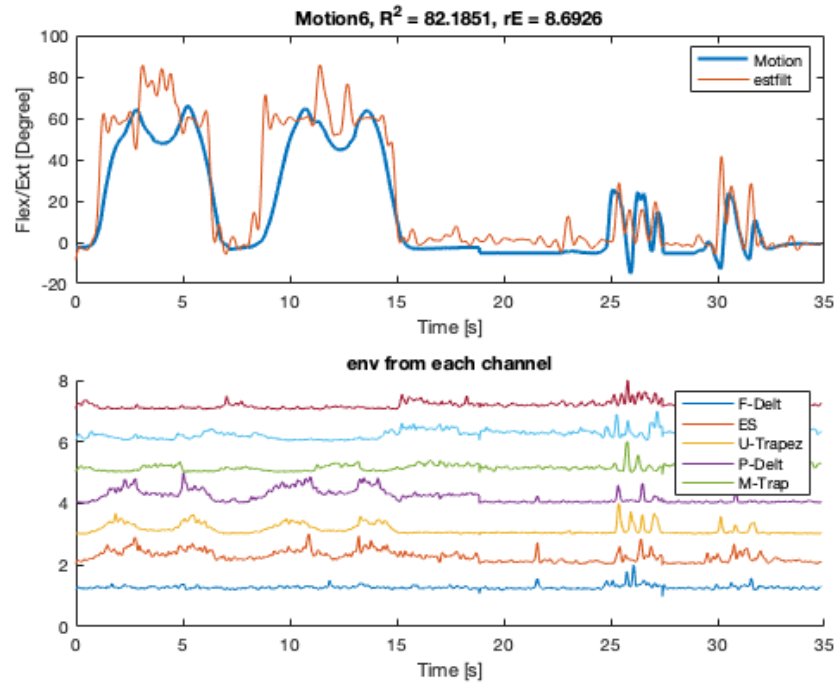


Figure 8.1: In the top, the estimation of the left hip angles, in orange, during performing of sitting/standing and walking tasks superimposed to the target signal calculated from the motion capture, in blu. In the bottom, the seven muscles activation envelopes used as input features for the Neural Networks and concurrently recorded.

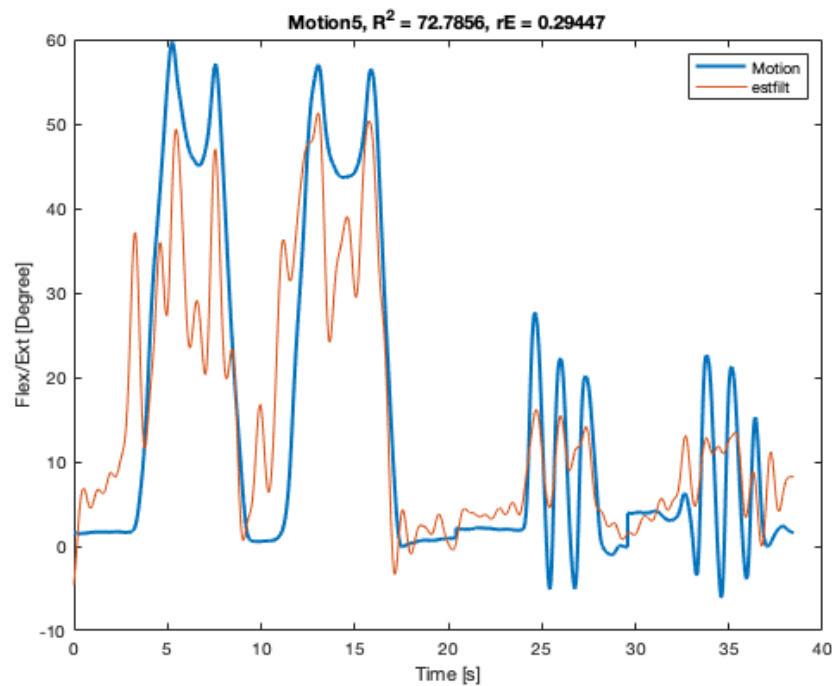


Figure 8.2: The right hip motion, in blue, during two sitting/standing and two walking tasks; superimposed to the Neural Network estimated angles, in orange.

In order to qualitatively compare the estimation between the joints, in figure 8.3 is shown a right ankle angle estimation which is usually always the worst one. In general, the estimation always follows the target pattern but not as good as for the hip or knee joints. This could be due to the larger distance between the joints and the selected muscles, or to the easier possibility of movements' variation during the execution of the tasks. Some subjects, for example, during the sitting/standing task slightly laterally rotate the feet. Therefore, the minor prediction's accuracy in the ankles angles could mean either that the relation between the muscles activation and the kinematics is not strong enough for a robust estimation either that the ankles have too many degrees of freedom to be perfectly estimated by only using back muscles.

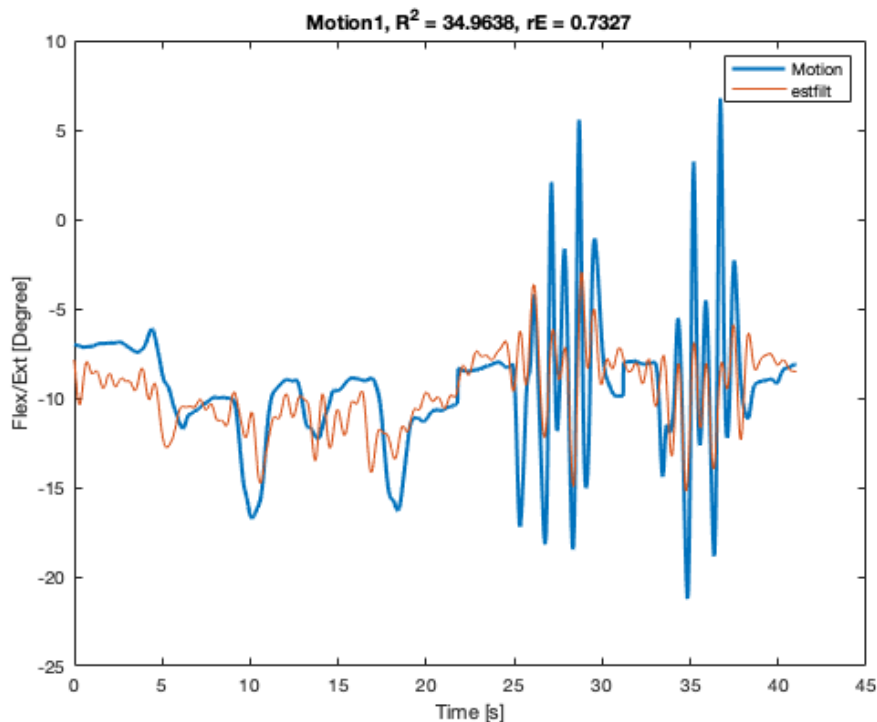


Figure 8.3: The right ankle motion, in blue, during two sitting/standing and two walking tasks; superimposed to the Neural Network estimated angles, in orange.

Looking at the results in a quantitative way, the previous evaluations are confirmed. Figure 8.4 shows the group average results obtained from ten able subjects performing the described experimental protocol. The group results allow describing the average results obtained for each joint and from each architecture tested. Moreover, a comparison between each different flexion/extension joint can be easily done. In terms of rE, it confirms that relation is always present, even with the distal ankles joints, because the error between the target and the prediction is always under 15% of the range of motion. These results are not obtainable if the muscles' activations are completely uncorrelated to the kinematics. Moreover, the rE is almost the same in each degree of freedom estimated and for every architecture tested, this means that all the NNs used to behave in the same way for each motion signals. These homogeneities in the results thus confirm that the Neural Networks are able to learn the relation EMG-force and the consequent force-motion relationship. The

R^2 instead, easily allows to analyze the differences between each joint. Figure 8.4 shows that for the hip and knee joints the kinematics prediction is good and robust, because the average R^2 between all the subjects is respectively 75% and 70%. Considering the ankle joint, instead, which shows an average R^2 of 45-50%, it is clear that the relationship is not that strong. The ankle kinematics is also more complex than the Hip and Knee one, due to the contact with the floor, in the stance phase of the gait, and the free movement of it, during the oscillation phase. This is not such a huge problem because most of the exoskeleton in commerce does not even have a powered ankle joint, therefore, these estimations of the ankle joint angles can also be seen as an improvement compares to the actual technologies.

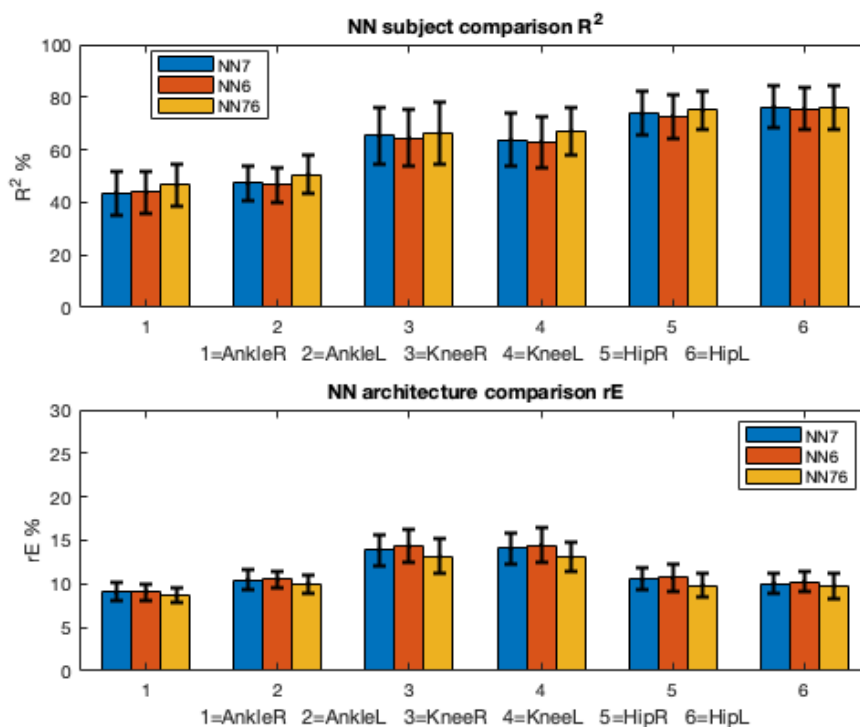


Figure 8.4: Ten able subjects' averaged group data of the coefficient of determination R^2 , in the top, and mean relative error rE , in the bottom. Each group of three bar is a lower limbs degree of freedom to estimate. Each bar of the group is a different Neural Network architecture. In blue and orange MLPs with one hidden layer with 7 and 6 neurons, respectively. In yellow the MLP with two hidden layers.

The group results in figure 8.4 also allows a comparison between the three different architecture tested for each degree of freedom. It is clear from these average results that the difference in the Neural Networks architectures do not influence the estimations. The R^2 and rE averaged values between ten subjects are in fact almost the same for each different architecture. These quantitative results, moreover, allow analyzing the difference in the prediction between the right lower limb and the left ones. It is clear that, even if the muscles activation is detected only from the right, both sides are perfectly predictable indifferently. Therefore, it could either mean that the left muscles activations detectable are completely redundant either that they could bring complementary activation which could increase or not increase the prediction quality.

8.2 Angles estimation from EMG and IMU

Analyzing the results obtained from the NNs with the EMG features and the IMU information as input in a qualitative way, the better performance of these networks comparing to the previous, from the EMG inputs only, is immediately appreciable. Figure 8.5 shows an example of the right hip kinematics prediction. As always, the reported example presents respectively two sitting/standing actions followed by two walking tasks. The prediction is improved since the joints kinematics is strictly related to the pelvis tilt, obliquity, and rotation. The estimation made is, with these input features, robust enough for stable control. Moreover, the already present and visible relationship between the muscles activations and the concurrent change in the kinematics is confirmed and improved with the new features. In figure 8.6 an example of right hip angles joints estimation, where the first two tasks in the signals are due to a sitting/standing actions and the following two are due to gait, is shown. Differently from the first analyzed results, the prediction is stable and perfectly correct in both tasks.

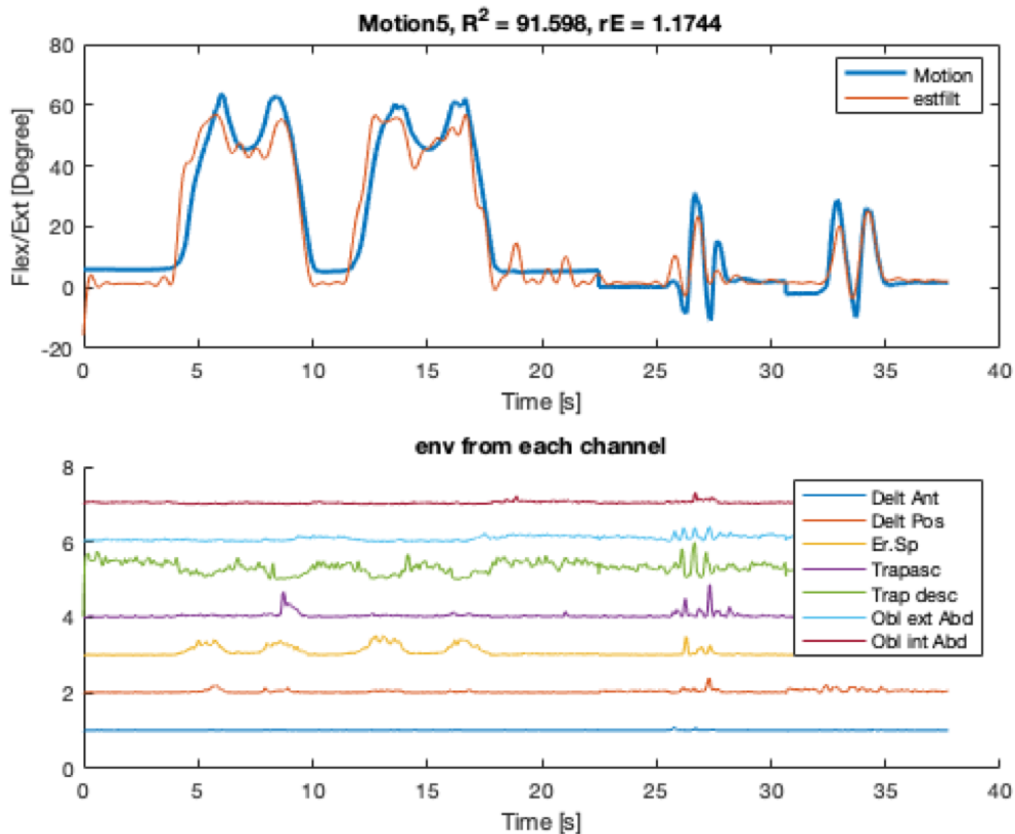


Figure 8.5: In the top, the estimation of the right hip angles, in orange, during performing of sitting/standing and walking tasks superimposed to the target signal calculated from the motion capture, in blu. In the bottom, the seven muscles activation envelopes used as input features, together with the pelvis tilt-obliquity-rotation, for the Neural Networks and concurrently recorded.

In order to qualitatively compare the estimation between the joints, in figure 8.7 is shown right ankle angles estimations which is usually always the worst one.

Comparing the prediction now obtained with the previous one, in figure 8.3 the IMU features show an improvement also in the ankle joint angles estimation. Beside that, the prediction is still not robust and stable enough or as good as for the hip and knee joints.

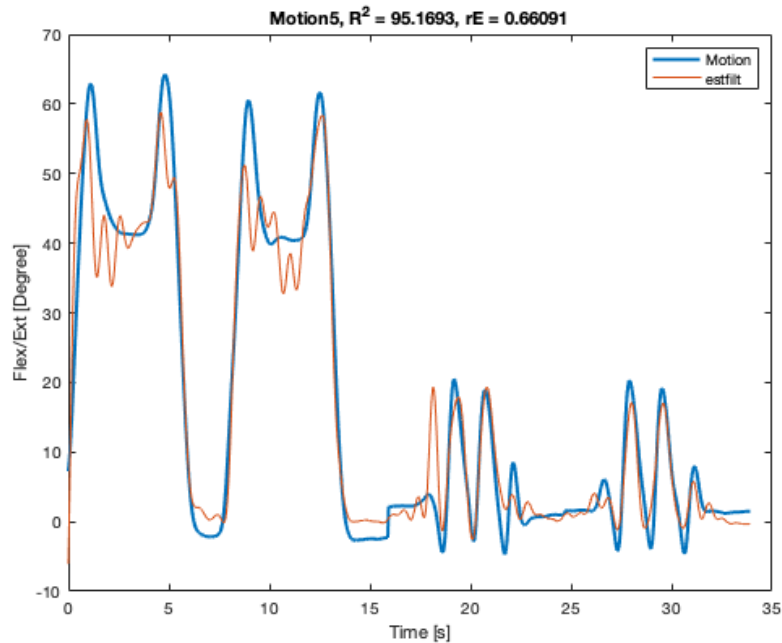


Figure 8.6: The right hip motion, in blue, during two sitting/standing and two walking tasks; superimposed to the Neural Network estimated angles, in orange.

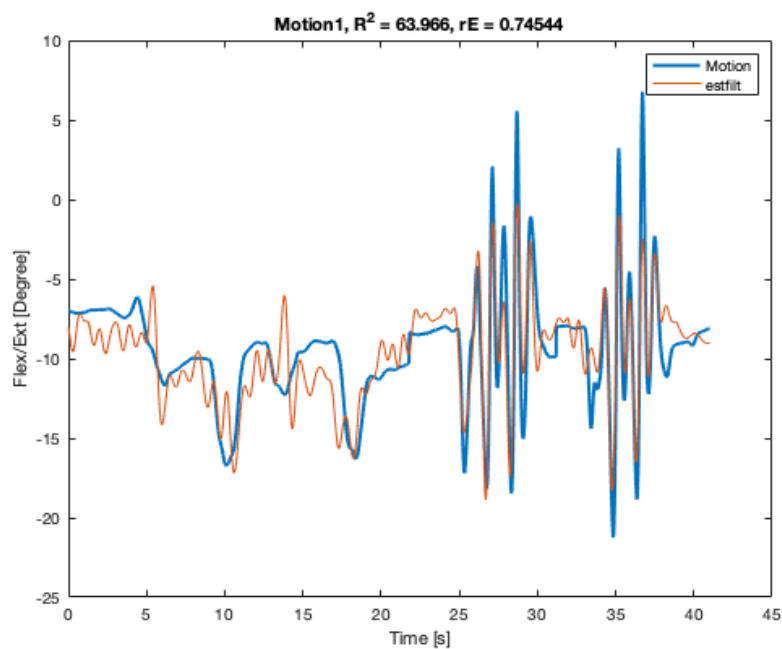


Figure 8.7: The right ankle motion, in blue, during two sitting/standing and two walking tasks; superimposed to the Neural Network estimated angles, in orange.

Looking at the results in a quantitative way, the improvement for every angle estimation is clearly visible. Figure 8.8 shows the average group results obtained from the angles' estimation in ten able participants. In terms of rE , it confirms the strong relationship between the input and the joints angles, because the error is always under 10% of the range of motion. Thus, 5% of the range of motion decrements in the mean relative error compared to the previous results. Moreover, R^2 shows that for the hip and knee joints angles the prediction is improved and thus completely utilizable for stable and robust control. The average R^2 between all the participants is respectively 85% and 80% for the Hip and Knee angles prediction. Considering the ankle joint, instead, a high improvement is visible, because the average R^2 is 60% of correlation, but still not enough for stable control. Obviously, the reasons for the worst estimation of the ankle joints are the same as before.

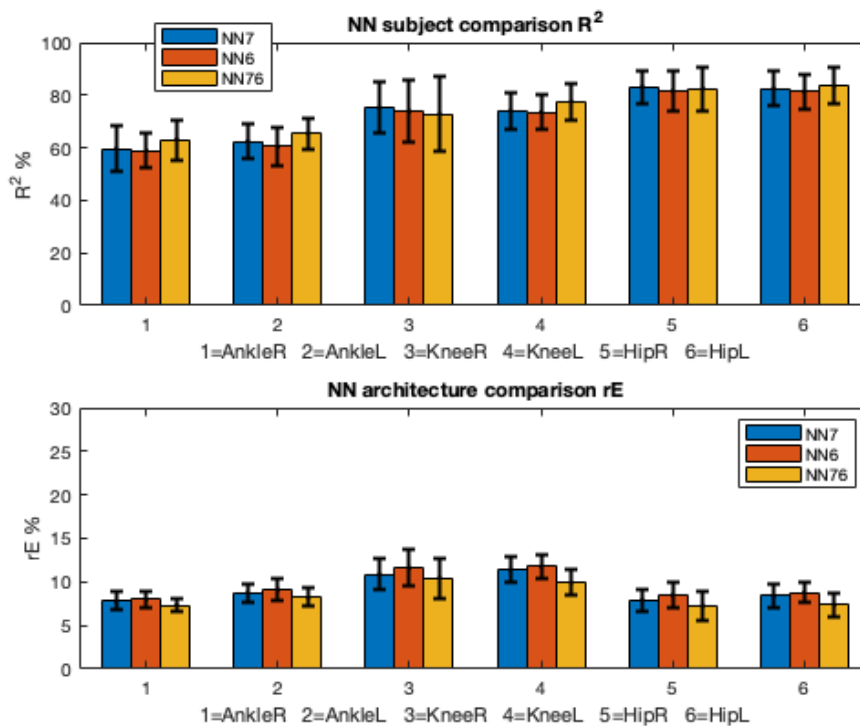


Figure 8.8: Ten able participants' averaged group data of the coefficient of determination R^2 , in the top, and mean relative error rE , in the bottom. Each group of three bar is a lower limbs degree of freedom to estimate. Each bar of the group is a different Neural Network architecture. In blue and orange MLPs with one hidden layer with 7 and 6 neurons, respectively. In yellow the MLP with two hidden layers.

The group results in figure 8.8 also allow a comparison between the three different architecture tested for each degree of freedom. It is clear from these average results that, even with three more inputs, the difference in the Neural Networks architectures do not influence the estimations. The R^2 and rE averaged values between ten participants are in fact almost the same for each different architecture. The aforementioned improvements are of course valid in both lower limbs, because the IMU features added from the pelvis are common to both sides. As well as before, adding the activation of the left upper body muscles side the prediction could improve more or anyway remain constant.

Chapter 9

Conclusion and Future steps

During this thesis work, I have developed an intuitive and proportional myoelectric control of an exoskeleton for a Spinal Cord Injury people. The developed Multi Layer Perceptron allowed a robust prediction and, thus, control of the hip, knee and ankle flexion/extension angles from EMG features and from the combination of them with three IMU information. These results are verified through the coefficient of determination and the mean relative error between the estimation and the target signals. It has been understood that myoelectric control is a great issue in the study of exoskeleton control, and in particular for Spinal Cord Injury. The development of assisting device for these people appears to me necessary and indispensable for the progress of the quality of life of them. Moreover, the existence of competition like Cybathlon is essential for the improvement of these assistive technologies and for the progress of human-machine interface methods. This dissertation also provided an overview of past and current research on exoskeleton control for paraplegic people. My proposed methods allow accurate and intuitive control also for other lower limb disabilities people. Moreover, the controller is based on present hardware, but it is applicable to whichever other devices with the same available degree of freedom.

All of this work is an absolute novelty in terms of myoelectric intuitive control for exoskeleton and of muscles kinematics relation. In the scientific literature, no other myoelectric control exists applicable to paraplegic people. I presented two different control strategies both applicable to the goal of the thesis. The presented study is perfectly utilizable for an active Hip-Knee exoskeleton. However, the control of ankle joint kinematics still lacks the desired level of accuracy and needs further improvement.

As a future development, it is proposed to use a multi joint lower limb sensing powered exoskeleton in a zero-impedance mode for the kinematics recording, instead of a motion capture acquisition system, and a wireless high density EMG (HD-sEMG) acquisition system [18], instead of the bipolar. The substitution of the motion capture system will allow having a complete time continuous and more various data set of movement. In this way, the user will be able to move freely outside the limited lab's space and it will be possible to add more complex daily life activity in the experimental protocol, like climbing stairs or avoiding obstacles. Substituting the bipolar system with a wireless high density will have the advantage of having an increased amount of EMG information and, of course, without the motion artifact problem faced in this study. It will also allow exploring new and more elaborated EMG features for the control. Secondly, in order to improve the estimation, a more

performant memory based recurrent neural network, like LSTM, should be tested for the regression. Last but not least, the final goal would be to test the intuitive controller with a Spinal Cord Injured persons and take part in the Cybathlon 2020 with the developed control system.

Progress in this area seems feasible in the short term. Lately, the exoskeleton field and, more in general, wearable technologies based on human-machine interface topics are rapidly growing in interest and founding. The aim of developing these technologies now is not only on rehabilitation or assistive point of view but also in a collaborative and supportive way for able people doing heavy jobs. Therefore, this higher demand and commercial interest will increase the research about these topics and will consequently help to improve the life of lots of people.

Appendices

Appendix A

Estimation of 6 DoF from EMG features: Results per Subject

Figure A.1: SUBJECT 01

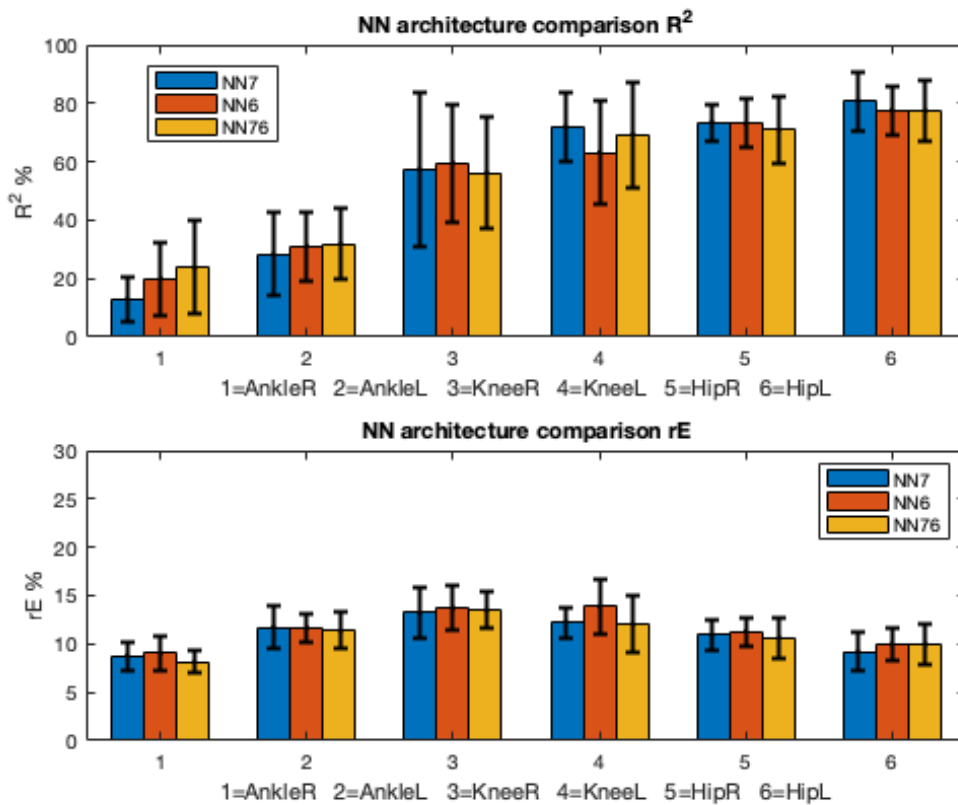


Figure A.2: SUBJECT 02

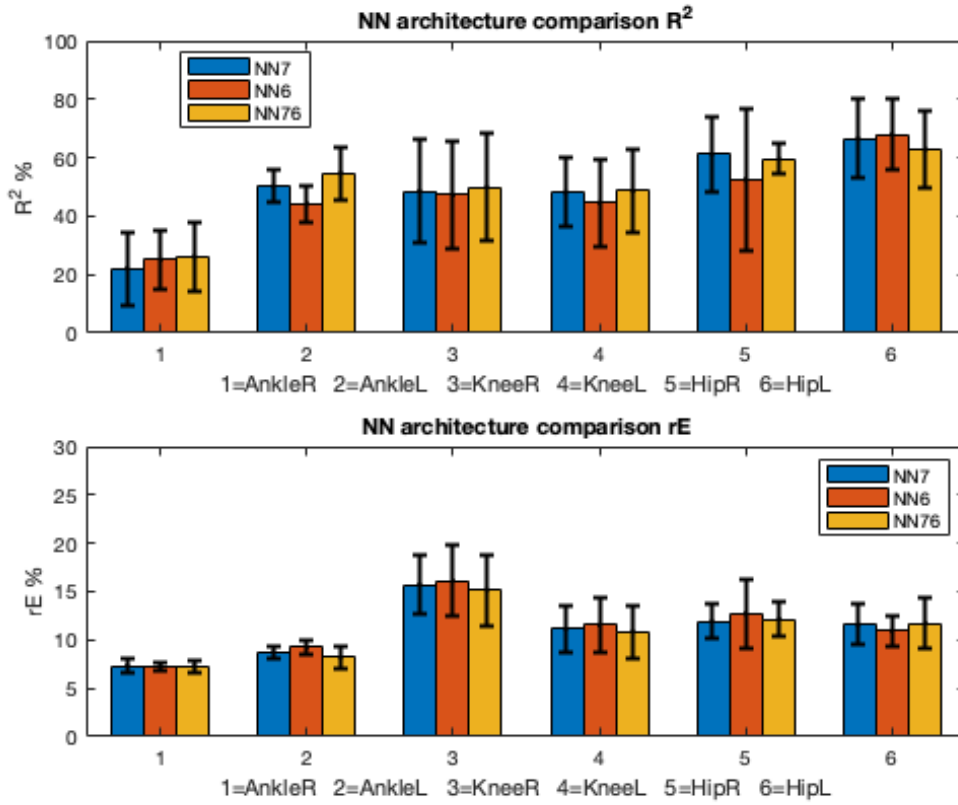


Figure A.3: SUBJECT 03

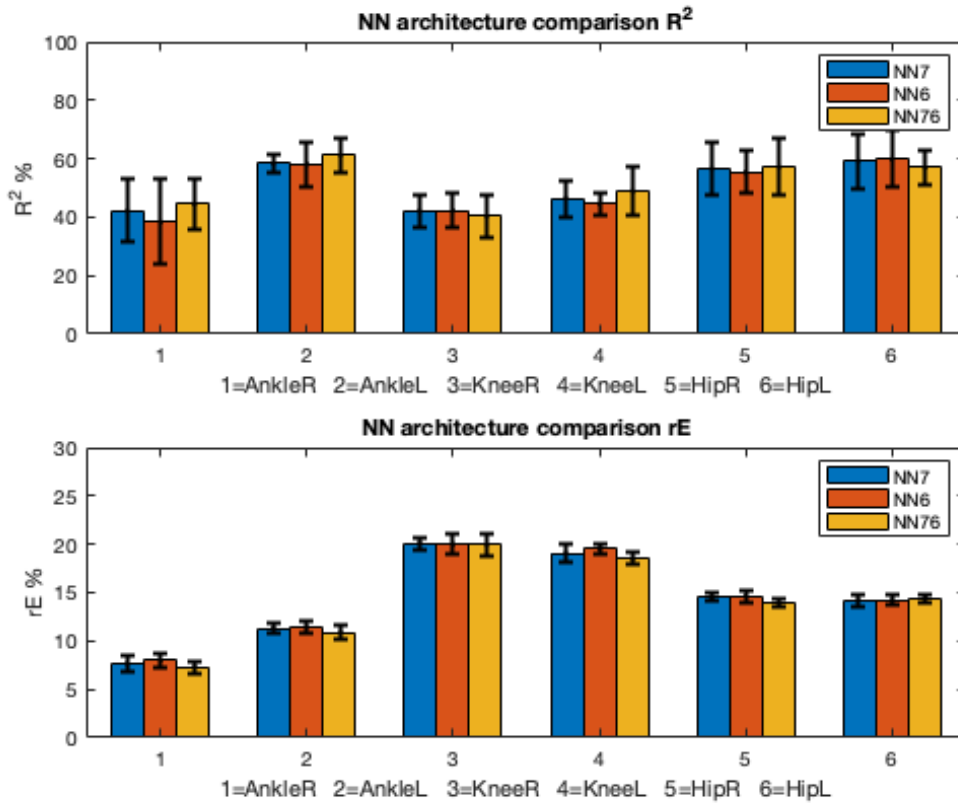


Figure A.4: SUBJECT 04

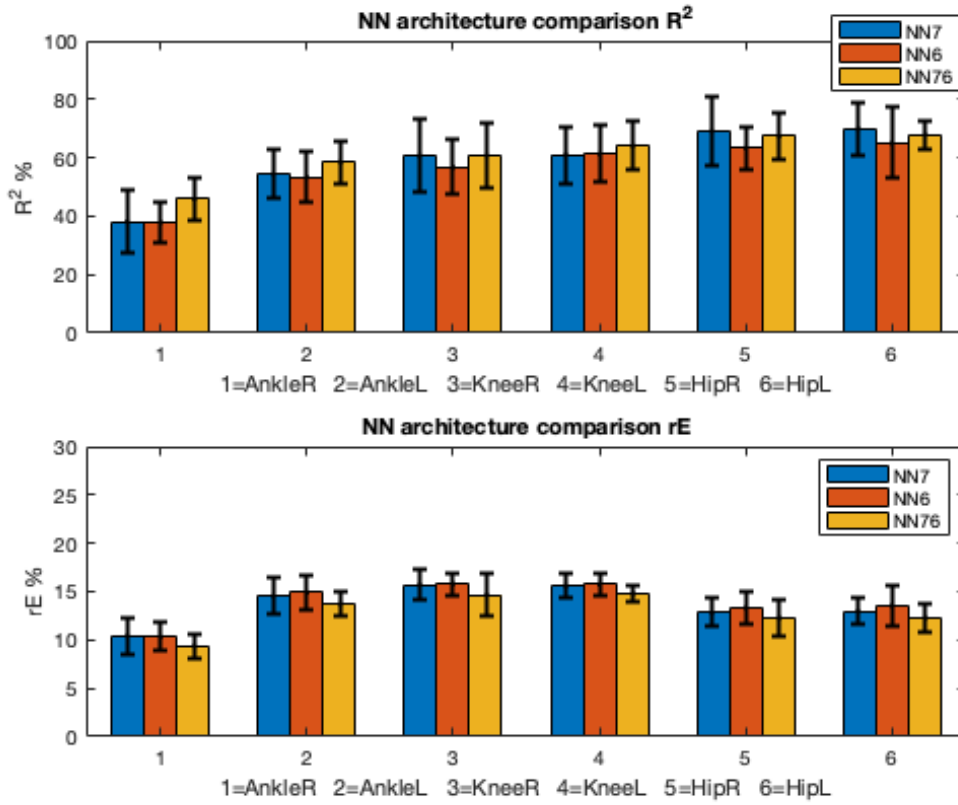


Figure A.5: SUBJECT 05

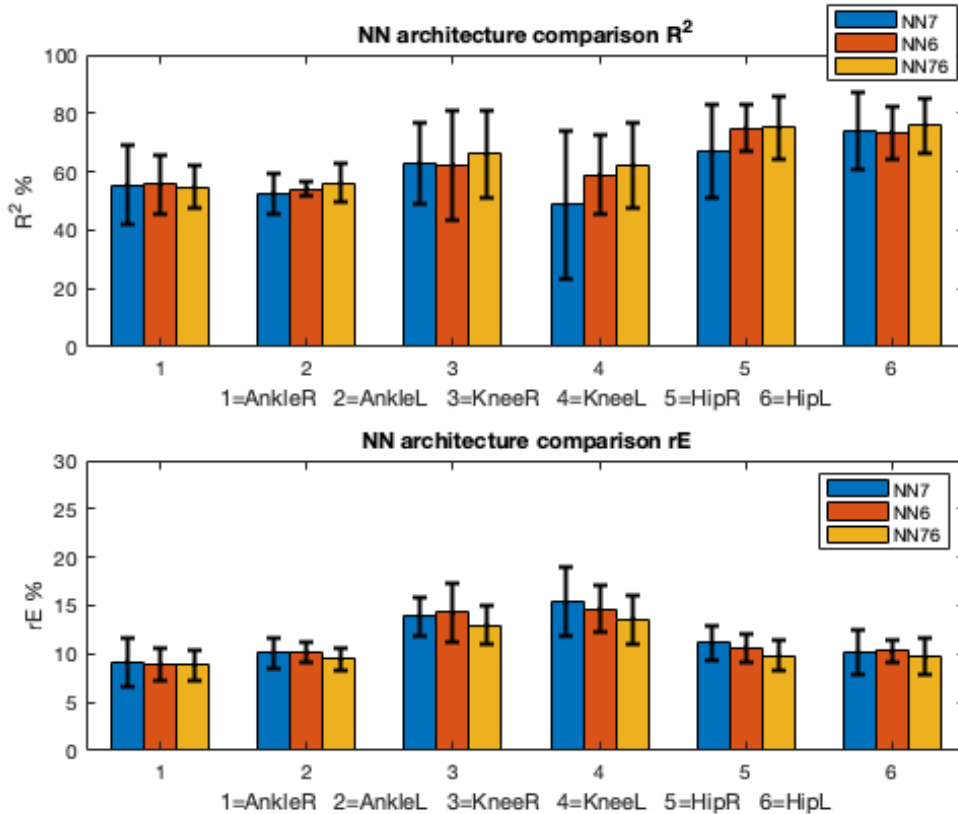


Figure A.6: SUBJECT 06

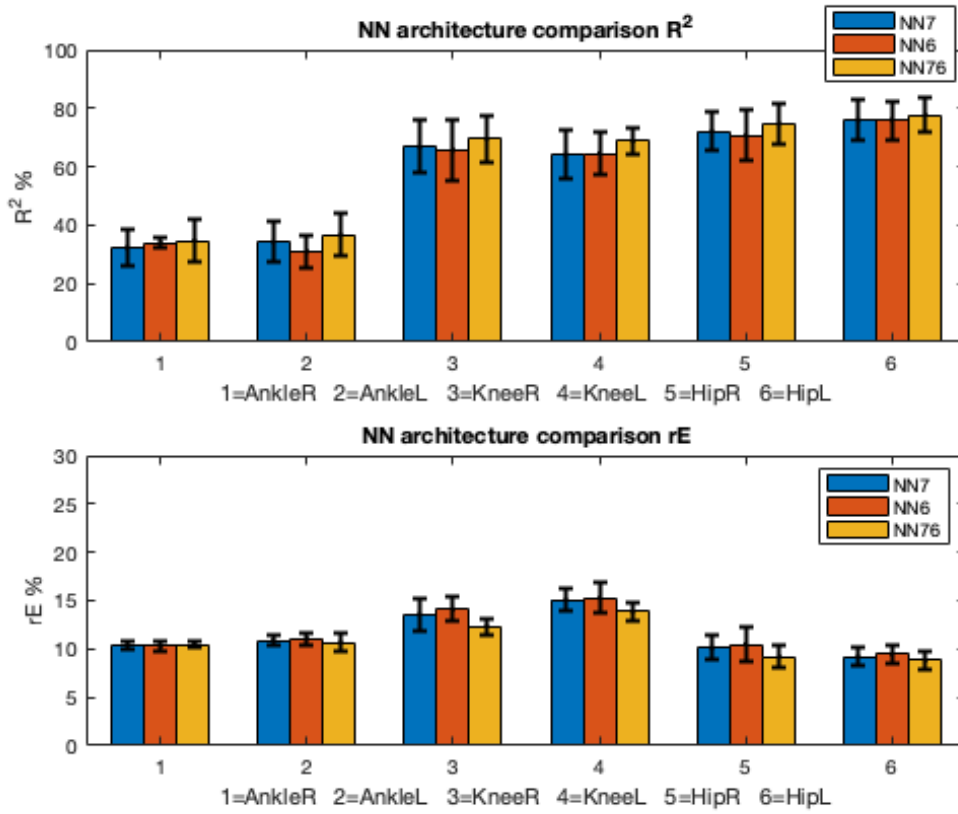


Figure A.7: SUBJECT 07

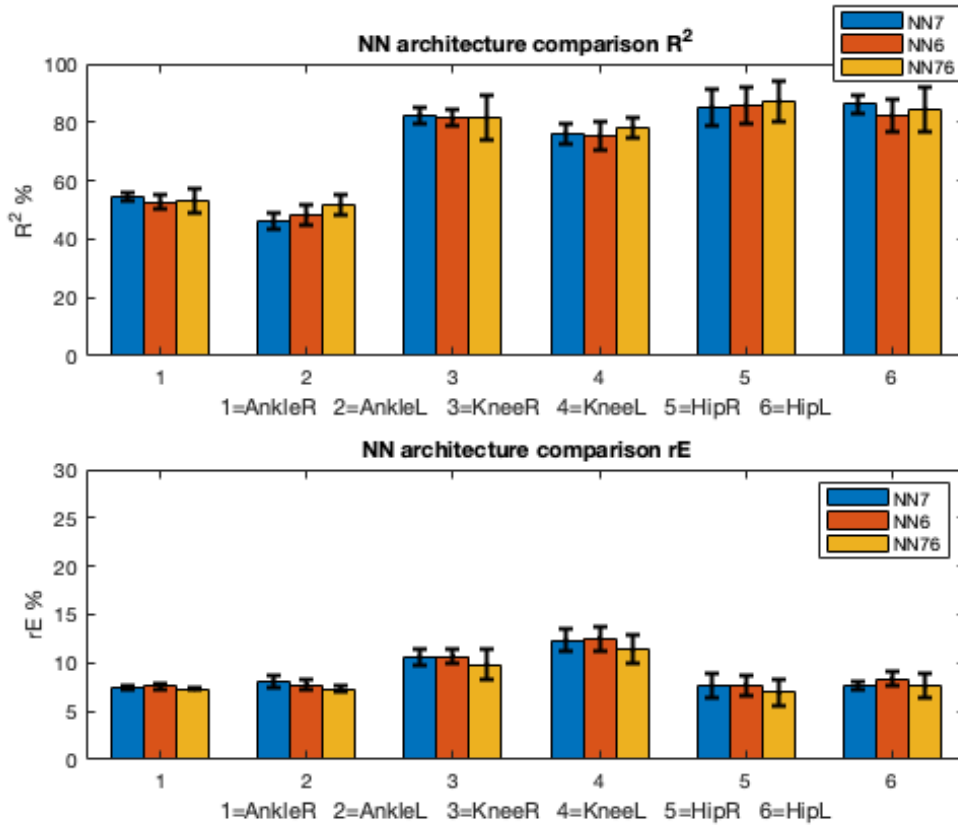


Figure A.8: SUBJECT 08

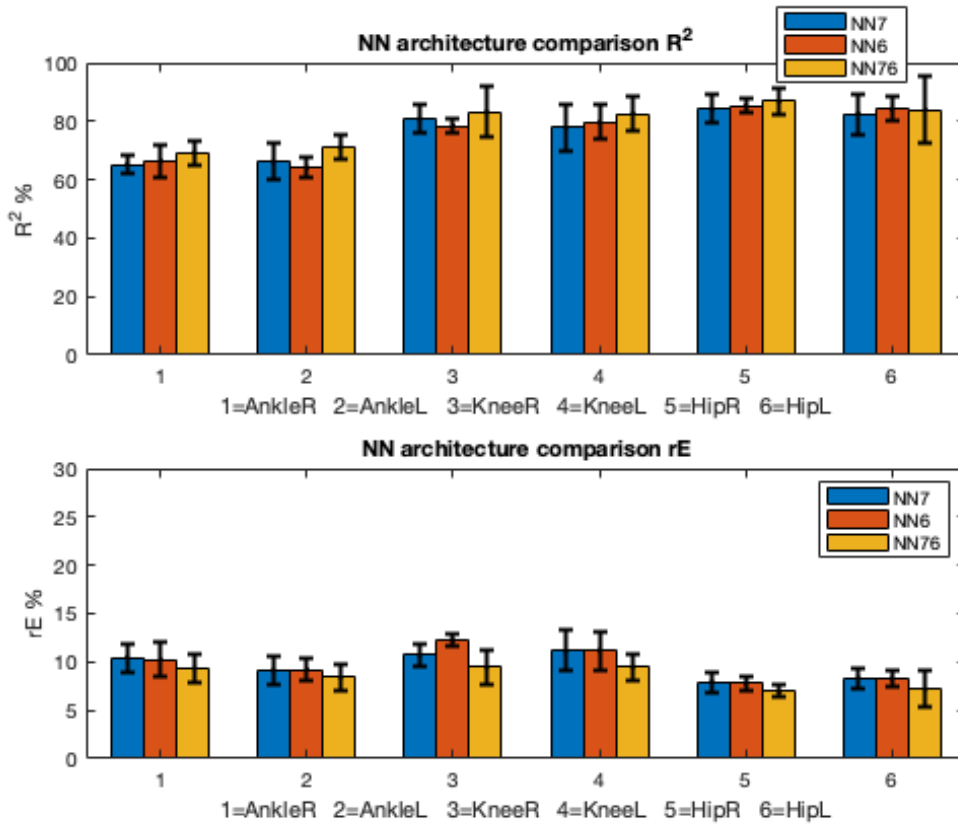


Figure A.9: SUBJECT 09

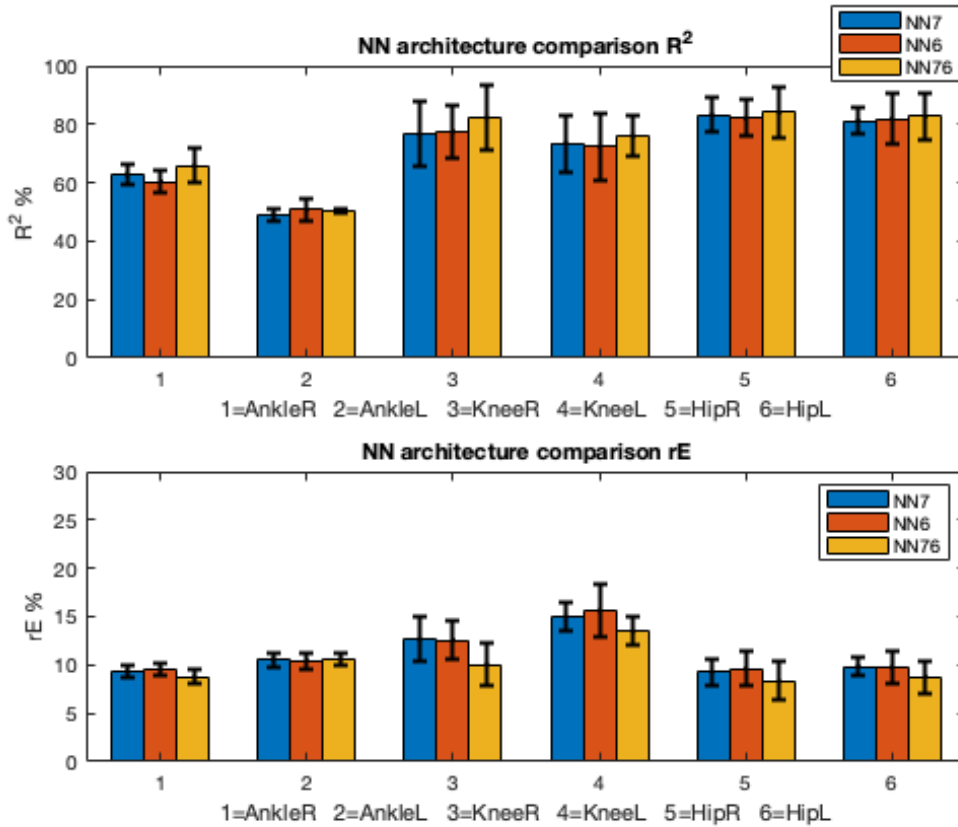
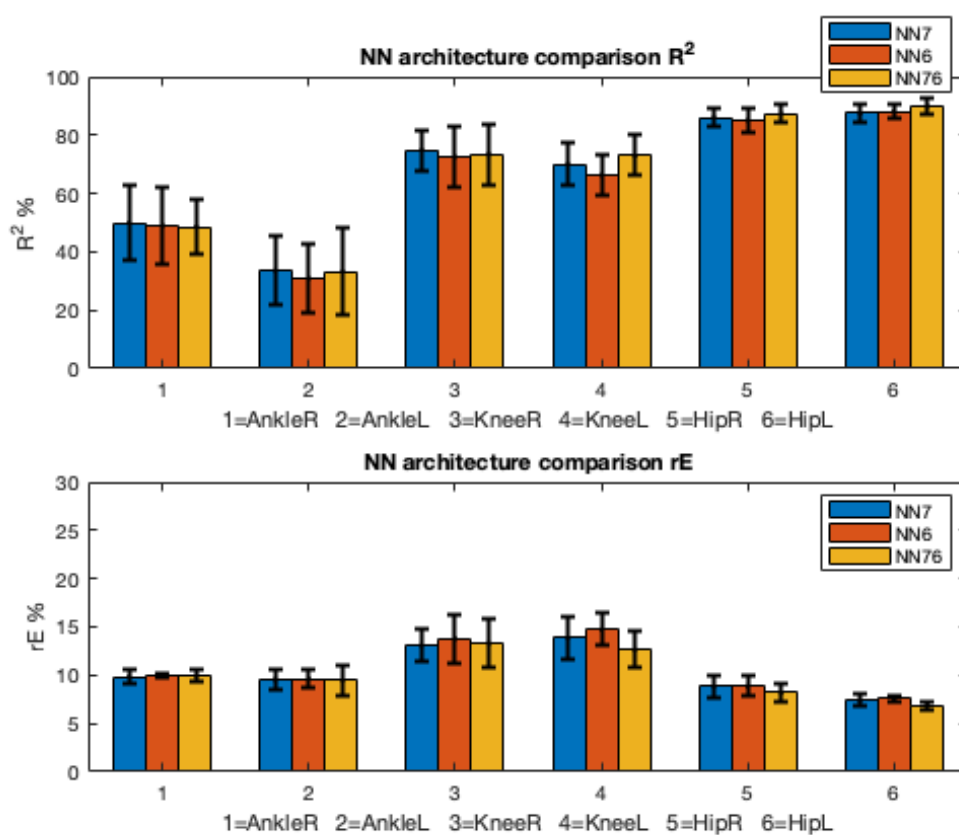


Figure A.10: SUBJECT 10



Appendix B

Estimation of 6 DoF from EMG and IMU features: Results per Subject

Figure B.1: SUBJECT 01

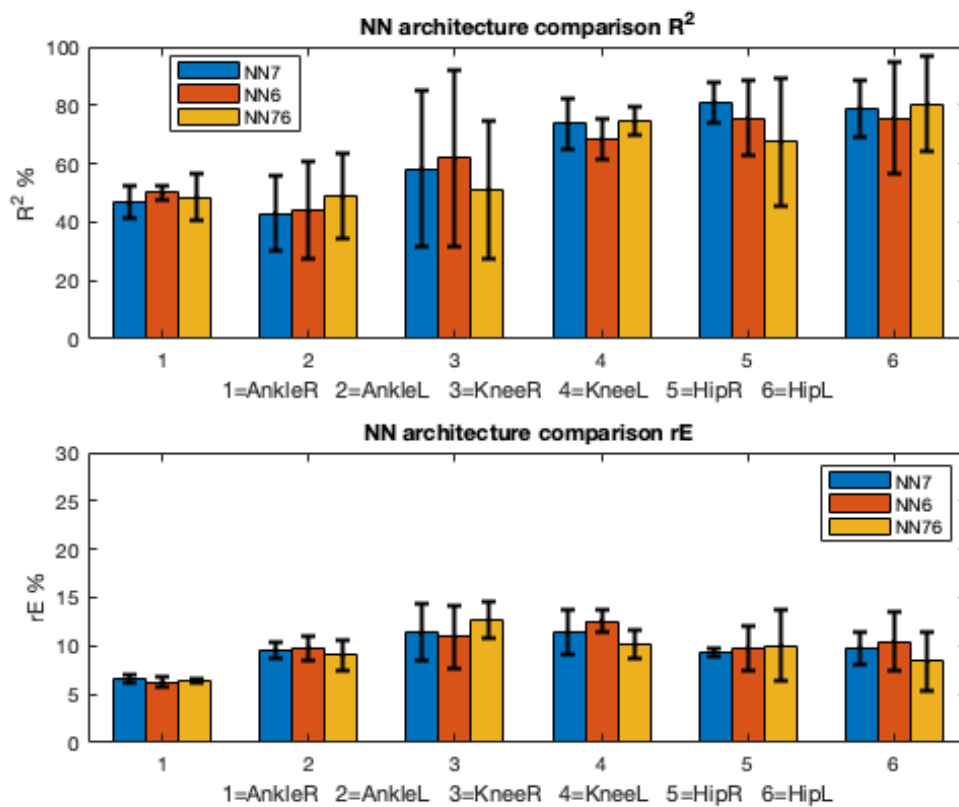


Figure B.2: SUBJECT 02

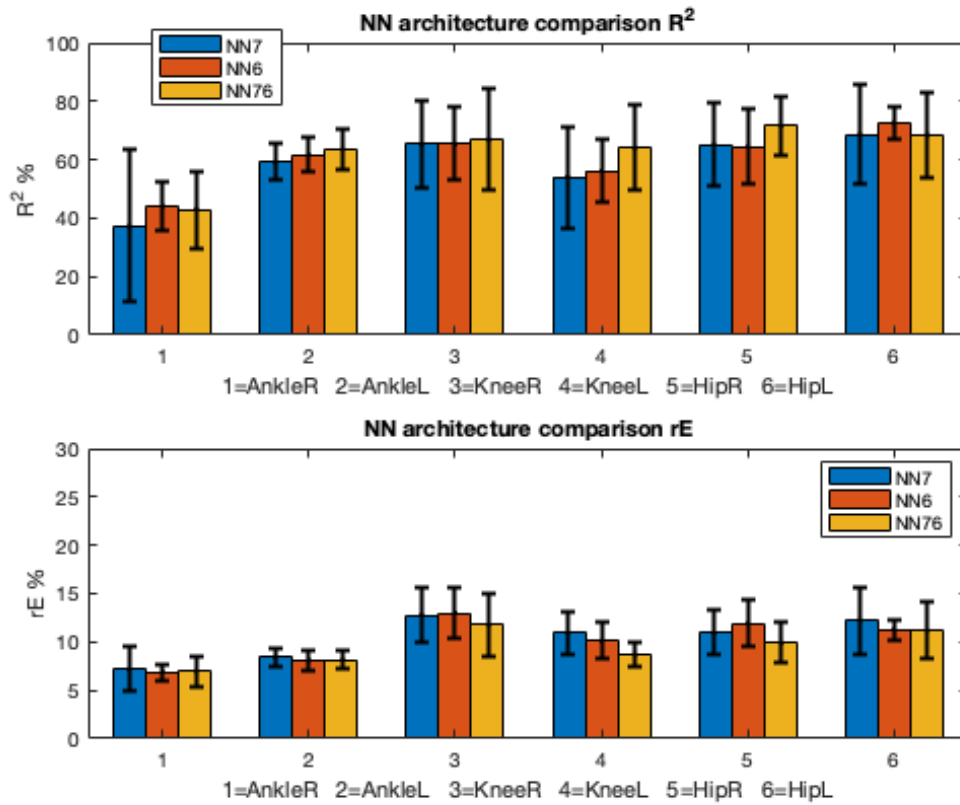


Figure B.3: SUBJECT 03

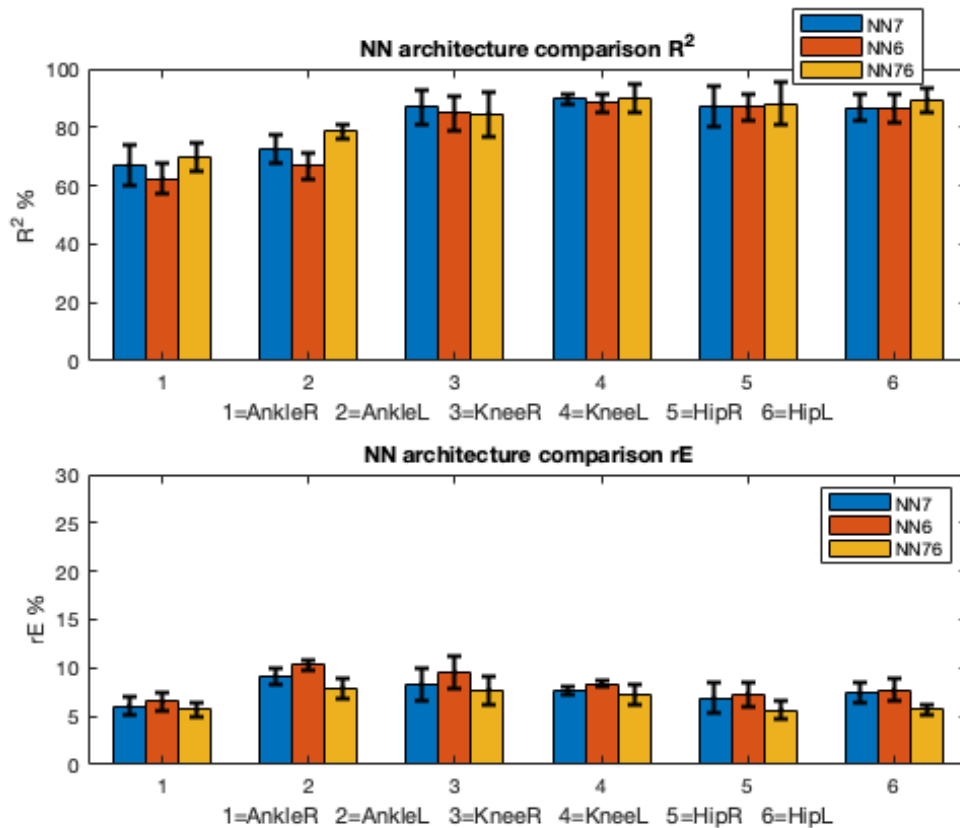


Figure B.4: SUBJECT 04

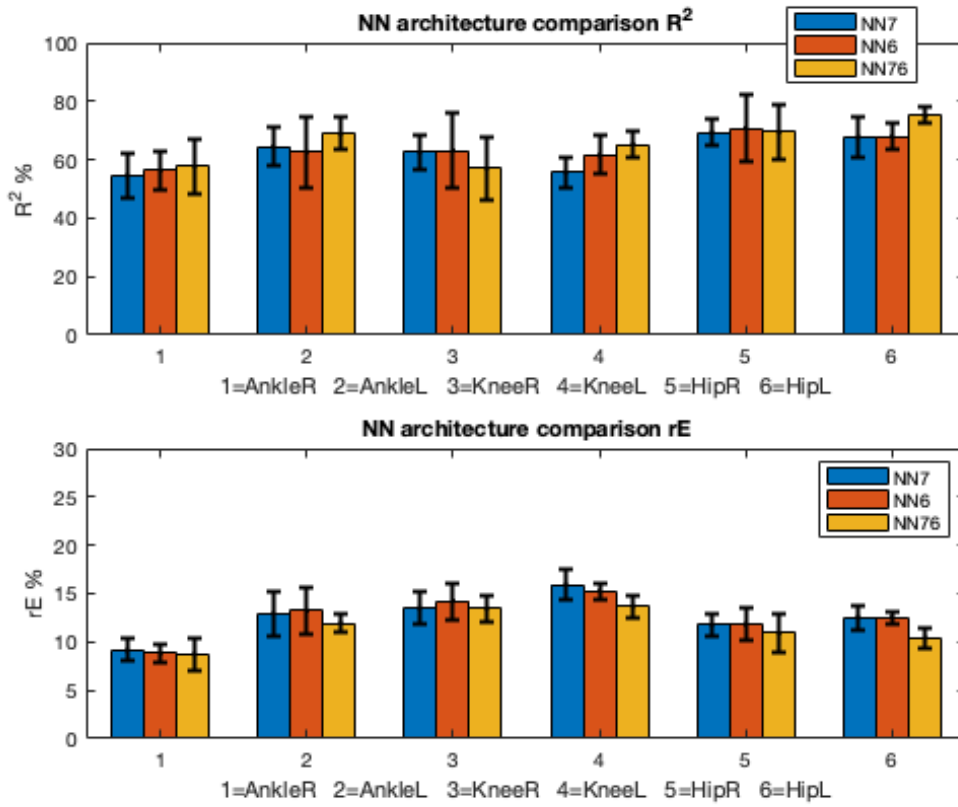


Figure B.5: SUBJECT 05

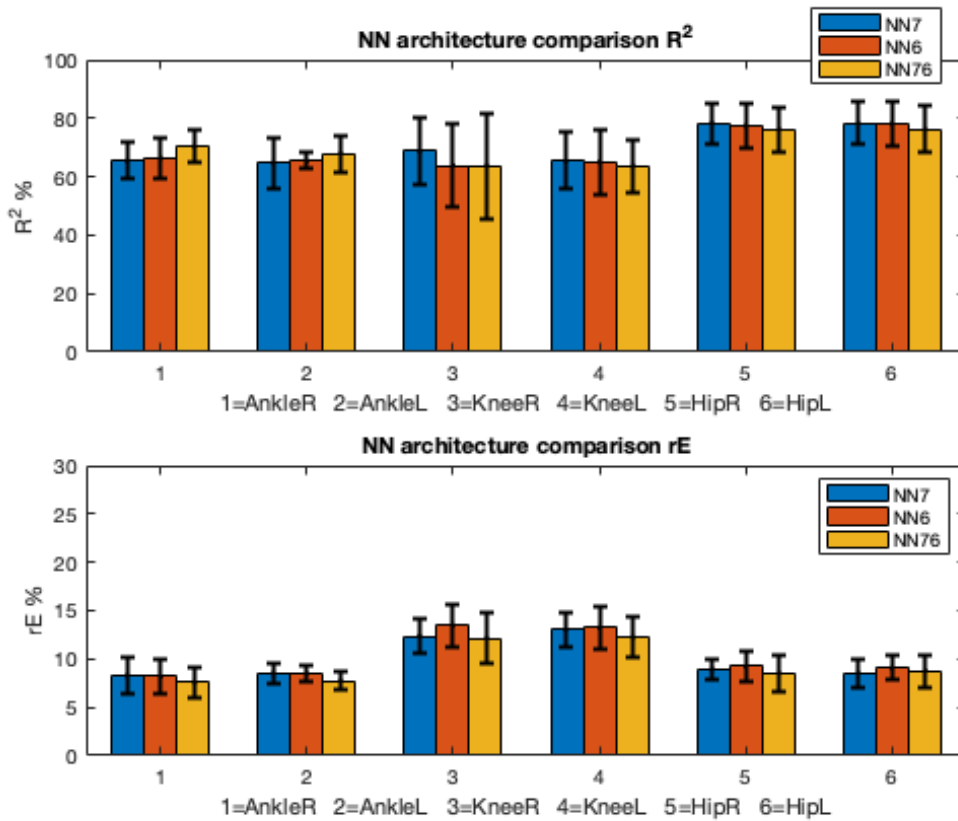


Figure B.6: SUBJECT 06

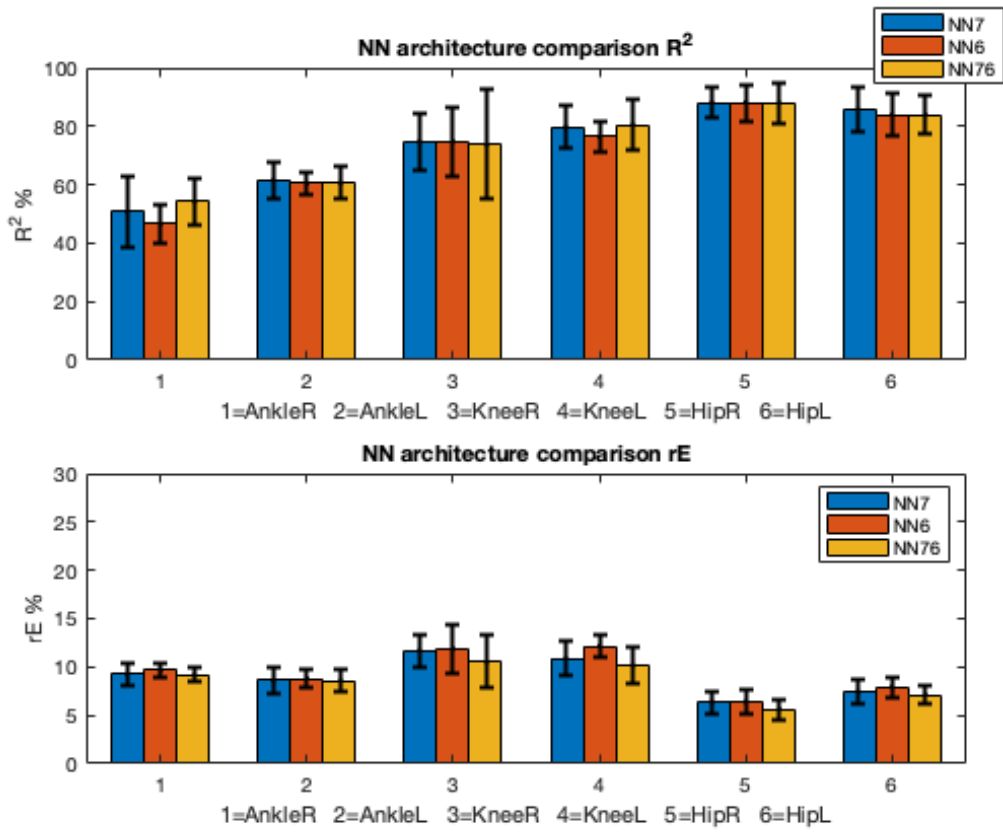


Figure B.7: SUBJECT 07

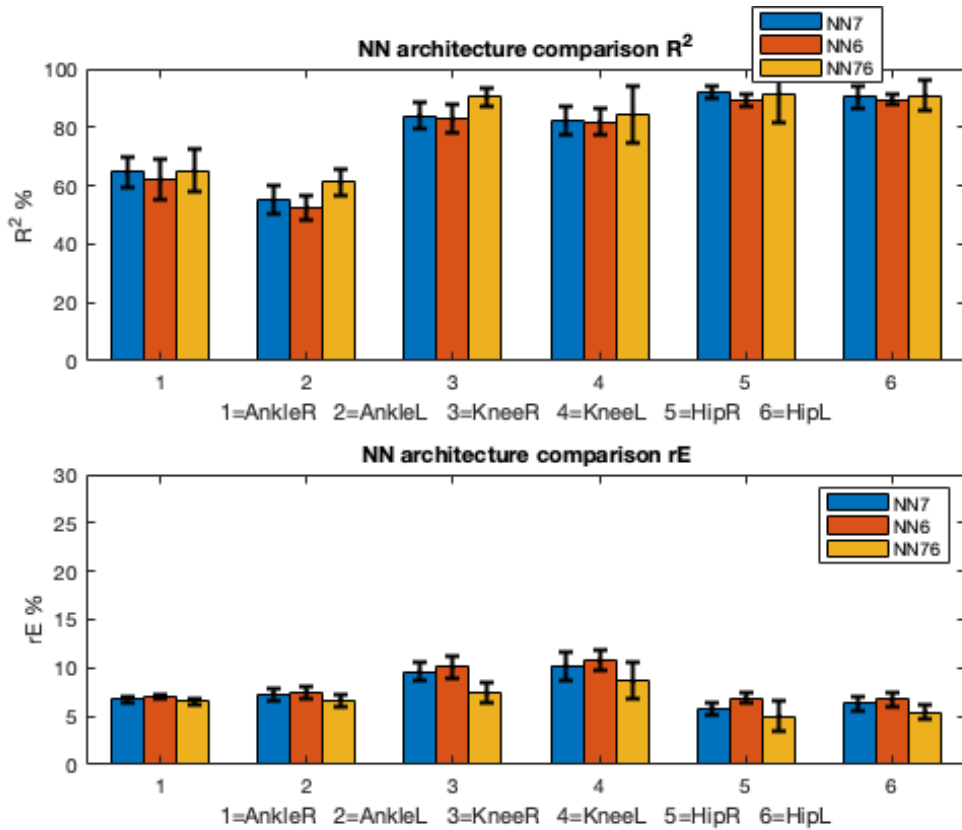


Figure B.8: SUBJECT 08

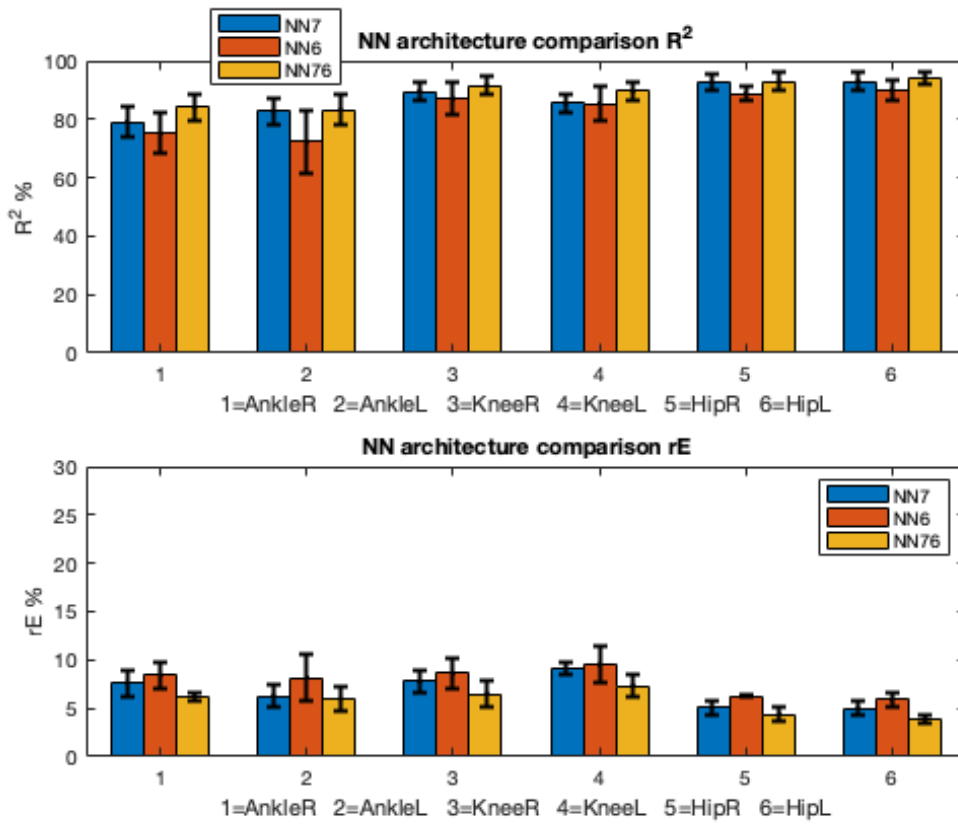


Figure B.9: SUBJECT 09

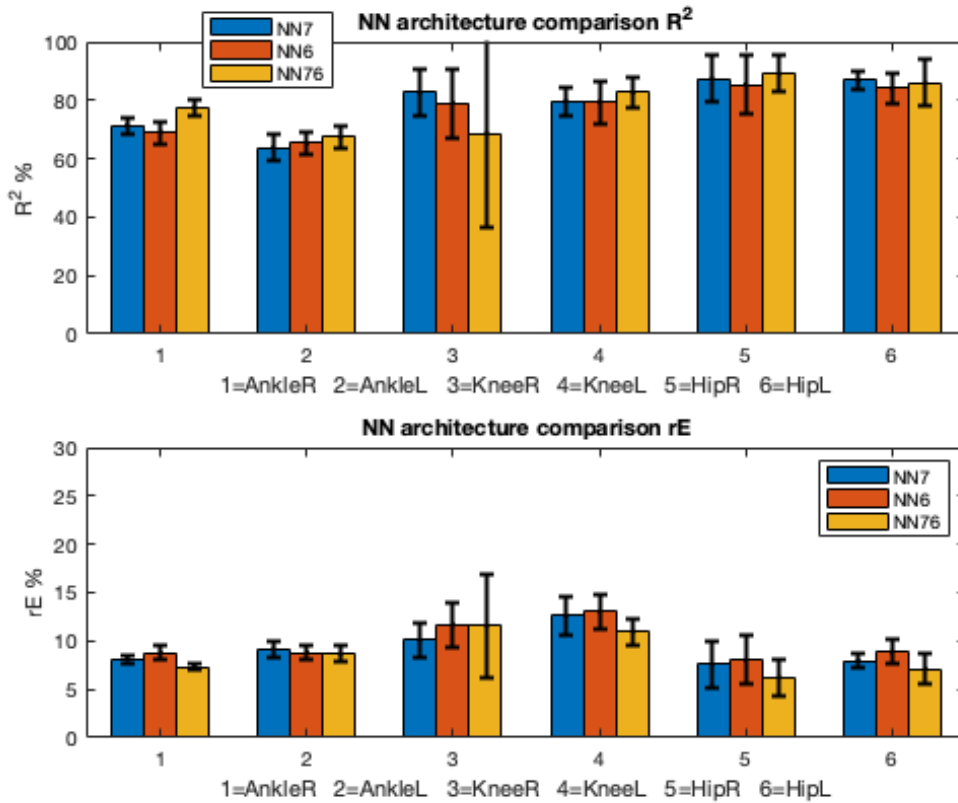
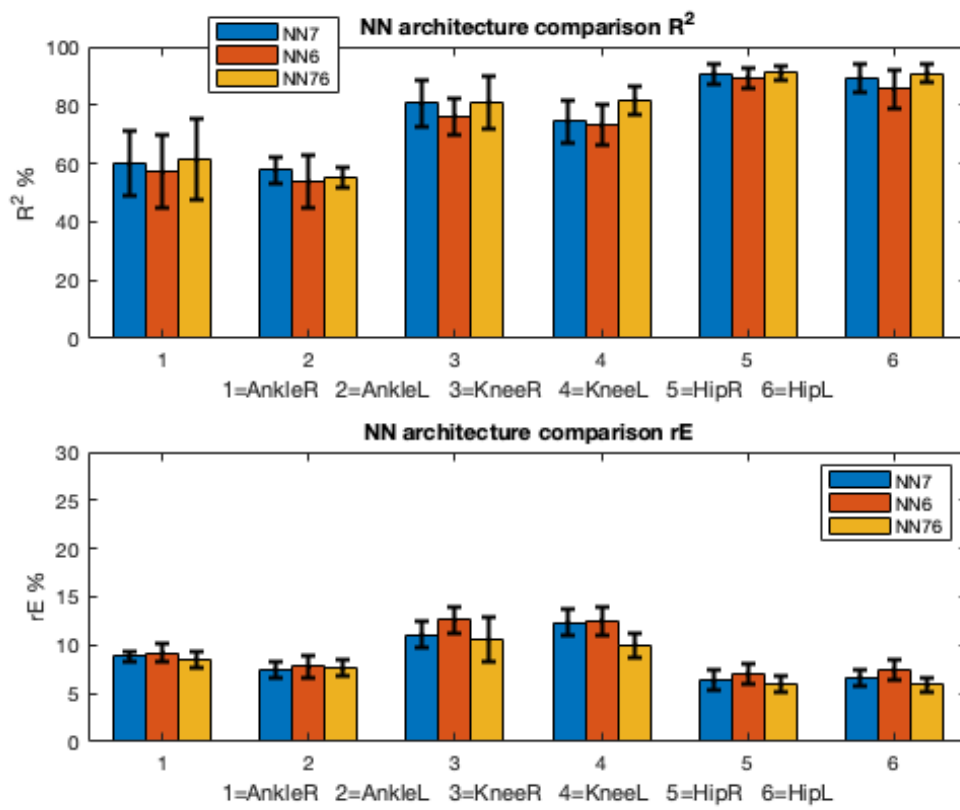


Figure B.10: SUBJECT 10



Bibliography

- [1] Christopher L Vaughan, Brian L Davis, and Jeremy C O'Connor. *The Three-Dimensional and Cyclic Nature of Gait*. 1999, pp. 16–17.
- [2] Sean G T Gibbons and Mark J Comerford. “Strength Versus Stability Part I ; Concept and Terms”. In: *Orthopaedic Divison Review* March/April (2001), pp. 21–27.
- [3] “ISB recommendation on definitions of joint coordinate system of various joints for the reporting of human joint motion—part I: ankle, hip, and spine”. In: *Journal of Biomechanics* 35 (2002), pp. 543–548.
- [4] Peter B O Sullivan et al. “The Effect of Different Standing and Sitting Postures on Trunk Muscle Activity in a Pain- Free Population The Effect of Different Standing and Sitting Postures on Trunk Muscle Activity in a Pain-Free Population”. In: *Spine* 27.11 (2002), pp. 1238–1244.
- [5] Wise Young. *Spinal Cord Injury Levels Classification*. 2002. URL: <https://www.sci-info-pages.com/levels.html>.
- [6] M. Zecca et al. “Control of Multifunctional Prosthetic Hands by Processing the Electromyographic Signal”. In: *Critical Reviews? in Biomedical Engineering* 30.4-6 (2002), pp. 459–485. URL: <http://www.dl.begellhouse.com/journals/4b27cbfc562e21b8,5b51f41866ab7f77,5d2cbc051cfa16a4.html>.
- [7] Y. P. Ivanenko, R. E. Poppele, and F. Lacquaniti. “Five basic muscle activation patterns account for muscle activity during human locomotion”. In: *Journal of Physiology* 556.1 (2004), pp. 267–282.
- [8] G. Cappellini et al. “Motor Patterns in Human Walking and Running”. In: *journal of Neurophysiol* (2006).
- [9] Dario Farina. “Interpretation of the Surface Electromyogram in Dynamic Contractions”. In: (2006), pp. 121–127.
- [10] Juan C. Moreno et al. “Design and Implementation of an inertial measurement unit for control of artificial limbs: Application on leg orthoses”. In: *Sensor and Actuators B: Chemical* 118 (2006), pp. 333–337.
- [11] Christoph Anders et al. “Trunk muscle activation patterns during walking at different speeds”. In: *Journal of Electromyography and Kinesiology* 17.2 (2007), pp. 245–252.
- [12] Aleš Holobar et al. “Clinical Neurophysiology Estimating motor unit discharge patterns from high-density surface electromyogram”. In: 120 (2009), pp. 551–562. DOI: 10.1016/j.clinph.2008.10.160.

-
- [13] Dario Farina et al. “Clinical Neurophysiology Decoding the neural drive to muscles from the surface electromyogram”. In: *Clinical Neurophysiology* 121.10 (2010), pp. 1616–1623. ISSN: 1388-2457. DOI: 10.1016/j.clinph.2009.10.040. URL: <http://dx.doi.org/10.1016/j.clinph.2009.10.040>.
- [14] Silvia Muceli and Dario Farina. “Simultaneous and proportional estimation of hand kinematics from EMG during mirrored movements at multiple degrees-of-freedom”. In: *IEEE Transactions on Neural Systems and Rehabilitation Engineering* 20.3 (2012), pp. 371–378.
- [15] Brian Lawson et al. “A Robotic Leg Prosthesis: Design, Control, and Implementation”. In: *IEEE Robotics and Automation Magazine* 21 (2014), pp. 70–81.
- [16] Magdo Bortole et al. “The H2 robotic exoskeleton for gait rehabilitation after stroke: Early findings from a clinical study Wearable robotics in clinical testing”. In: *Journal of NeuroEngineering and Rehabilitation* 12.1 (2015), pp. 1–14. URL: <http://dx.doi.org/10.1186/s12984-015-0048-y>.
- [17] M. Burke and J. Lasenby. “Estimating missing marker positions using low dimensional Kalman smoothing”. In: *Journal of Biomechanics* 49 (2016), pp. 1854–1858.
- [18] Giacinto Luigi Cerone, Alberto Botter, and Marco Gazzoni. “A Modular, Smart, and Wearable System for High Density sEMG Detection”. In: *IEEE Transactions on Biomedical Engineering* (2019).
- [19] W J Suntay. “A Joint Coordinate System for the Clinical Description of Three-Dimensional Motions : Application to the Knee 1”. In: 105.May 1983 (2019).
- [20] ETH Zurich. *CYBATHLON 2020 disciplines and races*. 2020. URL: <http://www.cybathlon.ethz.ch/races-and-disciplines.html>.
- [21] BTS Bioengineering. *Smart DX motion capture system, BTS Bioengineering*. URL: <https://www.btsbioengineering.com/products/smart-dx/>.
- [22] F Rosenblatt and Contract Nonr-. “THE PERCEPTRON : A PROBABILISTIC MODEL FOR INFORMATION STORAGE AND ORGANIZATION”. In: 65.6 (), pp. 386–408.
- [23] SENIAM Surface ElectroMyoGraphy for the Non-Invasive Assessment of Muscles. *Sensor location recommendations*. URL: <http://www.seniam.org>.
- [24] Vicon. *Lower limb modelling with plug-in gait*. URL: <https://docs.vicon.com/display/Nexus25/Lower+body+modeling+with+Plug-in+Gait>.
- [25] Nicola Vitiello et al. “Review of assistive strategies in powered lower-limb orthoses and exoskeletons”. In: (). URL: <https://www.journals.elsevier.com/robotics-and-autonomous-systems>.